European scale modeling of sulfur, oxidized nitrogen and photochemial oxidants. Model development and evaluation for the 1994 growing season

Joakim Langner, Robert Bergström SMHI
Karin Pleijel Swedish Environmental Research Institute IVL

Cover: Observed and model calculated (35 m) AOT40 April-September. Units: ppmh(v).

European scale modeling of sulfur, oxidized nitrogen and photochemical oxidants. Model development and evaluation for the 1994 growing season

Joakim Langner, Robert Bergström SMHI
Karin Pleijel Swedish Environmental Research Institute IVL

Report Summary / Rapportsammanfattning

Issuing Agency/Utgivare	Report number/Publikation
Swedish Meteorological and Hydrological Institute	RMK No. 82

S-601 76 NORRKÖPING Sweden	Report date/Utgivningsdatum September 1998

Author (s)/Författare

Joakim Langner, Robert Bergström SMHI and Karin Pleijel IVL

Title (and Subtitle/Titel

European scale modeling of sulfur, oxidized nitrogen and photochemical oxidants. Model development and evaluation for the 1994 growing season

Abstract/Sammandrag

A chemical mechanism, including the relevant reactions leading to the production of ozone and other photochemical oxidants, has been implemented in the MATCH regional tracer transport/chemistry/deposition model. The aim has been to develop a model platform that can be used as a basis for a range of regional scale studies involving atmospheric chemistry, including assessment of the importance of different sources of pollutants to the levels of photochemical oxidants and air pollutant forecasting. Meteorological input data to the model were taken from archived output from the operational version of HIRLAM at SMHI. Evaluation of model calculations over Europe for a six month period in 1994 for a range of chemical components show good results considering known sources of error and uncertainties in input data and model formulation. With limited further work the system is sufficiently good to be applied for scenario studies and for regional scale air pollutant forecasts.

Key words/sök-, nyckelord

Eulerian, long-range transport, air pollution

Supplementary notes/Tillägg	Number of pages/Antal sidor	Language/Språk
	71	English

Report available from/Rapporten kan köpas från:

SMHI
SE-601 76 NORRKÖPING
Sweden

CONTENTS

Page

European scale modeling of sulfur, oxidized nitrogen and photochemical oxidants. Model development and evaluation for the 1994 growing season

Joakim Langner and Robert Bergström, SMHI
and

Karin Pleijel, IVL

Abstract

A chemical mechanism, including the relevant reactions leading to the production of ozone and other photochemical oxidants, has been implemented in the MATCH regional tracer transport/chemistry/deposition model. The aim has been to develop a model platform that can be used as a basis for a range of regional scale studies involving atmospheric chemistry, including assessment of the importance of different sources of pollutants to the levels of photochemical oxidants and air pollutant forecasting. Meteorological input data to the model were taken from archived output from the operational version of HIRLAM at SMHI. Evaluation of model calculations over Europe, for a six-month period in 1994, for a range of chemical components show good results considering known sources of error and uncertainties in input data and model formulation. With limited further work the system is sufficiently good to be applied for scenario studies and for regional scale air pollutant forecasts.

1. Introduction

Concentration of surface ozone at many locations in Europe currently exceeds the critical levels, where damage to vegetation and health may occur. This is true also in northern Europe regarding vegetation damage. In southern Sweden even the critical levels for human health are occasionally exceeded. Optimizing measures to reduce the surface ozone concentration requires a better understanding of the interactions of ozone precursor emissions and processes influencing the distribution of photochemical oxidants.

Work on developing models for studying the contribution to the production of photochemical oxidants from individual countries, or activities, has been underway for several years in Europe. Both Lagrangian and Eulerian type models have been used for longer simulations (months) and scenario calculations (e.g. Simpson, 1992; Simpson, 1995; Builtjes, 1988; Zlatev et al., 1993). These studies have employed rather coarse horizontal resolution (100-150 km) and limited vertical resolution. Studies covering northern Europe using higher resolution over extended periods are lacking.

The chemical system describing the production of photochemical oxidants is strongly nonlinear and the range of simulated concentration levels depends on model resolution. It is therefore of great interest to carry out calculations with higher horizontal and vertical resolution.

During the last five years SMHI has developed an Eulerian atmospheric transport and chemistry modeling system called MATCH (Multiscale Atmospheric Transport and Chemistry model). The MATCH system is used in a wide range of applications, from high resolution assessment studies for sulfur and nitrogen compounds in regions of Sweden to continental scale studies in developing parts of the world (Langner et al., 1995; Robertson, et

al., 1995; Robertson et al. 1998). It is also used in emergency response applications over Europe (Langner et al., 1998)

In the work presented here a photochemical module has been implemented in MATCH. The intention is to use MATCH as a tool for assessing the importance of different sources of pollutants to the levels of photochemical oxidants over Sweden and to study control strategies. Details about the basic transport model, chemical mechanism and input data are given in Section 2. In Section 3 a detailed evaluation of a six-month simulation against observed chemical data is presented and Section 4 contains a summary and conclusions.

2. *Model*

The MATCH model solves the advection diffusion equation for atmospheric tracers in a three-dimensional, Eulerian framework:

nur Skalärprodukt ?

$$\frac{\partial c_i}{\partial t} = -\nabla(\mathbf{v}c_i) + \nabla(\mathbf{K}\nabla c_i) + Q_i + S_i \qquad (1)$$

Skalärprodukt.

where c_i represents the mass mixing ratio of the trace species of interest, $\mathbf{v}$ is the three-dimensional wind, $\mathbf{K}$ is the turbulent diffusion tensor and Q_i and S_i represents internal sources and sinks. The formulation of the model is similar to other limited area Eulerian transport models, e.g., Carmichel and Peters (1984), Chang et al. (1987), Hass et al. (1990) and Pudykiewiz (1989).

The basic transport model includes modules describing emissions, advection, turbulent diffusion and dry and wet deposition. Depending on the application specific modules describing, e.g., chemistry can be added to the basic transport model. MATCH is an "off-line" model. This means that atmospheric weather data are taken from some external source, usually a numerical weather prediction (NWP) model, and fed into the model at regular time intervals, currently every three or six hours. Such data are then interpolated in time to yield hourly data. Special attention is given to interpolation of the horizontal wind where vector increments are applied. The vertical wind is calculated internally to assure mass consistency of the atmospheric motion after the time interpolation of the horizontal winds.

The model design is flexible with regard to the horizontal and vertical resolution, principally defined by the input weather data, and allows for an arbitrary number of chemical compounds. The model is written in η (or hybrid) vertical co-ordinates which is a linear combination of pressure and σ vertical co-ordinates. Pressure and σ vertical co-ordinates can be obtained as special cases.

2.1 Advection

Advection is modeled using a Bott-type advection scheme (Bott, 1989), which means that polynomials are fitted to the concentration distribution in order to reduce numerical diffusion. The scheme has been rewritten using integral functions to be applicable in situations with variable grid distances (Robertson et al. (1996)). The scheme is also written in flux form in order to ensure mass conservation (Bott, 1992). For the calculations presented here, fifth order integral functions were used in the horizontal and an upstream scheme in the vertical direction.

2.2 Boundary layer parameterization

In order to maintain a flexible off-line model an optional boundary layer parameterization package has been developed. For the calculations presented here this package has been used. It is, however, also possible to use boundary layer parameters from an NWP model, if available.

Boundary layer processes, such as turbulent vertical mixing in the boundary layer and dry deposition, are parameterized using three primary parameters; the surface friction velocity ($u*$), the surface sensible heat flux (H_0) and the boundary layer height (z_{PBL}). The friction velocity is calculated for neutral stratification in order to avoid unrealistic values of numerical origin for strongly stable and unstable conditions:

$$u_* = \frac{ku(z_1)}{\ln(z_1/z_0)} \qquad (2)$$

where k is von Karmans constant, u is the wind speed, z_0 is the roughness length and z_1 is the height above the surface of the lowest model level.

The sensible heat flux is given by the surface energy balance equation, utilizing different formulations for land and ice covered sea and for open sea. For land and ice covered sea H_0 is defined from similarity theory, using the surface friction velocity, $u*$, and the temperature scale, $\theta*$ (van Ulden and Holtslag, 1985):

$$H_0 = -\rho c_p u_* \theta_* \qquad (3)$$

where c_p is the specific heat of dry air at constant pressure. For open water a formulation suggested by Burridge and Gadd (1977) is used:

$$H_0 = C_H \Delta\theta \qquad (4)$$

where $\Delta\theta = \theta_s - \theta_z$ is the potential temperature difference between the water surface and the first model level (at height $z = z_1$) and C_H is an exchange coefficient defined by

$$C_H = \begin{cases} ku_*/\ln(z_1/z_0)(1+0.1\Delta\theta) & ; \Delta\theta > -10K \\ 0 & ; \Delta\theta \le -10K \end{cases} \qquad (5)$$

The calculation of the boundary layer height for unstable conditions is based on a bulk Richardson number approach (Holtslag et al., 1995), where the boundary layer height is defined as the height where the bulk Richardson number, Ri, reaches a critical value of 0.25. The bulk Richardson number at height z is defined as

$$Ri_z = \frac{gz(\theta_z - \theta_s)}{\theta_1 |v_H|^2} \qquad (6)$$

where

3

$$\theta_s = \theta_1 + 8.5 \frac{H_0}{\rho c_p w_m} \qquad (7a)$$

$$w_m = \left(u_*^3 + 0.6w_*^3\right)^{1/3} \qquad (7b)$$

where θ_1 is the potential temperature at the first model level, v_H is the horizontal wind vector at height z and w_* is the convective velocity scale (Holtslag et al., 1995).

For neutral and stable conditions a formulation proposed by Zilitinkevich and Mironov (1996) for the equilibrium stable boundary layer is used. The formulation accounts for the combined effects of rotation, surface momentum flux and static stability in the free flow and remains applicable in the limits of a rotation-free stable layer and a perfect neutral layer subject to rotation.

The horizontal diffusive fluxes are assumed to be small compared to the advection along the direction of the horizontal wind. Therefore only the vertical turbulent mixing is taken into account. Two different formulations of the vertical turbulent exchange coefficient, K_z, are applied. The exchange coefficient within the boundary layer for neutral and stable conditions follows Holtslag et al. (1995):

$$K_z(z) = \frac{ku_* z}{\Phi_H(z, z_0, L)} (1 - z/z_{PBL})^2 \qquad (8)$$

where Φ_H is the stability function, following Businger et al. (1971), and L is the Monin-Obukhow length. For unstable conditions the convective turn-over time, z_{PBL}/w_*, is used directly to determine K_z:

$$K_z = \frac{\Delta z^2}{\Delta t} (1 - e^{-w_* \Delta t/z_{PBL}}) \qquad (9)$$

where Δz is the layer thickness and Δt is the time step. The convective case is limited by $-z_{PBL}/L \geq 4$ or $w_*/u_* \leq 2.3$ (Holtslag et al., 1995). Above the boundary layer K_z is set to zero. Given the uncertainties in convective fluxes derived from current NWP models, transport by deep convection is not yet included in the standard version of the model. Work is currently in progress to include this process in the future.

2.3 Dry deposition

Dry deposition is modeled using a resistance approach (Chamberlain and Chadwick, 1965), where the component dry deposition flux, F_{di}, is proportional to the concentration of component i and the inverse of the sum of the aerodynamic resistance, r_a, and a species specific surface resistance, r_{di},

$$F_{di} = c_i \cdot \frac{1}{r_a + r_{di}} \qquad (10)$$

For simplicity we use the same aerodynamic resistance for all surfaces in a grid square and only account for variations in the surface resistance. For some components the deposition

Table 2.1. Removal parameters employed in the model. Maximum 1-m dry deposition velocities to different surfaces (cm s^{-1}) and wet scavenging coefficients (s^{-1} mm^{-1} hour)

Component	Dry deposition					Wet deposition
	rural day	rural night	sea	forest day	forest night	scavenging coefficient
NO$_2$	0.4	0.1	0	0.6	0.2	0
SO$_2$	0.8	0.3	0.8	1.3	0.6	6.95e-5
HCHO	0.4	0.1	0.3	0.4	0.1	1.4e-5
CH$_3$CHO	0.6	0.1	0.5	0.6	0.1	3.89e-4
CH$_3$COC$_2$H$_5$	0.4	0.1	0.3	0.4	0.1	1.4e-5
O$_3$	0.8	0.3	0.05	0.8	0.3	0
HNO$_3$	4.0	4.0	4.0	5.0	5.0	3.89e-4
H$_2$O$_2$	0.8	0.8	0.8	0.8	0.8	3.89e-4
SULFATE	0.1	0.1	0.05	0.5	0.5	2.78e-4
CH$_3$OOH	0.6	0.1	0.5	0.6	0.1	3.89e-4
PAN	0.25	0.05	0	0.25	0.05	0
METHYLGLYOXAL	0.4	0.1	0.3	0.4	0.1	0
GLYOXAL	0.4	0.1	0.3	0.4	0.1	1.4e-5
NO$_3$	0.25	0.25	0.1	0.25	0.25	0
N$_2$O$_5$	4.0	4.0	4.0	5.0	5.0	0
ISOPROD	0.4	0.1	0.3	0.4	0.1	0
C$_2$H$_5$OH	0.6	0.1	0.5	0.6	0.1	3.89e-4
NITRATE	0.1	0.1	0.05	0.5	0.5	2.78e-4
C$_2$H$_5$OOH	0.6	0.1	0.5	0.6	0.1	0
CH$_3$OH	0.6	0.1	0.5	0.6	0.1	3.89e-4

velocity is scaled with the solar elevation during daytime. The surface deposition velocities are given in Table 2.1.

The surface characteristics are important in determining the turbulence in the atmospheric surface layer and the surface resistances for different compounds. In this study we have used the land-use information available in the HIRLAM model (Bringfelt, 1996). Currently the dry deposition model differentiates between water surfaces, forested surfaces, low-vegetation land and no-vegetation land. Information about the fraction of each of these surface types is available for each grid square. The forest cover is taken from The Remote Sensing Forest Map of Europe (ESA, 1992). Information about the dominating types of forests and low vegetation is derived from the land-use data set of Henderson-Sellers et al. (1986). The physiographic data available from HIRLAM is given in Table 2.2. Currently the deposition model does not distinguish between different types of forests and low-vegetation. This information is, however, used in the calculation of biogenic emissions of hydrocarbons.

2.4 Wet scavenging

Wet scavenging is assumed to be proportional to the precipitation intensity and a species-specific scavenging coefficient:

$$\frac{dc_i}{dt} = -c_i \Lambda_i P \qquad (11)$$

where c_i is the concentration of species i, Λ_i is the scavenging coefficient given in s^{-1} mm^{-1} hour and P is the precipitation rate in mm hour^{-1}. The scavenging coefficients employed in this study are given in Table 2.1.

Table 2.2. Physiographic data available from HIRLAM.

Main surface type	Subclass
Sea/lake	
Ice (on lakes and oceans)	
No vegetation land	Desert
	Ice cap/glacier
Low vegetation land	Crop
	Short grass
	Tall grass
	Tundra
	Irrigated crop
	Semi-desert
	Bog and marsh
	Evergreen shrub
	Deciduous shrub
Forest	Evergreen needle
	Deciduous needle
	Deciduous broadleaf
	Evergreen broadleaf
	Mixed woodland

2.5 Radiation

Estimates of radiation are needed in the calculation of photolysis rates and in the calculation of biogenic emissions. So far simple models have been used to estimate global radiation and photosynthetically active radiation (PAR), using model calculated total cloud cover from HIRLAM as the main input. The calculation of photolysis rates has been linked to the global radiation and is treated in a simplified manner.

2.5.1 Global radiation and PAR

The global radiation, G, is given by

$$G = G_{ext} \cdot t \cdot g_m \tag{12}$$

where G_{ext} is the extraterrestrial global irradiance (W m^{-2}), t is the total transmittance of the atmosphere, adjusted for cloud effects, and g_m is a factor correcting for multiple reflection between the earth's surface, atmosphere and clouds. G_{ext} is given by

$$G_{ext} = r \cdot I_0 \sin h \tag{13}$$

where I_0 is the solar constant (1370 W m^{-2}) and r accounts for the variation in the solar irradiation due to the variation in distance between the sun and the earth. h is the solar elevation. The total transmittance, t, is related to the total cloud cover, TCC, the cloud transmittance, t_c, and the clear sky atmospheric transmittance, t_a,

$$t = t_a(1 - TCC + TCC \cdot t_c) \tag{14}$$

The total cloud cover, TCC, is taken from HIRLAM. For the present study we have used values of t_c of 0.30 and 0.35 for precipitating and non-precipitating clouds respectively. The clear sky transmittance of the atmosphere over bare ground, t_a, is given by empirical relations based on measurements in Sweden (Josefsson, 1989):

$$t_a = \begin{cases} 0.5 + 0.3 \cdot \sin h^{0.75} & ; \sin h > 0.08 \\ 1 - 6 \cdot \sin h & ; \sin h \le 0.08 \end{cases} \qquad (15)$$

These relations account roughly for the geometric variation in path length with solar elevation and for average effects of aerosols. The multiple reflection factor, g_m, is given by

$$g_m = \frac{1 - \rho_{bg}\rho_{cs}}{1 - \rho_g\rho_s} \qquad (16)$$

where ρ_g is the surface albedo, ρ_{bg}, is the bare ground surface albedo, ρ_{cs} is the clear sky reflectance and ρ_s is the sky reflectance with clouds taken into account. The multiple reflection factor equals one for clear sky and bare ground, which corresponds to the conditions for t_a. The sky reflectance, ρ_s, is finally given by

$$\rho_s = TCC \cdot \rho_c + 0.07 \cdot (1 - TCC) \qquad (17)$$

where ρ_c is the cloud reflectance and the factor 0.07 is the clear sky reflectance. For the present study we have used values of ρ_c of 0.6 and 0.4 for precipitating and non-precipitating clouds respectively. Hourly values of photosyntethically active radiation (PAR) are calculated as half the value of the global radiation using eq. (12) (Blackburn and Proctor, 1983). The information about PAR is then used as input to the calculation of biogenic emissions.

2.5.2 Calculation of photolysis rates

The rates for photolytical reactions in the lower troposphere depends on a number of factors, the most important being the solar elevation, the presence of clouds, the surface albedo and the vertical distribution of gases absorbing at the wave lengths for which the photolytic reaction in question can take place. On-line calculation of the photolysis rates is rather computationally demanding and for the present study a simplified approach has been used. Expressions for the photolysis rates depending on solar elevation derived for clear sky situations were taken from Derwent and Jenkin (1990). To account for the effect of clouds the photolysis rates given by Derwent and Jenkin were scaled by the ratio of the actual global radiation (corrected for clouds) to the clear sky global radiation. This ratio was estimated using a simple analytical expression for the global radiation, based on measurements in Denmark, (Nielsen et al., 1981):

$$G = (A_0(TCC_o) + A_1(TCC_o) \cdot \sin h + A_3(TCC_o) \cdot (\sin h)^3)/A_4(TCC_o) - L_0(TCC_o)$$

(18)

where A_0, A_1, A_3, A_4 and L_0 are empirical parameters, depending on total cloud cover, TCC_o, given in octas. Since the photolysis rates are adjusted every timestep this relationship is used, instead of the relations (12) – (17), for global radiation in order to further reduce the computational requirements. The expressions for the photolysis are calculated for a given ozone column, but we have used them for all levels and independent of the actual ozone column.

2.6   Emissions and boundary conditions

The basic version of the MATCH transport model includes modules for inclusion of area emissions of the simulated species. Emissions can be introduced at any height in the model and at different heights simultaneously. Emissions are initially distributed in the vertical based on a Gaussian plume formulation (Berkowicz et al., 1986), evaluated at a downwind distance of x=u_h Δt, where u_h is the wind speed at the effective plume height. If desired, standard plume-rise calculations can be performed (Berkowicz et al., 1986), based on stack parameters (stack diameter, effluent temperature and volume flux) that are given as input to the model. It is also possible to specify temporal variations in the emissions over the diurnal time scale as well as variations between days. The emissions that enter the model calculations are updated every hour to account for temporal variations and the influence of the stability on the plume rise and initial vertical spread calculations.

2.6.1   Anthropogenic emissions

Anthropogenic emissions for the simulations presented below were derived from the 50x50 km emission data provided by EMEP MSC-W at the Norwegian Meteorological Institute. The EMEP emission data are divided into emissions below and above 100m. The emissions for 1994 for NO_x, SO_2, nonmethane hydrocarbons (NMHC) and CO were used in the model calculations. Simple variations of the emissions with the time of day and with the day of the week were used. The annual emission fields interpolated to the model grid are shown in Figure 2.1. The total emissions are given in Table 2.3.

Table 2.3.   Annual European emissions used in the model calculations. Anthropogenic emissions are for 1994 from the EMEP database. Biogenic emissions have been calculated on-line in the model (see text). Units: ktonnes as SO_2, NO_2, CO, NMVOC and C_5H_8-C.

| Component | Annual emission ktonnes | | |
	Low	High	Total
SO_2	12982	18410	31392
NO_x	13169	8194	21363
NMVOC	18723	1534	20257
CO	75110	1186	76296
C_5H_8	4000	-	4000
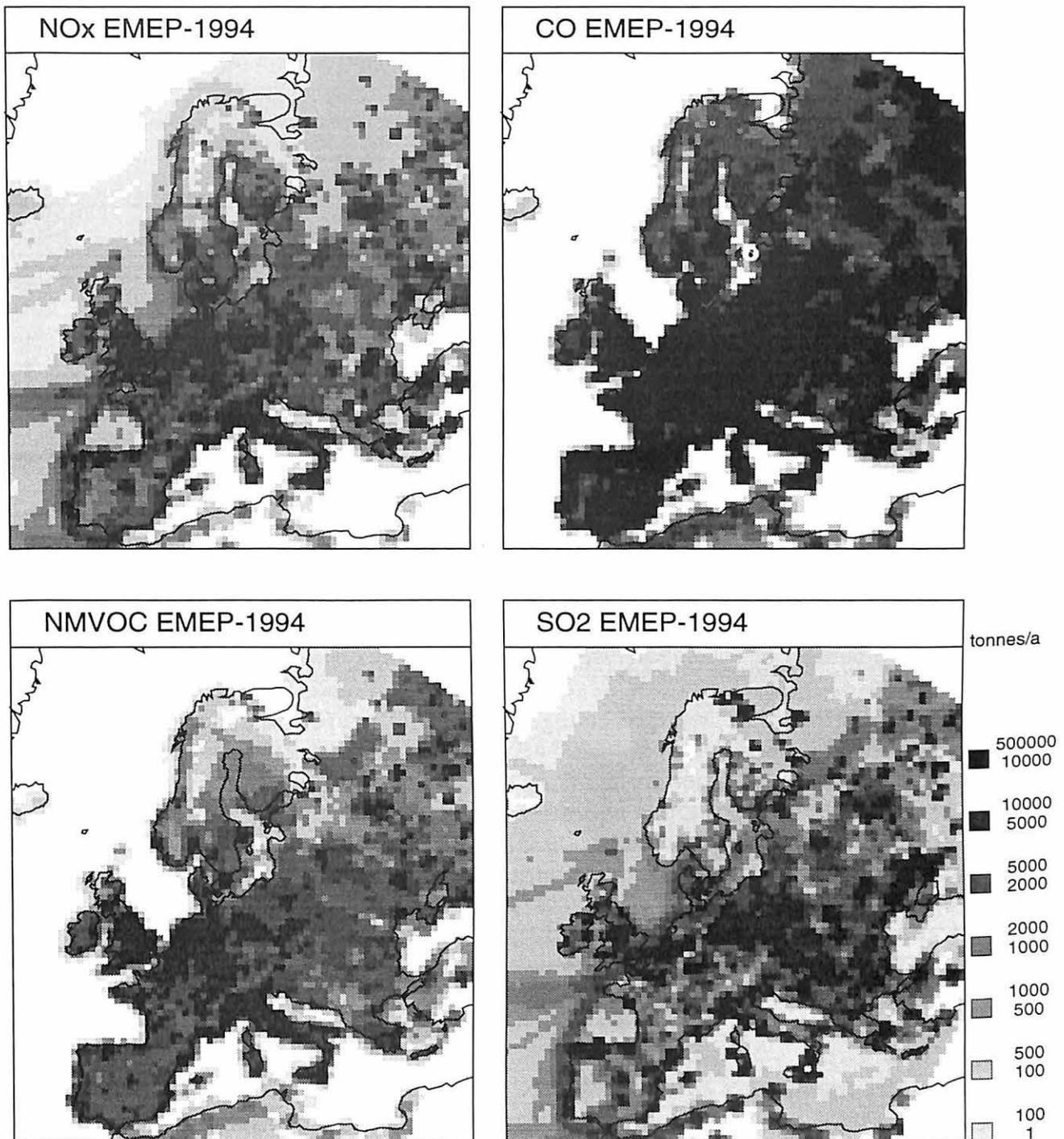
Figure 2.1   Annual gridded emissions of SO_2, NO_x, NMHC and CO used in the model
calculations. Units: tonnes/year of SO_2, NO_2, NMHC and CO.

Uncertainties for these emission data are difficult to estimate. Comparisons between the
EMEP and CORINAIR emission estimates for 1990 as well as information about reported
national emissions are discussed in Berge et al. (1995). Based on this the uncertainty in annual
total emissions is likely to be around ±20%. For individual gridpoints the uncertainties are
considerably larger.

The emission of anthropogenic hydrocarbons was split on the components used in the
chemical scheme using data from the UK (Derwent and Jenkin, 1991). The resulting split is
given in Table 2.4.

9

Table 2.4. Model split of hydrocarbon emissions

Component	Mass%
C_2H_4	3.6
C_2H_6	6.7
C_3H_6	3.8
n-C_4H_{10}	37.1
o-XYLENE	24.5
CH_3OH	1.0
C_2H_5OH	14.0
HCHO	0.9
CH_3CHO	0.1
$CH_3COC_2H_5$	3.3
unreactive	4.9

2.6.2 *Biogenic emissions*

Biogenic emissions of isoprene (C_5H_8) were estimated using the E-94 isoprene emission methodology proposed by Simpson et al. (1995). The emission rate, *ER*, is given as,

$$ER = \sum_{j=1}^{m} \left[A_j \cdot AEF_j \cdot ECF \left(PAR, T \right) \right]$$ (12)

where m is the number of vegetation categories, A_j is the area of vegetation category j, AEF_j is the area-based emission factor for vegetation category j and *ECF(PAR,T)* is a unitless environmental correction factor representing the effects of temperature and solar radiation on emissions. Following Simpson et al. (1995) five vegetation categories are used: Oak, Other broadleaf, Spruce, Other coniferous and Crop. The distribution of these five categories over Europe is derived by combining the information about coverage of forest and low-vegetation land from HIRLAM and the information on a national basis given by Simpson et al. (1995). The emission calculation was included in the model using the two-meter temperature available from HIRLAM and *PAR* calculated as described in section 2.5. The emissions were updated hourly based on current values of *T* and *PAR*. The resulting emission for the six-month period is shown in Figure 2.2. The estimated isoprene emission for the period April-September 1994 was 4000 kt C a^{-1}, which is almost identical to the value given for 1989 by Simpson et al. (1995) (3966 kt C a^{-1}, for a slightly different area).

2.6.3 *Initial and boundary concentrations*

For some components in the chemical mechanism it is necessary to specify mixing ratios on the boundaries. In the present study the boundary conditions were treated in a rather simplified way. For each boundary (the four sides and the top of the model domain) a concentration (c_{north}, c_{east}, c_{south}, c_{west} and c_{top}) was assigned for each of the components. c_{top} represents the concentration at the top *surface* boundary, while the four lateral boundary concentrations represent the ground level concentrations at the *midpoints* of the four sides. Linear interpolation is used to get the boundary values between these points.

The boundary concentrations were as far as possible based on measurements of the various components at sites which were considered representative for the model boundaries. For peroxyacetyl nitrate (PAN) results from a large-scale simulation (Moxim et al., 1996) were used to estimate reasonable boundary values. Due to lack of observational data for many of the components the boundary values are in many cases fairly crude estimates. The situation is
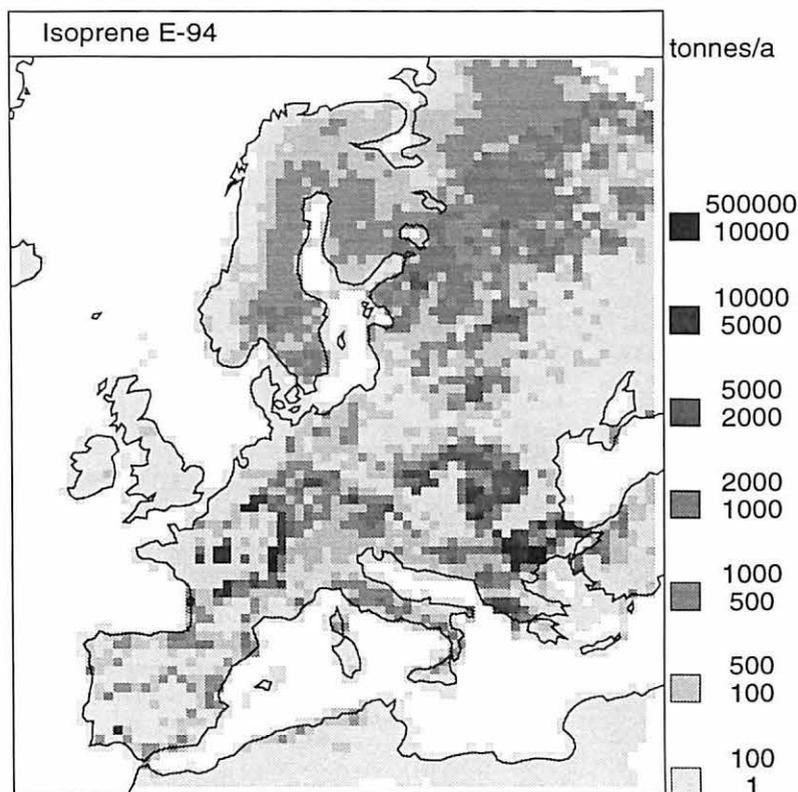
Figure 2.2   Annual emissions of C_5H_8 used in the model calculations. Units: tonnes C/year.

especially uncertain for the eastern and southern boundaries, where suitable measurements are scarce. This is also true for the top boundary.

Different boundary values were used for different months for some components, due to seasonal variability in the background concentration. The boundary conditions used in these runs are given in Table 2.5. For further studies it will be necessary to estimate the sensitivity of the results to variations in the boundary concentrations.

The initial concentrations for the entire model domain (at April 1) were set equal to the minimum of the c_{top} and c_{west} boundary values.

2.7   Chemistry

The gas-phase chemical mechanism used is mainly based on the EMEP MSC-W model chemistry (Simpson et al., 1993). The main difference is that for the isoprene chemistry an adapted version of the so-called Carter 1-product mechanism (Carter, 1996) has been used instead of the EMEP mechanism. The behavior of three different isoprene chemistry models has been investigated in detail by Pleijel, in this study, and the comparison is presented in Appendix A.

A key feature of the chemical scheme is that a simplified mixture of a dozen *representative compounds* is used to model the many different organic molecules emitted to the atmosphere. The model compounds are chosen to span the normal range of ozone creation potentials for the most important organic pollutants (Pleijel et al., 1996).

The chemical model includes ca. 130 thermal and photochemical reactions between 58 chemical components and it is designed to provide a good description of the chemistry for both high and low NO_x conditions. The details of the reaction scheme are given in Appendix B. In order to simulate ozone concentrations, the error connected to the use of a more simplified chemical model, as the EMEP model, is comparatively small (Pleijel et al., 1996; Andersson-Sköld and Simpson, 1997).

11

Table 2.5. Boundary concentrations used in the model

Component	month	C_{top}	C_{west}	C_{east}	C_{south}	C_{north}
O_3	Apr	6.4e-8	4.3e-8	4.e-8	3.6e-8	4.1e-8
	May	6.4e-8	4.1e-8	4.e-8	3.6e-8	2.7e-8
	Jun	6.4e-8	3.5e-8	4.e-8	3.6e-8	3.0e-8
	Jul	6.2e-8	3.1e-8	4.e-8	3.6e-8	2.5e-8
	Aug	6.2e-8	3.1e-8	4.e-8	3.6e-8	2.8e-8
	Sep	6.2e-8	3.4e-8	4.e-8	3.6e-8	3.1e-8
$^{\times}$NO		1e-11	1e-11	1e-11	1e-11	1e-11
$\vee$NO$_2$		3.e-11	3.e-10	1.e-9	3.e-10	1.e-10
HNO$_3$		5.e-11	5.e-11	1.e-10	5.e-11	5.e-11
NITRATE		5.e-11	2.e-10	2.e-10	2.e-10	5.e-11
H$_2$O$_2$		2.8e-10	1.e-10	5.e-10	5.e-10	1.e-12
$\searrow$H$_2$		5.e-7	5.e-7	5.e-7	5.e-7	5.e-7
$\times$SO$_2$	Apr	4.e-11	1.2e-10	3.e-10	1.2e-10	1.2e-10
	May-Sep	4.e-11	4.e-11	3.e-10	4.e-11	4.e-11
SULFATE	Apr	2.6e-11	1.5e-10	4.e-10	3.e-10	1.8e-10
	May	2.6e-11	1.5e-10	4.e-10	3.e-10	9.e-11
	Jun	2.6e-11	1.5e-10	4.e-10	3.e-10	7.e-11
	Jul-Sep	2.6e-11	1.5e-10	4.e-10	3.e-10	3.e-11
$\searrow$CO		1.e-7	1.e-7	1.e-7	1.e-7	1.e-7
$\rightarrow$CH$_4$		1.5e-6	1.5e-6	1.5e-6	1.5e-6	1.5e-6
$\vee$C$_2$H$_4$	Apr	3.4e-10	3.4e-10	2.8e-10	5.e-11	3.4e-10
	May	3.3e-10	1.9e-10	2.e-10	5.e-11	3.3e-10
	Jun	2.7e-10	1.8e-10	2.e-10	5.e-11	2.7e-10
	Jul	2.3e-10	1.8e-10	2.e-10	5.e-11	2.3e-10
	Aug	2.8e-10	1.7e-10	2.e-10	5.e-11	2.8e-10
	Sep	3.2e-10	2.e-10	2.e-10	5.e-11	3.2e-10
$\searrow$ C$_2$H$_6$	Apr	3.4e-9	3.6e-9	2.9e-9	1.7e-9	3.4e-9
	May	2.4e-9	3.1e-9	2.0e-9	1.7e-9	2.4e-9
	Jun	1.9e-9	2.2e-9	2.e-9	1.4e-9	1.9e-9
	Jul	1.6e-9	1.3e-9	2.e-9	1.e-9	1.6e-9
	Aug	1.5e-9	1.6e-9	2.e-9	1.e-9	1.5e-9
	Sep	1.8e-9	1.9e-9	2.e-9	1.e-9	1.8e-9
$\times$ C$_3$H$_6$		5.e-11	5.e-11	5.e-11	1.6e-11	5.e-11
$\searrow$n-C$_4$H$_{10}$	Apr	1.4e-9	1.1e-9	1.e-9	2.5e-10	1.4e-9
	May	4.2e-10	4.6e-10	1.e-9	1.6e-10	4.2e-10
	Jun	2.e-10	2.9e-10	1.e-9	1.3e-10	2.e-10
	Jul	2.e-10	1.2e-10	1.e-9	1.e-10	2.e-10
	Aug	1.6e-10	1.9e-10	1.e-9	1.e-10	1.6e-10
	Sep	3.2e-10	3.5e-10	1.e-9	5.e-11	3.2e-10
o-XYLENE	Apr	4.e-10	4.e-10	2.e-10	4.e-11	4.e-10
	May	2.4e-10	1.2e-10	2.e-10	4.e-11	2.4e-10
	Jun	1.4e-10	7.5e-11	2.e-10	4.e-11	1.4e-10
	Jul	1.4e-10	3.1e-11	2.e-10	4.e-11	1.4e-10
	Aug	1.5e-10	6.6e-11	2.e-10	4.e-11	1.5e-10
	Sep	1.8e-10	7.9e-11	2.e-10	4.e-11	1.8e-10
$\times$ C$_5$H$_8$		5.e-18	1.e-11	1.5e-10	3.e-11	1.e-11
$\searrow$CH$_3$OH		5.e-11	5.e-11	7.e-11	8.e-12	5.e-11
χC$_2$H$_5$OH		4.e-10	4.e-10	6.e-10	7.e-11	4.e-10
$\searrow$CH$_3$OOH		7.5e-11	1.e-10	1.e-10	1.e-10	1.e-12
$\times$ C$_2$H$_5$OOH		1.e-12	1.e-12	1.e-12	1.e-12	1.e-12
$\swarrow$HCHO		4.3e-11	4.9e-10	7.5e-10	2.4e-10	2.4e-10
$\curlyvee$CH$_3$CHO		1.4e-10	2.0e-10	3.2e-10	1.4e-10	1.4e-10
$\searrow$CH$_3$COC$_2$H$_5$		2.5e-11	2.5e-11	5.e-11	2.5e-11	2.5e-11
$\searrow$GLYOXAL		5.e-18	6.e-12	1.3e-11	4.e-12	4.e-12
$\times$METHYL-GLYOXAL		5.e-18	2.e-12	1.5e-11	2.e-12	2.e-12
$\curlyvee$PAN	Apr	3.e-10	3.e-10	3.e-10	6.e-11	3.e-10
	May	3.e-10	2.e-10	3.e-10	6.e-11	2.e-10
	Jun	2.0e-10	1.e-10	2.e-10	5.0e-11	1.e-10
	Jul	1.5e-10	5.e-11	2.e-10	3.e-11	3.e-11
	Aug	1.5e-10	8.e-11	2.e-10	3.e-11	7.e-11
	Sep	1.5e-10	1.e-10	3.e-10	3.e-11	1.e-10

Standard numerical integration techniques following the work by Verver et al. (1996) are used to integrate the chemical mechanism. This leads to stable integrations, where the accuracy of the calculations can be controlled. We have used the Kinetics Pre-Processor

(KPP) developed at the University of Iowa. The use of a standard solver coupled with KPP makes it easy to change the chemical mechanism without having to recode the solver.

Table 2.6. Meteorological fields available from HIRLAM.

Field	Note
Temperature	16 model levels
Specific humidity	"
Horizontal wind components	"
Mean sea level pressure	
Surface pressure	
Two meter temperature	
Surface temperature	
Large scale precipitation	Accumulated for three- and six-hour forecasts
Convective precipitation	"
Sensible heat flux	
Latent heat flux	
Ice concentration	
Albedo	
Total cloud cover	
Snow depth	

2.8   Meteorological data

Meteorological data were taken from archived output of the operational HIRLAM model at SMHI. A selection of fields for a sub-area of the operational grid was archived specially for the purpose of dispersion modeling. The fields available are listed in Table 2.6. Initialized analysis, three- and six-hour forecasts for every six hours were archived. Precipitation and cloud cover were taken from the six-hour forecast while the three-hour forecast was used to get wind fields with three-hourly resolution. The horizontal resolution was approximately 55 km on a rotated latitude longitude grid. The vertical resolution was 16 levels. The approximate height and thickness of the ten lowest model layers are given in Table 2.7.

The wind field at all 16 levels was used together with the tendency of the surface pressure to achieve a balanced wind field as described in Robertson et al. (1996). In the transport calculation however, only nine levels were used in order to reduce computing and storage requirements.

Table 2.7. Approximate height of model levels and thickness of corresponding model layers for HIRLAM as used in the model calculations. Only the ten lowest levels are shown for brevity. Units: m.

Level/Layer	height (m)	thickness (m)
1	35	70
2	155	170
3	395	310
4	790	480
5	1360	660
6	2105	830
7	3015	990
8	4080	1140
9	5295	1290
10	6590	1300

13

3.   *Evaluation*

In this section we will present comparisons between the model calculations and observations of air- and precipitation-chemistry and an attempt to evaluate the model performance. Before going into the details some general comments regarding evaluation of large-scale atmospheric transport/chemistry/deposition models are appropriate.

The model calculations are subject to a number of uncertainties. Some important factors that must be considered when interpreting comparisons between the present model calculations and observations are:

- Emission data, temporal variation, biogenic emissions
- Representativity and siting of stations (e.g. coastal, mountains and valleys)
- Model resolution (horizontal and vertical)
- Model formulation of physical and chemical processes

Errors in the emission data are important sources of uncertainty. Estimates of the uncertainties pertaining to annual anthropogenic emissions were given in Section 2.6. For these emissions day-to-day and diurnal variations were applied. The same time variations were applied for the whole model domain. This could lead to large errors in the estimated emissions on short time-scales (hours to days) and consequently to large errors in the calculated concentrations averaged over these time-scales. This is especially true for primary (emitted) components.

For naturally emitted components the uncertainties in the emissions are large, both for annual averages and for shorter time-scales. For anthropogenic hydrocarbon emissions another potential source of error is the fact that we have assumed the same division of the total emission on the model hydrocarbons over the whole model area, while the ideal split is likely to vary with location (c.f. Section 2.6).

A major problem when comparing model calculations with point measurements is the representativity of the observations. The model calculation represents an average both in the horizontal and vertical direction. In our case the horizontal grid distance is ~55 km and the model calculated values therefore represent horizontal averages over an area 55x55 km. Difficulties with the representativity are worst in areas with abrupt transitions in, e.g., emission density, physiography and topography. Typical cases, where one can expect problems with representativity, are coastal sites, mountain peaks and valleys.

The thickness of the lowest model layer is about 70 m. Model calculated surface concentrations therefore represent averages over this depth. For components subject to dry deposition, we have used similarity theory for the atmospheric surface layer to adjust the model calculated concentrations to a level of 1 m above ground, which corresponds better to the actual height where observations are made. However, this adjustment accounts only for the effect of dry deposition. Other effects, such as strong vertical gradients resulting from surface emissions, are not resolved. Such effects can be important, especially for primary components and under stably stratified conditions.

Other uncertainties are related to the model formulation and input meteorological data, in particular the precipitation fields. Here we will just use the uncertainties discussed above as a background when comparing the model calculations and observations. A more detailed sensitivity analysis will be the subject of future work.

3.1 Observations

Most observations used in the model evaluation are taken from work within the EMEP-programme (Co-operative Programme for Monitoring and Evaluation of the Long-range Transmission of Air Pollutants in Europe). Figure 3.1 shows a map with the sampling locations and station codes used by EMEP. Table 3.1 provides further details for each station, including station height and the corresponding height used in the model. The observations from EMEP represent only surface measurements. We have not been able to get access to any height-resolved observations for the time period simulated. The main focus of this section will be on ozone but we will start by looking at observations of other components that are available.

Figure 3.1   Sampling locations for chemical measurements and corresponding EMEP station codes.

Table 3.1. Measurement stations (HC = hydrocarbons, totNO$_3$= total nitrate =HNO$_3$+NO$_3^-$)

CODE	STATION NAME	LAT	LON	ALT. (m)	MODEL ALT. (m)	MEASURED COMPONENTS in gas phase	in precipitation
AT02	Illmitz	47.77	16.77	117	176	O$_3$	NO$_3$, SO$_4$
AT03	Achenkirch	47.55	11.72	960	1034	O$_3$	NO$_3$, SO$_4$
AT04	St. Koloman	47.65	13.20	851	1085	O$_3$	NO$_3$, SO$_4$
CH01	Jungfraujoch	46.55	7.98	3573	1349	NO$_2$, SO$_2$, SO$_4$	
CH02	Payerne	46.82	6.95	500	1549	O$_3$, NO$_2$, SO$_2$, SO$_4$	NO$_3$, SO$_4$
CH03	Taenikon	47.48	8.90	540	809	O$_3$, NO$_2$, SO$_2$, SO$_4$, HC	
CH04	Chaumont	47.05	6.97	1130	645	O$_3$, NO$_2$, SO$_2$, SO$_4$	
CH05	Rigi	47.07	8.45	1028	719	O$_3$, NO$_2$, SO$_2$, SO$_4$	
CH31	Sion	46.22	7.33	480	692	O$_3$	
CS01	Svratouch	49.73	16.03	737	493	O$_3$, NO$_2$, NO$_3$, HNO$_3$, SO$_2$, SO$_4$	NO$_3$, SO$_4$
CS03	Kosetice	49.58	15.08	633	514	O$_3$, NO$_2$, NO$_3$, HNO$_3$, SO$_2$, SO$_4$, HC, Carbonyls	NO$_3$, SO$_4$
DE01	Westerland	54.92	8.30	12	5	O$_3$, NO$_2$, SO$_2$, SO$_4$	NO$_3$, SO$_4$
DE02	Waldhof	52.80	10.75	74	70	O$_3$, NO$_2$, SO$_2$, SO$_4$, HC, Carbonyls	NO$_3$, SO$_4$
DE03	Schauinsland	47.90	7.90	1205	520	O$_3$, NO$_2$, SO$_2$, SO$_4$	NO$_3$, SO$_4$
DE04	Deuselbach	49.75	7.05	480	354	O$_3$, NO$_2$, SO$_2$, SO$_4$	NO$_3$, SO$_4$
DE05	Brotjacklriedel	48.82	13.22	1016	526	O$_3$, NO$_2$, SO$_2$, SO$_4$	NO$_3$, SO$_4$
DE07	Neuglobsow	53.17	13.03	65	62	O$_3$, NO$_2$, SO$_2$, SO$_4$	NO$_3$, SO$_4$
DE08	Schmucke	50.65	10.77	937	393	O$_3$, NO$_2$, SO$_2$, SO$_4$	NO$_3$, SO$_4$
DE09	Zingst	54.43	12.73	1	8	O$_3$, NO$_2$, SO$_2$, SO$_4$	NO$_3$, SO$_4$
DE11	Hohenwestedt	54.10	9.67	75	15	O$_3$	
DE12	Bassum	52.85	8.70	52	24	O$_3$, SO$_4$	
DE14	Meinerzhagen	51.12	7.63	510	234	SO$_4$	
DE17	Ansbach	49.30	10.57	481	400	O$_3$, SO$_4$	
DE18	Rottenburg	48.48	8.93	427	443	SO$_4$	
DE19	Starnberg	48.02	11.35	729	600	SO$_4$	
DE26	Uckermunde	53.75	14.07	1	12	O$_3$	
DE31	Wiesenburg	52.12	12.47	107	70	O$_3$	
DE35	Luckendorf	50.83	14.77	490	361	O$_3$	
DK03	Tange	56.35	9.60	13	42	TotNO$_3$, SO$_2$, SO$_4$	NO$_3$, SO$_4$
DK05	Keldsnor	54.73	10.73	9	0	TotNO$_3$, SO$_2$, SO$_4$	NO$_3$, SO$_4$
DK08	Anholt	56.72	11.52	40	0	NO2, TotNO$_3$, SO$_2$, SO$_4$	
DK31	Ulborg	56.28	8.43	10	17	O$_3$	
DK32	Frederiksborg	55.97	12.33	10	14	O$_3$, TotNO$_3$, SO$_2$, SO$_4$	
ES01	Toledo	39.55	-4.35	917	694	O$_3$, NO$_2$, TotNO$_3$, SO$_2$, SO$_4$	NO$_3$, SO$_4$
ES02	La Cartuja	37.20	-3.60	720	910	O$_3$, NO$_2$, TotNO$_3$, SO$_2$, SO$_4$	NO$_3$, SO$_4$
ES03	Roquetas	40.82	-0.50	50	878	O$_3$, NO$_2$, TotNO$_3$, SO$_2$, SO$_4$	NO$_3$, SO$_4$
ES04	Logrono	42.45	-2.35	370	753	O$_3$, NO$_2$, TotNO$_3$, SO$_2$, SO$_4$	NO$_3$, SO$_4$
ES05	Noia	42.73	-8.92	685	280	O$_3$, NO$_2$, TotNO$_3$, SO$_2$, SO$_4$	NO$_3$, SO$_4$
FI04	Ähtäri	62.53	24.22	160	33	O$_3$, NO$_2$, TotNO$_3$, SO$_2$, SO$_4$	NO$_3$, SO$_4$
FI09	Utö	59.77	21.37	7	0	O$_3$, NO$_2$, TotNO$_3$, SO$_2$, SO$_4$	NO$_3$, SO$_4$
FI17	Virolahti	60.52	27.68	8	14	O$_3$, NO$_2$, TotNO$_3$, SO$_2$, SO$_4$	NO$_3$, SO$_4$
FI22	Oulanka	66.32	29.40	310	269	O$_3$, NO$_2$, TotNO$_3$, SO$_2$, SO$_4$	NO$_3$, SO$_4$
FR03	La Crouzille	45.83	1.27	497	303	SO$_2$, SO$_4$	NO$_3$, SO$_4$
FR05	La Hague	49.62	-1.83	133	43	SO$_2$, SO$_4$	NO$_3$, SO$_4$
FR08	Donon	48.50	7.13	775	368	SO$_2$, SO$_4$, Carbonyls	NO$_3$, SO$_4$
FR09	Revin	49.90	4.63	390	219	SO$_2$, SO$_4$	NO$_3$, SO$_4$
FR10	Morvan	47.27	4.08	620	296	SO$_2$, SO$_4$	NO$_3$, SO$_4$
FR11	Bonnevaux	46.82	6.18	836	545	SO$_2$, SO$_4$	NO$_3$, SO$_4$
FR12	Iraty	43.03	-1.08	1300	960	SO$_2$, SO$_4$	NO$_3$, SO$_4$
GB02	Eskdalemuir	55.30	-3.20	269	201	O$_3$, TotNO$_3$, SO$_4$	
GB04	Stoke Ferry	52.57	0.50	15	78	SO$_4$	
GB06	Lough Navar	54.43	-7.87	130	122	O$_3$, SO$_4$	NO$_3$, SO$_4$
GB07	Barcombe Mills	50.87	-0.03	8	76	SO$_4$	
GB13	Yarner Wood	50.58	-3.70	119	147	O$_3$, SO$_4$	NO$_3$, SO$_4$
GB14	High Muffles	54.33	-0.80	267	85	O$_3$, TotNO$_3$, SO$_4$	NO$_3$, SO$_4$
GB15	Strath Vaich	57.73	-4.77	270	224	O$_3$, SO$_4$	NO$_3$, SO$_4$
GB16	Glen Dye	56.97	-2.42	85	192	SO$_4$	
GB31	Aston Hill	52.50	-3.03	370	177	O$_3$	
GB32	Bottesford	52.92	-0.80	32	113	O$_3$	
GB33	Bush	55.85	-3.20	180	172	O$_3$	
GB34	Glazebury	53.45	-2.47	21	125	O$_3$	
GB35	Great Dun Fell	54.68	-2.43	847	253	O$_3$	
GB36	Harwell	51.57	-1.32	137	120	O$_3$, Carbonyls	
GB37	Ladybower Res.	53.38	-1.75	420	195	O$_3$	
GB38	Lullington Hth	50.78	0.17	120	76	O$_3$	
GB39	Sibton	52.28	1.47	46	33	O$_3$	
GB41	Wharley Croft	54.60	-2.47	206	253	O$_3$	
GBWB	Weybourne	52.96	1.13	15	39	HC	

GR01	Aliartos	38.37	23.08	110	316	NO₂, SO₂, SO₄	
GR01	Aliartos	38.37	23.08	110	316	NO_2, SO_2, SO_4	
HR02	Puntijarka	45.90	15.97	988	242	NO_2	NO_3, SO_4
HR04	Zavizan	44.82	14.98	1594	442	NO_2	NO_3, SO_4
HU02	K-puszta	46.97	19.58	125	116	NO_2, NO_3, HNO_3, SO_2, SO_4	NO_3, SO_4
IE01	Valentina Obs.	51.93	-10.25	9	145	NO_2, SO_2, SO_4	NO_3, SO_4
IE02	Turlough Hill	53.03	-6.40	420	127	SO_2, SO_4	NO_3, SO_4
IE31	Mace Head	53.17	-9.50	15	86	O_3, Carbonyls	
IT01	Montelibretti	42.10	12.63	48	198	NO_3, HNO_3, SO_2, SO_4, Carbonyls	NO_3, SO_4
IT04	Ispra	45.80	8.63	209	689	O_3, NO_2, NO_3, HNO_3, SO_2, SO_4, Carbonyls	NO_3, SO_4
LT15	Preila	55.35	21.07	5	17	O_3, NO_2, NO_3, SO_2, SO_4	NO_3, SO_4
LV10	Rucava	56.22	21.22	5	0	O_3, NO_2, NO_3, $TotNO_3$, SO_2, SO_4, Carbonyls	NO_3, SO_4
LV16	Zoseni	57.13	25.92	183	115	NO_2, NO_3, SO_2, SO_4	
NL02	Witteveen	52.81	6.67	17	0	O_3	
NL09	Kollumerwaard	53.33	6.28	0	0	O_3, NO_2, NO_3, SO_2, SO_4, HC, PAN	NO_3, SO_4
NL10	Vreedepeel	51.54	5.85	28	48	O_3, NO_2, NO_3, SO_2, SO_4	
NO01	Birkenes	58.38	8.25	190	138	O_3, NO_2, $TotNO_3$, SO_2, SO_4, HC, Carbonyls	NO_3, SO_4
NO08	Skreaadalen	58.82	6.72	475	504	NO_2, $TotNO_3$, SO_2, SO_4	NO_3, SO_4
NO15	Tustervatn	65.83	13.92	439	501	O_3, NO_2, $TotNO_3$, SO_2, SO_4	NO_3, SO_4
NO30	Jergul	69.45	24.60	255	362	O_3, NO_2, $TotNO_3$, SO_2, SO_4	NO_3, SO_4
NO39	Kaarvatn	62.78	8.88	210	890	O_3, NO_2, $TotNO_3$, SO_2, SO_4	NO_3, SO_4
NO41	Osen	61.25	11.78	440	605	O_3, NO_2, $TotNO_3$, SO_2, SO_4	NO_3, SO_4
NO43	Prestebakke	59.00	11.53	160	120	O_3, NO_2, NO_3, HNO_3, SO_2, SO_4	NO_3, SO_4
NO44	Nordmoen	60.27	11.10	200	266	O_3, NO_2, NO_3, HNO_3, SO_2, SO_4	NO_3, SO_4
NO45	Jeloeya	59.43	10.60	3	85	O_3	
NO47	Svanvik	69.45	30.03	30	166	O_3	
NO48	Voss	60.60	6.53	500	517	O_3	
NO51	Sogne	58.08	7.85	15	138	O_3	
PL02	Jarczew	51.32	21.98	180	180	NO_2, NO_3, $TotNO_3$, SO_2, SO_4	NO_3, SO_4
PL03	Sniezka	50.73	15.73	1604	447	NO_2, NO_3, $TotNO_3$, SO_2, SO_4	NO_3, SO_4
PL04	Leba	54.75	17.53	2	30	NO_2, NO_3, $TotNO_3$, SO_2, SO_4	NO_3, SO_4
PL05	Diabla Gora	54.15	22.07	157	130	NO_2, $TotNO_3$, SO_2, SO_4	NO_3, SO_4
PT01	Braganca	41.82	-6.77	691	895		NO_3, SO_4
PT03	V. d. Castelo	41.70	-8.80	16	140		NO_3, SO_4
PT04	Monte Velho	38.08	-8.80	43	78	O_3, SO_2, SO_4	NO_3, SO_4
RU01	Janiskoski	68.93	28.85	118	159	NO_2, NO_3, SO_2, SO_4	NO_3, SO_4
RU13	Pinega	64.70	43.40	28	92	NO_2, NO_3, SO_2, SO_4	NO_3, SO_4
RU14	Pushinskie Gory	57.00	28.90	103	110	NO_2, NO_3, SO_2, SO_4	NO_3, SO_4
SE02	Rörvik	57.42	11.92	10	37	O_3, NO_2, $TotNO_3$, SO_2, SO_4, HC	NO_3, SO_4
SE05	Bredkälen	63.85	15.33	404	380	NO_2, $TotNO_3$, SO_2, SO_4	NO_3, SO_4
SE08	Hoburg	56.92	18.15	58	0	NO_2, $TotNO_3$, SO_2, SO_4	
SE11	Vavihill	56.02	13.15	175	48	O_3, NO_2, $TotNO_3$, SO_2, SO_4	NO_3, SO_4
SE12	Aspvreten	58.80	17.38	20	0	O_3, NO_2, $TotNO_3$, SO_2, SO_4	NO_3, SO_4
SE13	Esrange	67.88	21.07	475	426	O_3, NO_2, SO_2, SO_4	
SE32	Norra-Kvill	57.82	15.57	261	115	O_3	
SE35	Vindeln	64.25	19.77	225	233	O_3	
SI31	Zarodnje	46.43	15.00	770	680	O_3	
SI32	Krvavec	46.30	14.54	1740	680	O_3	
SI33	Kovk	46.13	15.11	600	493	O_3	
SK02	Chopok	48.93	19.58	2008	796	NO_2, NO_3, HNO_3, SO_2, SO_4	NO_3, SO_4
SK04	Stara Lesna	49.15	20.28	808	907	O_3, NO_2, NO_3, HNO_3, SO_2, SO_4	NO_3, SO_4
SK05	Liesek	49.37	19.68	892	940	NO_2, NO_3, HNO_3, SO_2, SO_4	NO_3, SO_4
SK06	Starina	49.05	22.27	345	434	O_3, NO_2, NO_3, HNO_3, SO_2, SO_4	NO_3, SO_4
TR01	Cubuk II	40.50	33.00	1169	1316	O_3, NO_2, NO_3, HNO_3, $TotNO_3$, SO_2, SO_4	NO_3, SO_4
YU05	Kamenichi vis	43.40	21.95	813	617	NO_2, SO_2	NO_3, SO_4
YU08	Zabljak	43.15	19.13	1450	1268	NO_2, SO_2	NO_3, SO_4

3.2 Concentrations of primary components

Figure 3.2 to 3.4 show average calculated concentrations of NO, NO_2, SO_2, CO, C_2H_4 (ethene), C_2H_6 (ethane), C_3H_6 (propene), n-C_4H_{10} (n-butane), 1,2-Dimethylbenzene (o-xylene), C_2H_5OH (ethanol) and C_5H_8 (isoprene) for the simulated six month period.

The components with mainly anthropogenic sources show rather similar distributions, with highest concentrations in the vicinity of densely populated and industrialized areas. There are some striking differences, though, related to variations in emission distribution and atmospheric life times. Large sources of sulfur on the Kola Peninsula show up in the SO_2 distribution.
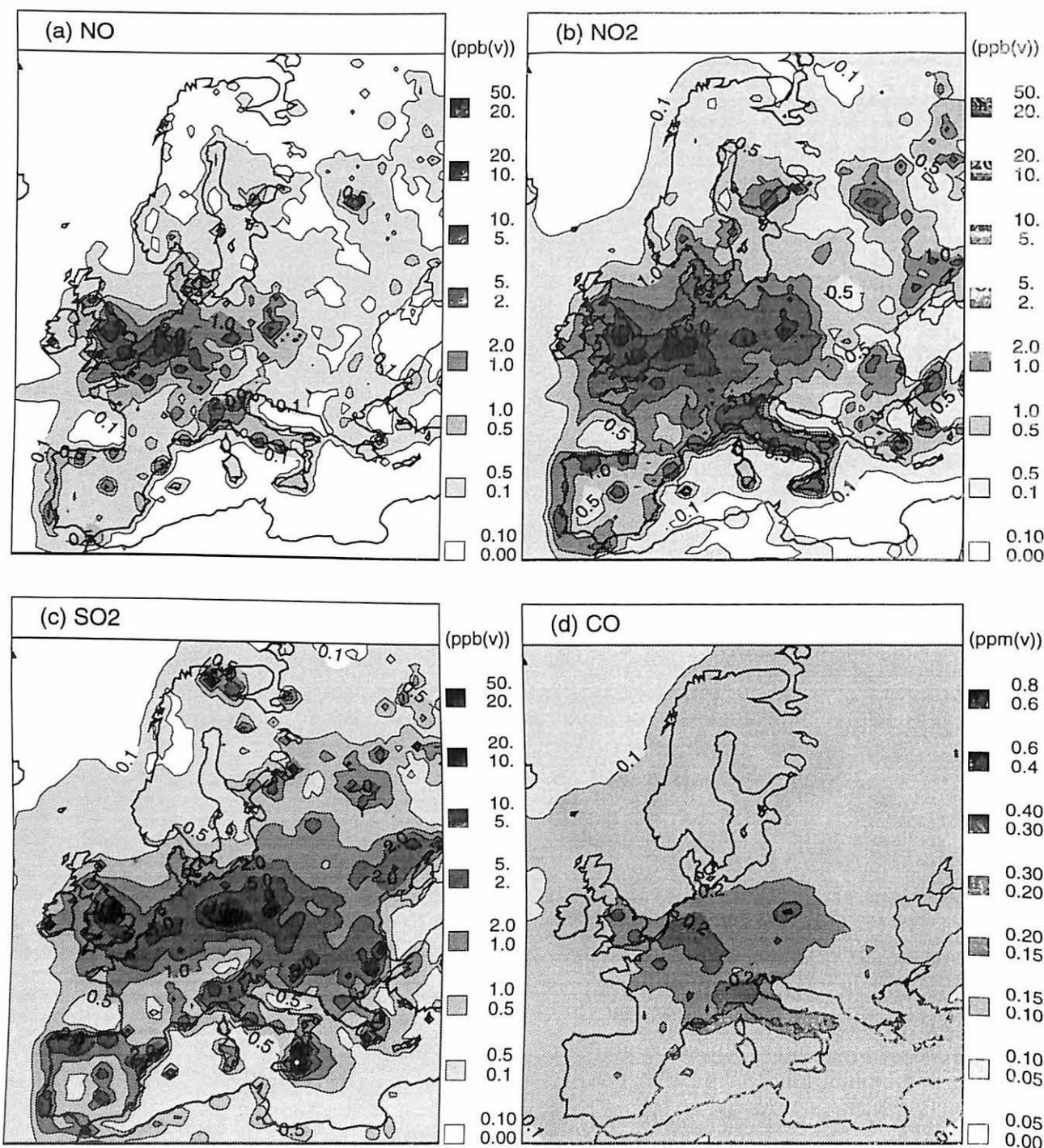
Figure 3.2   Six-month average (April-September 1994) model calculated surface concentrations of NO, NO₂, SO₂ (ppb(v)) and CO. (ppm(v)).

Ethane exhibits a smoother distribution than the other hydrocarbons, reflecting its lower reactivity, which leads to a longer residence time. Ethene, propene and o-xylene have the shortest residence times of the anthropogenic hydrocarbons, with ethanol and n-butane taking intermediate positions. Isoprene, which is naturally emitted, has a completely different distribution, reflecting mainly the distribution of emitting tree species used in the emission calculation and a short residence time.
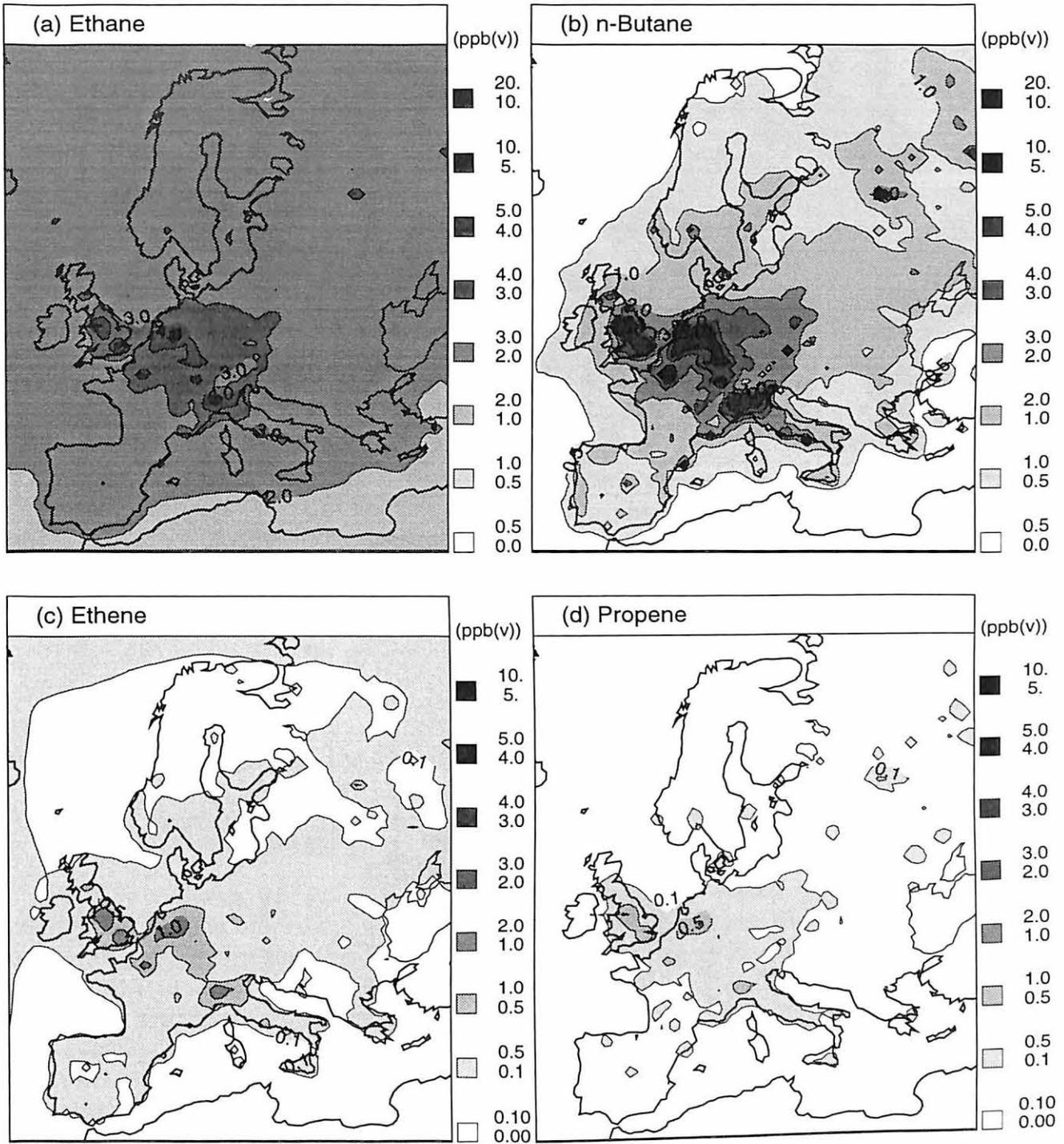
18

Figure 3.3   Six-month average (April-September 1994) model calculated surface
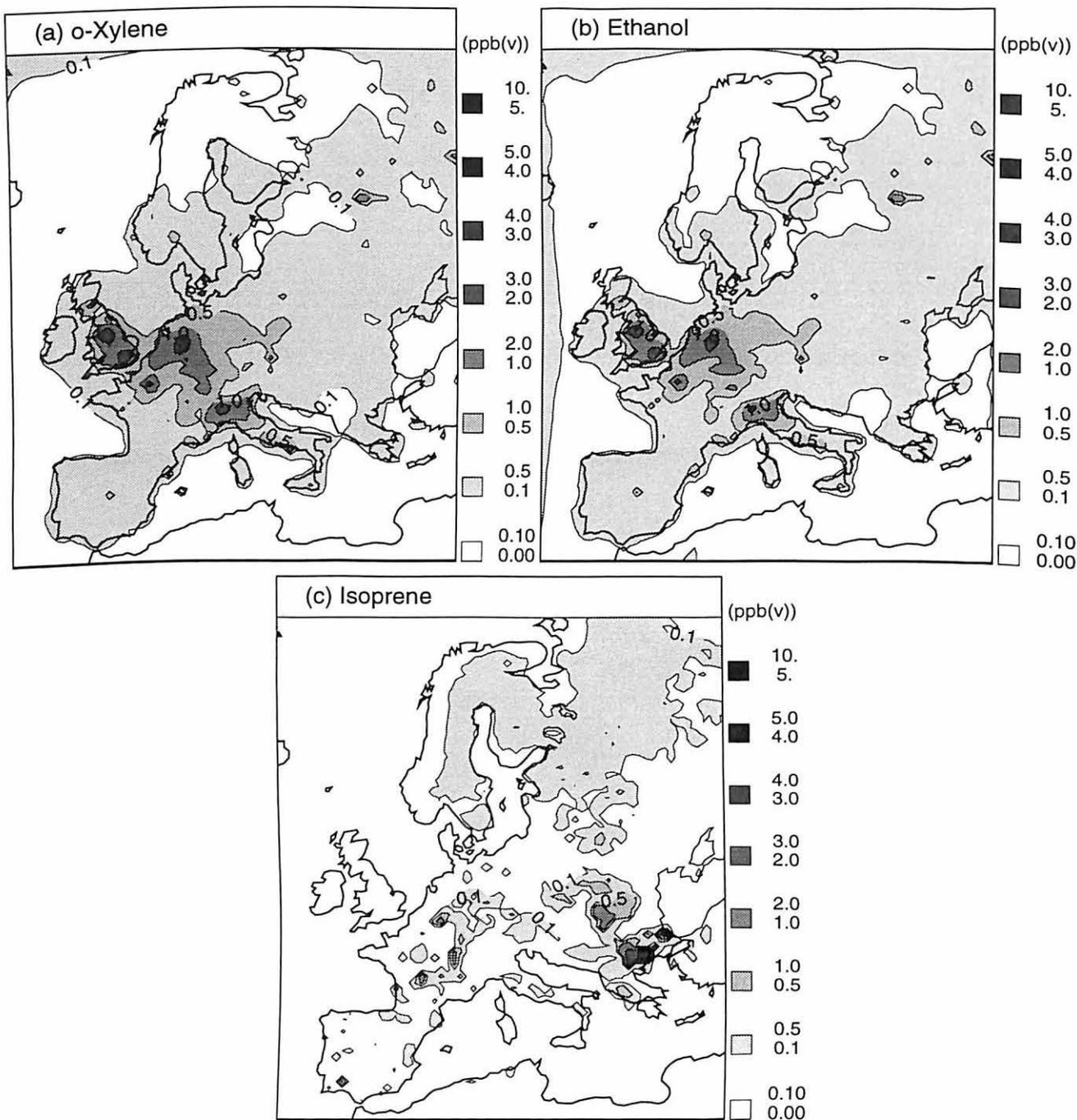concentrations of Ethane, n-Butane, Ethene and Propene. Units: ppb(v).

19

Figure 3.4 Six-month average (April-September 1994) model calculated surface concentrations of o-Xylene, Ethanol and Isoprene. Units: ppb(v).

3.2.1 NO₂

Figure 3.5 shows timeseries of observed and model calculated diurnal average concentrations of NO_2 at eight selected stations. For these stations the approximate levels of observed and calculated concentrations are about equal but the correlation is not excellent.

Figure 3.6 shows a scatterplot comparing average concentrations for the whole six-month period. A majority of the calculated averages are within a factor of two of the observations.
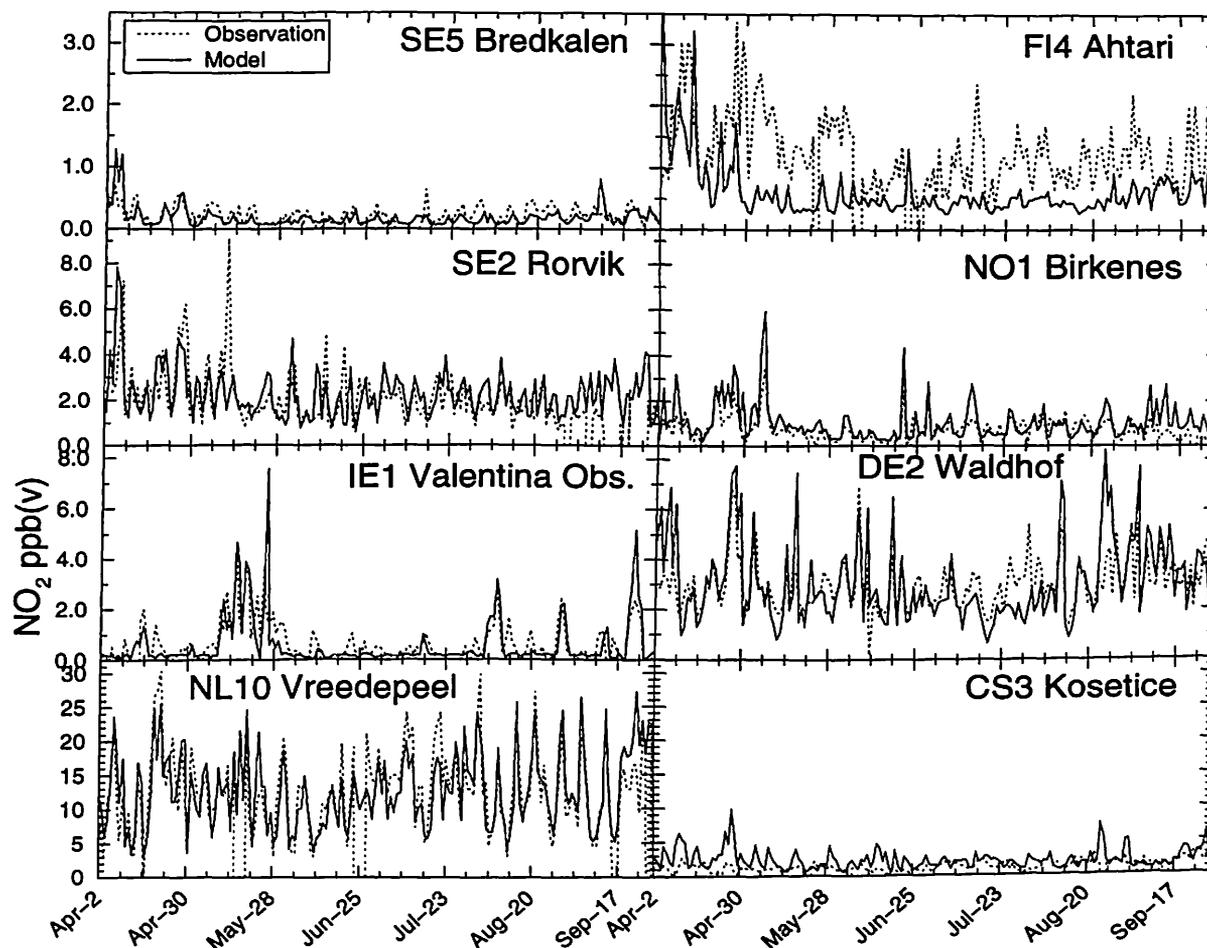
Figure 3.5   Observed and model calculated timeseries of diurnal average concentration of NO₂ at Bredkälen, Ähtäri, Rörvik, Birkenes, Valentina Observatory, Waldhof, Vreedepeel and Kosetice in1994. Units: ppb(v).

Major exceptions are the Spanish stations, where the model predicts much lower concentrations than observed, and one station in Switzerland, where the model predicts much higher values. Four of the five Spanish stations show higher observed values than any of the other EMEP stations. This indicates either that these stations are sited differently than the majority of the other EMEP stations or that there are uncertainties in the emissions. The Swiss station (Jungfraujoch) is located on a mountaintop, which is not well resolved by the model.

Correlation coefficients for daily values as well as observed and calculated average concentrations for all the stations are listed in Table 3.2. The correlation is in general quite low and very variable between different stations, with several cases of negative correlation.

In summary the results for NO₂ are not very good. This can be understood considering the uncertainties discussed above, where model resolution is probably a major factor in combination with the rather short residence time of NO₂. We note that in a recent comparison of four other European regional air quality models (EMEP, EURAD, LOTOS and REM3) none of the models gave NO₂ concentrations in good agreement with observations (Hass et al. 1997).

21

Table 3.2. NO$_2$ and SO$_2$ concentrations (ppb(v)) and correlation coefficients between observed and calculated diurnal mean concentrations

| Station	NO$_2$ observed mean conc.	model mean conc.	correlation coefficient	SO$_2$ observed mean conc.	model mean conc.	correlation coefficient
CH01	0.21	3.23	0.44	0.086	0.70	0.07
CH02	6.17	2.34	0.28	0.54	0.61	0.27
CH03	5.23	3.02	0.53	0.84	0.73	0.44
CH04	2.73	3.79	0.24	0.81	0.95	0.29
CH05	3.50	2.11	0.63	0.42	0.76	0.23
CS01	1.68	4.35	0.37	4.05	11.17	0.69
CS03	1.33	2.26	0.20	3.30	5.74	0.65
DE01	2.94	2.53	0.80	0.80	1.16	0.56
DE02	3.05	3.14	0.70	1.19	3.16	0.81
DE03	1.73	3.60	0.47	0.11	1.29	0.67
DE04	3.09	4.98	0.46	0.58	2.71	0.47
DE05	2.32	1.72	0.47	0.57	1.91	0.68
DE07	2.37	2.36	0.64	0.86	3.22	0.72
DE08	2.81	3.38	0.49	1.33	5.52	0.73
DE09	2.57	1.72	0.40	0.54	1.84	0.77
DK03	-	-	-	0.59	1.24	0.67
DK05	-	-	-	0.92	1.21	0.45
DK08	2.55	2.45	0.59	0.71	0.78	0.66
DK32	-	-	-	0.60	2.09	0.62
ES01	13.04	0.61	-0.18	2.22	0.69	0.10
ES02	12.55	0.61	-0.02	2.10	0.68	0.06
ES03	14.61	1.43	0.09	1.75	6.68	-0.17
ES04	17.90	1.83	0.07	1.90	2.33	-0.07
ES05	19.45	1.82	0.01	2.31	2.68	0.09
FI04	1.24	0.63	0.25	0.14	0.26	0.60
FI09	2.04	0.69	0.25	0.42	0.31	0.18
FI17	0.90	1.58	0.54	0.48	0.78	0.66
FI22	0.69	0.17	0.22	0.19	0.31	0.52
FR03	-	-	-	0.48	0.64	0.39
FR05	-	-	-	0.60	2.63	0.02
FR08	-	-	-	0.88	2.33	0.42
FR09	-	-	-	1.00	3.17	0.65
FR10	-	-	-	0.54	0.97	0.45
FR11	-	-	-	0.51	0.74	0.61
FR12	-	-	-	0.66	0.93	-0.05
GR01	6.65	1.64	0.21	4.63	1.85	-0.31
HR02	0.81	1.95	-0.04	-	-	-
HR04	0.92	0.44	0.03	-	-	-
HU02	1.47	1.95	-0.07	0.47	5.63	-0.44
IE01	0.82	0.69	0.71	0.38	0.71	0.77
IE02	-	-	-	0.55	1.66	0.80
IT01	-	-	-	0.75	2.90	0.23
IT04	7.92	5.58	0.26	1.01	2.19	0.30
LT15	4.83	0.61	-0.03	2.41	1.07	-0.02
LV10	1.59	0.59	0.03	0.58	0.51	0.13
LV16	0.93	0.40	-0.15	0.88	0.62	0.02
NL09	4.57	4.17	0.80	0.85	2.15	0.54
NL10	12.87	12.74	0.82	1.67	5.87	0.64
NO01	0.78	1.05	0.74	0.26	0.60	0.68
NO08	1.24	0.72	0.26	0.21	0.48	0.74
NO15	0.25	0.23	0.12	0.070	0.12	0.82
NO30	0.20	0.10	0.31	0.20	0.20	0.33
NO39	0.36	0.36	0.17	0.082	0.17	0.60
NO41	0.42	0.43	0.42	0.16	0.19	0.50
NO43	0.99	1.03	0.39	0.27	0.55	0.52
NO44	1.53	1.16	0.55	0.16	0.27	0.49
PL02	4.33	2.65	0.25	1.35	4.70	0.39
PL03	1.53	3.44	-0.01	1.84	9.75	-0.06
PL04	2.07	0.94	0.25	1.31	1.46	0.49
PL05	1.00	0.84	0.58	0.66	1.61	0.56
PT04	-	-	-	1.10	3.19	-0.21
RU01	0.51	0.15	0.07	0.94	2.60	0.56
RU13	0.62	0.13	0.16	0.33	0.24	0.40
RU14	1.37	0.30	0.09	0.49	0.60	0.37
SE02	2.11	2.22	0.44	0.55	0.82	0.72
SE05	0.25	0.19	0.50	0.068	0.081	0.40
SE08	1.42	0.90	0.43	0.52	0.51	0.44
SE11	1.90	1.95	0.62	0.49	0.96	0.62
SE12	1.15	1.48	0.07	0.27	0.40	0.62
SE13	0.23	0.36	0.29	0.096	0.25	0.26
SK02	2.89	1.97	-0.05	0.95	3.87	0.29
SK04	2.73	1.87	0.10	0.81	3.85	0.24
SK05	3.50	2.57	0.27	1.47	4.38	0.21
SK06	2.74	1.55	0.05	1.07	3.03	0.43
TR01	1.28	0.14	0.14	0.23	0.23	0.14
YU05	2.98	0.50	0.31	4.57	2.89	-0.24
YU08	3.71	0.28	0.01	5.08	1.05	0.11
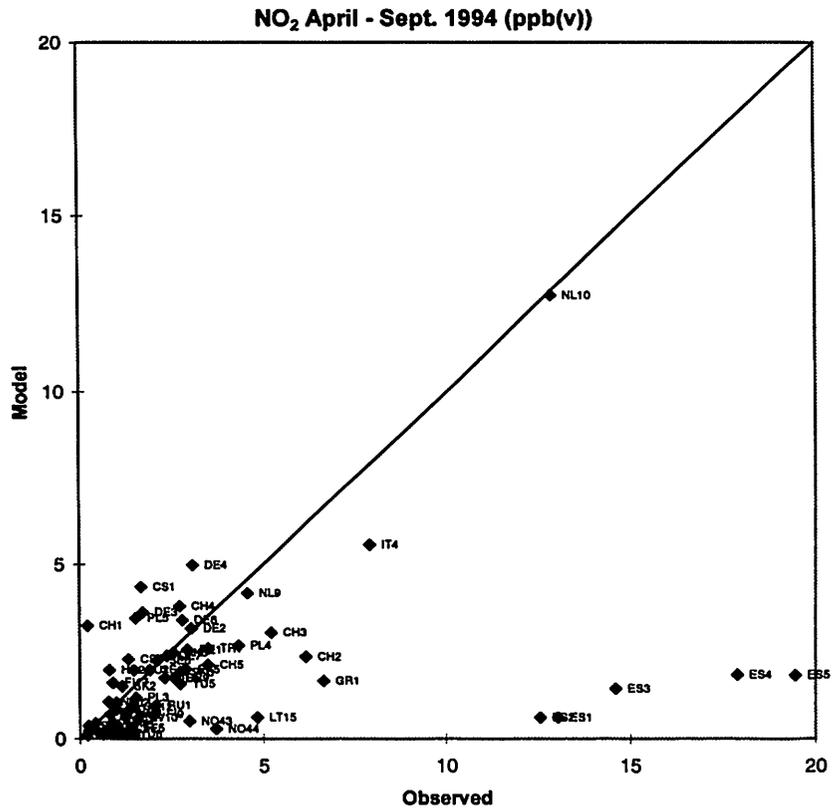
Figure 3.6   Scatterplot of observed and model calculated six-month average (April-September 1994) concentrations of NO₂. Units: ppb(v).
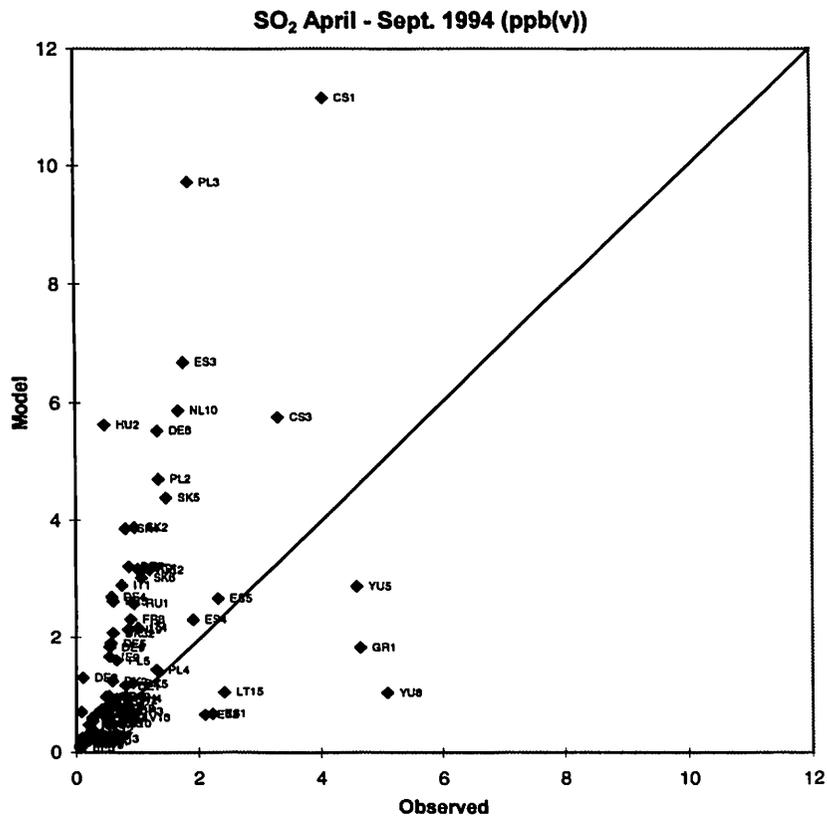

Figure 3.7   Scatterplot of observed and model calculated six-month average (April-September 1994) concentrations of SO₂. Units: ppb(v).
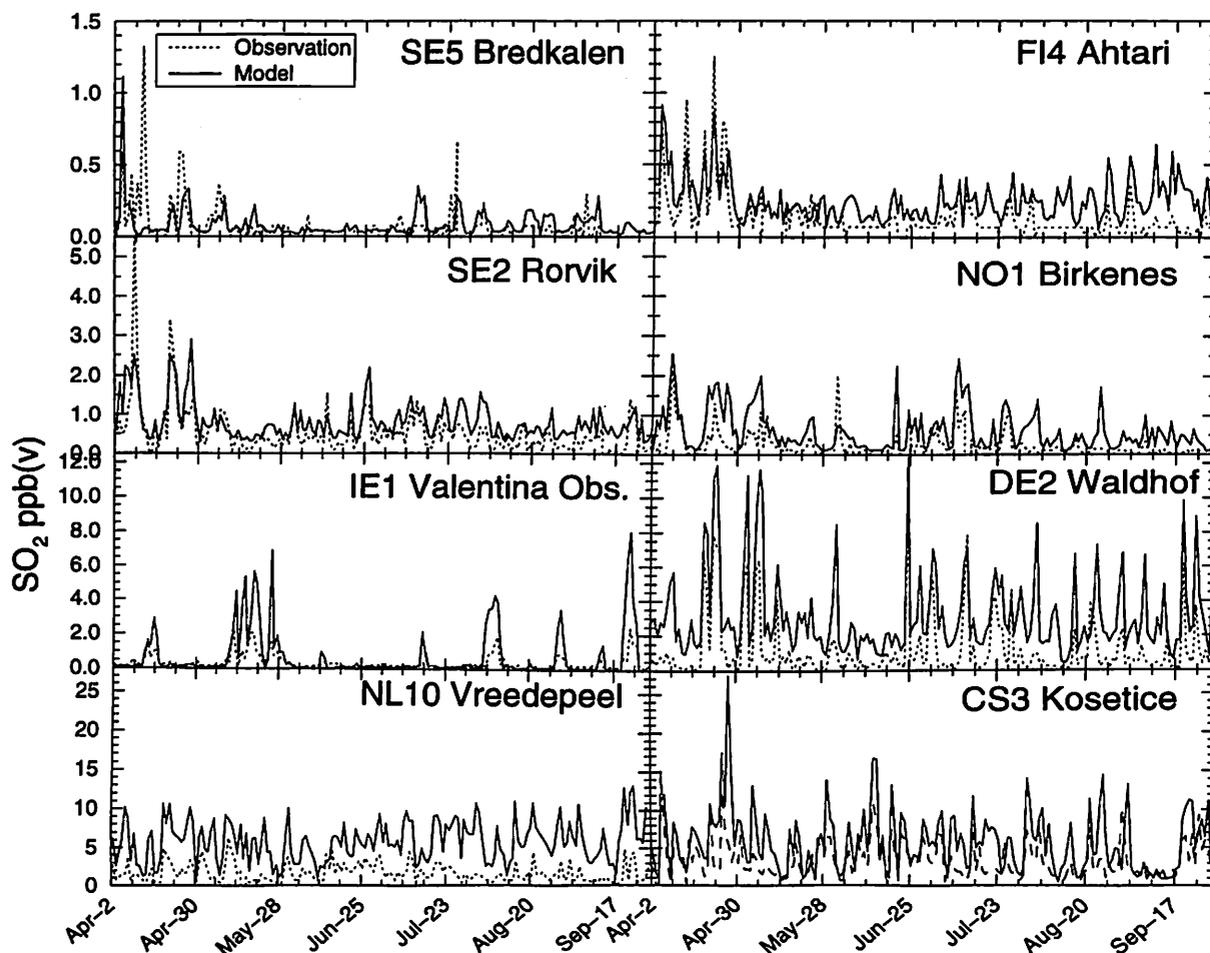
Figure 3.8   Observed and model calculated timeseries of diurnal average concentration of
SO₂ at Bredkälen, Ähtäri, Rörvik, Birkenes, Valentina Observatory, Waldhof,
Vreedepeel and Kosetice in 1994. Units: ppb(v).

3.2.2   *SO₂*

Figure 3.8 shows timeseries of observed and model calculated diurnal average concentrations of SO_2 at eight selected stations. The model overestimates the SO_2 concentration but at least for these stations, there is some positive correlation between the observed and calculated concentrations.

Figure 3.7 shows a scatterplot comparing average SO_2 concentrations for the whole six-month period. On the average the model overestimates the SO_2 concentrations by a factor of two. The overprediction is more pronounced in areas with high SO_2 emission, while the agreement is better further away from the main source areas. This result is probably due to the fact that the SO_2 emissions were distributed in the vertical in the same way as the NO and NO_2 emissions. This probably leads to an overestimation of the emissions close to the ground for SO_2. Correlation coefficients for daily values and observed and calculated averages for all the stations are listed in Table 3.2. The correlation is slightly better than for NO_2 but still in general quite low and very variable between different stations, with several cases of negative correlation.

In summary the results for SO_2 are not very good. Again this is probably to a large extent related to model resolution as well as to a too low emission height.

Table 3.3. Six-month mean hydrocarbon concentrations and correlation coefficients between observed and calculated concentrations

Model species	Station	Correlation coefficient	Observed conc. (ppb)	Model conc. (ppb)	Obs/Model	Observed components' fraction of the emission of the model species
Ethene	CH03	0.45	0.82	0.57	1.45	0.75
	CS03	0.51	0.46	0.21	2.17	0.75
	DE02	0.68	0.45	0.35	1.28	0.75
	GBWB	0.16	0.63	0.44	1.43	0.77
	NL09	0.6	6.14*	0.31	19.93*	0.77
	NO01	0.25	0.34	0.13	2.63	0.75
	SE02	0.47	0.19	0.15	1.27	0.75
	SK06	0.68	0.51	0.25	2.02	0.75
Ethane	CH03	0.58	2.7	3.85	0.7	0.6
	CS03	0.75	2.25	2.98	0.76	0.6
	DE02	0.82	2.28	3.22	0.71	0.6
	GBWB	0.55	2.13	2.64	0.81	0.6
	NL09	0.63	18.75*	2.46	7.63*	0.6
	NO01	0.87	2.05	2.66	0.77	0.6
	SE02	0.86	1.56	2.71	0.57	0.6
	SK06	0.85	2.89	2.63	1.1	0.6
Propene	CH03	0.46	0.25	0.21	1.16	0.28
	CS03	0.54	0.15	0.064	2.39	0.28
	DE02	0.56	0.16	0.12	1.4	0.28
	GBWB	0.33	0.14	0.15	0.96	0.87
	NL09	0.63	3.119*	0.17	18.9*	0.53
	SE02	0.45	0.045	0.058	0.78	0.87
	SK06	0.51	0.16	0.085	1.86	0.28
n-Butane	CH03	0.25	3.15	4.47	0.7	0.59
	CS03	0.53	1.47	2.2	0.67	0.59
	DE02	0.73	1.7	2.8	0.61	0.59
	GBWB	0.55	1.6	2.68	0.6	0.52
	NL09	0.69	32.97*	3.37	9.78*	0.58
	NO01	0.39	1.4	1.28	1.09	0.59
	SE02	0.56	0.86	1.36	0.63	0.39
	SK06	0.087	2.59	2.26	1.15	0.59
o-Xylene	CH03	0.36	1.33	0.87	1.52	0.7
	CS03	0.36	0.64	0.3	2.16	0.7
	DE02	0.55	0.66	0.54	1.23	0.7
	GBWB	0.39	0.44	0.58	0.76	0.7
	NL09	0.33	9.66*	0.61	15.91*	0.7
	NO01	0.3	0.52	0.17	3.08	0.7
	SE02	0.57	0.24	0.23	1.04	0.41
	SK06	0.17	0.91	0.36	2.54	0.7
Isoprene	CH03	0.037	0.094	0.0075	12.53	1
	CS03	0.004	0.064	0.005	12.75	1
	DE02	0.72	0.045	0.075	0.6	1
	GBWB	0.1	0.04	0.0019	20.74	1
	NL09	0.074	1.106*	0.0023	480.87*	1
	NO01	0.26	0.049	0.0069	7.12	1
	SE02	0.64	0.052	0.047	1.11	1
	SK06	0.74	0.16	0.84	0.19	1

*The observed values for the NL09 station appear to be reported with the wrong scaling factor in the TOR database and should probably be reduced by a factor of ten.

3.2.3 Hydrocarbons

The number of sites with observations of hydrocarbons is much smaller than for SO_2 or NO_2 (c.f. Table 3.1). Table 3.3 gives correlation coefficients and observed and calculated averages and ratios between observed and calculated averages for ethene, ethane, propene, n-butane, o-xylene and isoprene at eight stations. For some of these stations only a few measurements are available and therefore the values given in the table can not be considered as any "long-time averages" for the given station and components. For most stations only one short sample per day was taken so individual data points do not represent diurnal averages.

When looking at these results one should also keep in mind that the anthropogenic hydrocarbons included in the chemical mechanism are used as models for several different organic molecules. When making the comparison we have therefore added the observed concentrations according to the emission split that was used to partition the emission on the model hydrocarbons. Since the number of different hydrocarbons observed varies between the stations the "observed fraction" varies as indicated in Table 3.3. This is not a problem for isoprene since it is not used to model any other components.

Considering the number of uncertainties and complicating factors discussed above the results for the anthropogenic hydrocarbons are surprisingly good. The results are best for ethane, which is the component with the longest residence time. For ethane the correlation coefficient is above 0.8 for four of the eight measurement locations. Correlations for the other components are generally lower, but positive.

For isoprene the results are not so good with low correlation coefficients and large deviations between observed and calculated average concentrations, exceeding a factor of 10 at several locations. This indicates that the isoprene emissions are probably quite far from being realistic. The fact that isoprene is a rather short-lived component complicates the matter further.

3.3 Concentrations of secondary components

Figure 3.9 and 3.10 show average calculated concentrations of HNO_3, NO_3^- (nitrate), SO_4^{2-} (sulfate), peroxy-acetyl-nitrate (PAN), HCHO (formaldehyde) and CH_3CHO (acetaldehyde) for the simulated six-month period. In general the distributions of the secondary components are smoother than those for the primary components as a result of atmospheric transport and generally longer combined residence times for the precursors and secondary components.

3.3.1 $HNO_3 + NO_3^-$ and SO_4^{2-}

Figure 3.11 shows a scatterplot comparing average $HNO_3 + NO_3^-$ concentrations for the whole six month period. The calculated averages are within a factor of two from the observations at all stations except three. There is no clear bias. Correlation coefficients and observed and calculated averages for all the stations are listed in Table 3.4. The correlation coefficients, r, between observed and model concentrations are generally higher than for the primary components. For more than half of the stations r is above 0.5.

Figure 3.12 shows the corresponding scatterplot for sulfate. In this case the model has a clear tendency towards underprediction with a large fraction of the observed average concentrations being more than a factor of two higher than the calculated averages. This bias in the model is related to the overprediction seen for SO_2 and indicates that the oxidation of SO_2 to sulfate is too slow in the model. Part of the reason for the underprediction could also be the fact that no sea salt sulfate is included in the model.

Correlation coefficients and observed and calculated average sulfate concentrations for all the stations are listed in Table 3.5. The correlation is slightly better than for $HNO_3 + NO_3^-$, with r above 0.5 for more than half of the stations. In four cases the correlation coefficients are even above 0.8.

In summary the results are better for $HNO_3 + NO_3^-$ and SO_4^{2-} than for the corresponding primary components. This effect is quite common in large-scale transport/chemistry/deposition models. It is simply easier to model secondary components than primary components with short residence times.
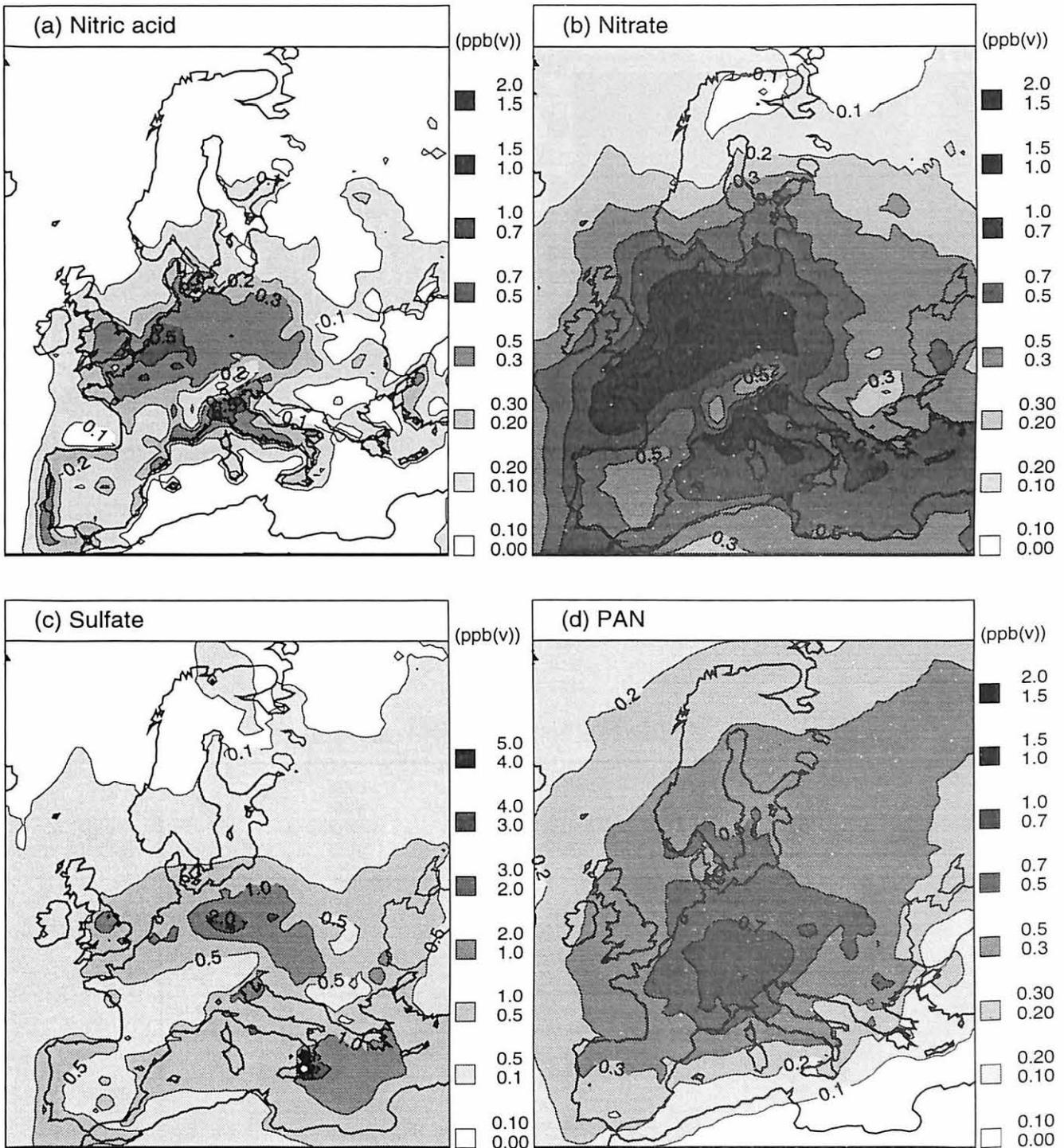
Figure 3.9   Six-month average (April-September 1994) model calculated surface concentrations of HNO_3, NO_3^-, SO_4^{2-} and PAN. Units: ppb(v).
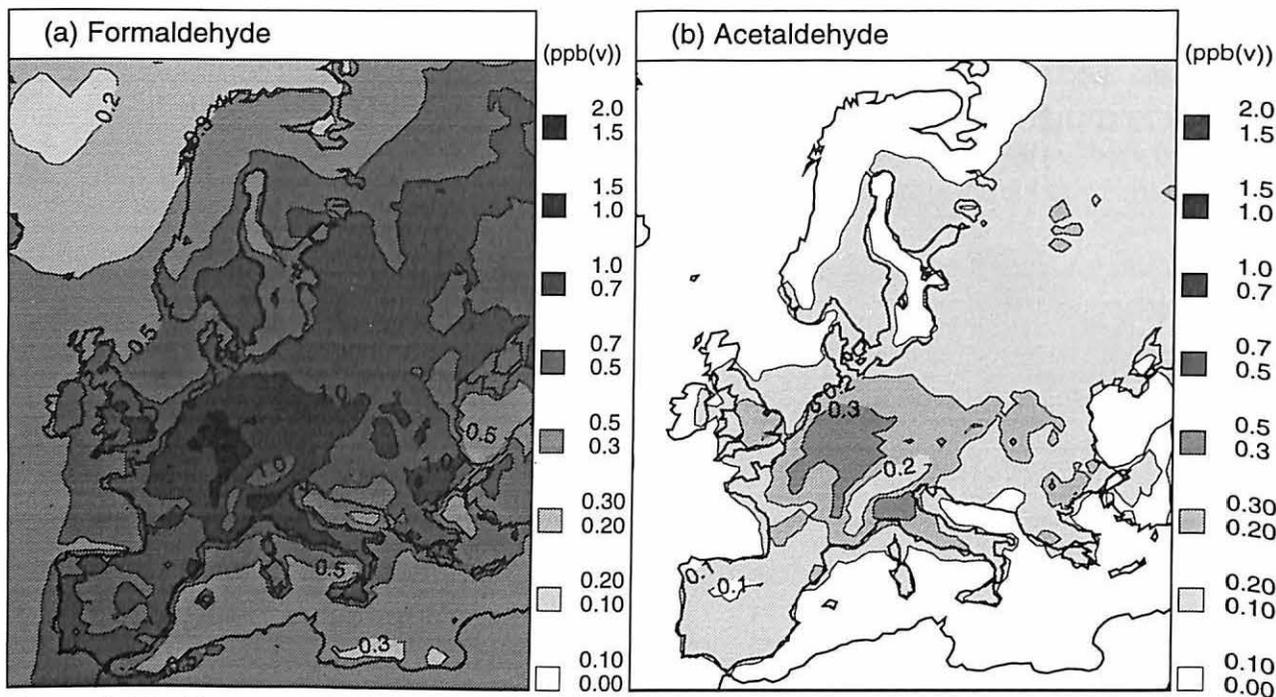
Figure 3.10 Six-month average (April-September 1994) model calculated surface
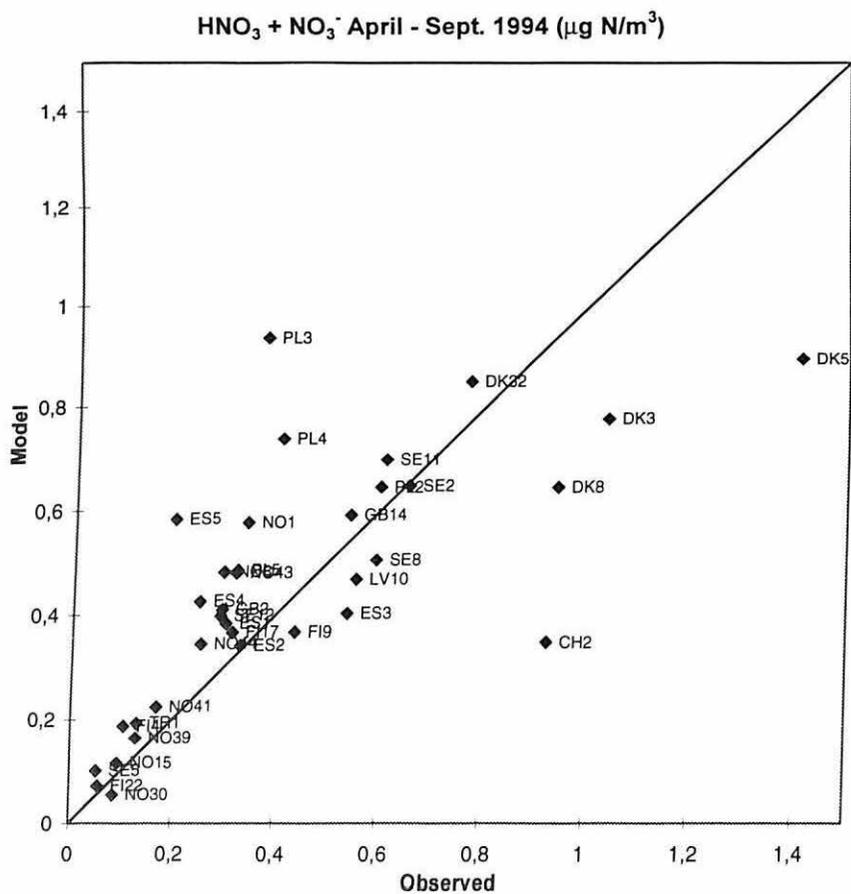concentrations of HCHO and CH₃CHO. Units: ppb(v).

Figure 3.11 Scatterplot of observed and model calculated six-month (April-September 1994
average surface concentrations of HNO₃ + NO₃⁻. Units: μg N/m³.

Table 3.4. $HNO_3 + NO_3^-$ concentration in air and correlation coefficients between observed and calculated diurnal mean concentrations

Station	Observed mean conc. ($\mu g\ N/m^3$)	Model mean conc. ($\mu g\ N/m^3$)	Correlation coefficient
CH02	1.56	0.58	0.31
DK03	1.75	1.30	0.57
DK05	2.38	1.50	0.50
DK08	1.59	1.08	0.61
DK32	1.29	1.43	0.57
ES01	0.50	0.64	0.17
ES02	0.55	0.57	-0.01
ES03	0.90	0.67	0.20
ES04	0.42	0.71	0.32
ES05	0.33	0.98	0.45
FI04	0.18	0.32	0.63
FI09	0.73	0.61	0.67
FI17	0.53	0.61	0.50
FI22	0.094	0.12	0.64
GB02	0.49	0.69	0.67
GB14	0.91	0.99	0.31
LV10	0.93	0.78	0.60
NO01	0.57	0.97	0.60
NO08	0.49	0.81	0.58
NO15	0.16	0.20	0.60
NO30	0.14	0.09	0.44
NO39	0.22	0.28	0.42
NO41	0.28	0.38	0.65
NO43	0.53	0.80	0.54
NO44	0.42	0.58	0.47
PL02	1.00	1.08	0.56
PL03	0.62	1.58	0.32
PL04	0.68	1.24	0.49
PL05	0.54	0.81	0.24
SE02	1.10	1.09	0.53
SE05	0.089	0.17	0.62
SE08	0.99	0.84	0.66
SE11	1.02	1.17	0.54
SE12	0.48	0.67	0.62
TR01	0.22	0.33	0.30

Table 3.5. SO_4^{2-} concentration in air and correlation coefficients between observed and calculated diurnal mean concentrations

Station	Observed mean conc. ($\mu g\ S/m^3$)	Model mean conc. ($\mu g\ S/m^3$)	Correlation coefficient
CH01	0.30	0.21	0.11
CH02	1.01	0.18	0.32
CH03	1.13	0.24	0.40
CH04	1.11	0.33	0.45
CH05	1.03	0.27	0.55
CS01	1.69	2.48	0.68
CS03	1.92	1.81	0.66
DE01	1.07	0.92	0.58
DE02	1.00	1.33	0.63
DE03	0.70	0.40	0.49
DE04	0.93	0.87	0.52
DE05	0.93	0.90	0.56
DE07	0.90	1.14	0.61
DE08	1.01	1.52	0.63
DE09	0.77	0.98	0.63
DE12	0.91	1.19	0.47
DE14	0.95	1.21	0.54
DE17	0.72	1.00	0.58
DE18	0.77	0.69	0.57
DE19	0.77	0.61	0.44
DK03	1.49	0.68	0.75
DK05	1.84	0.91	0.68

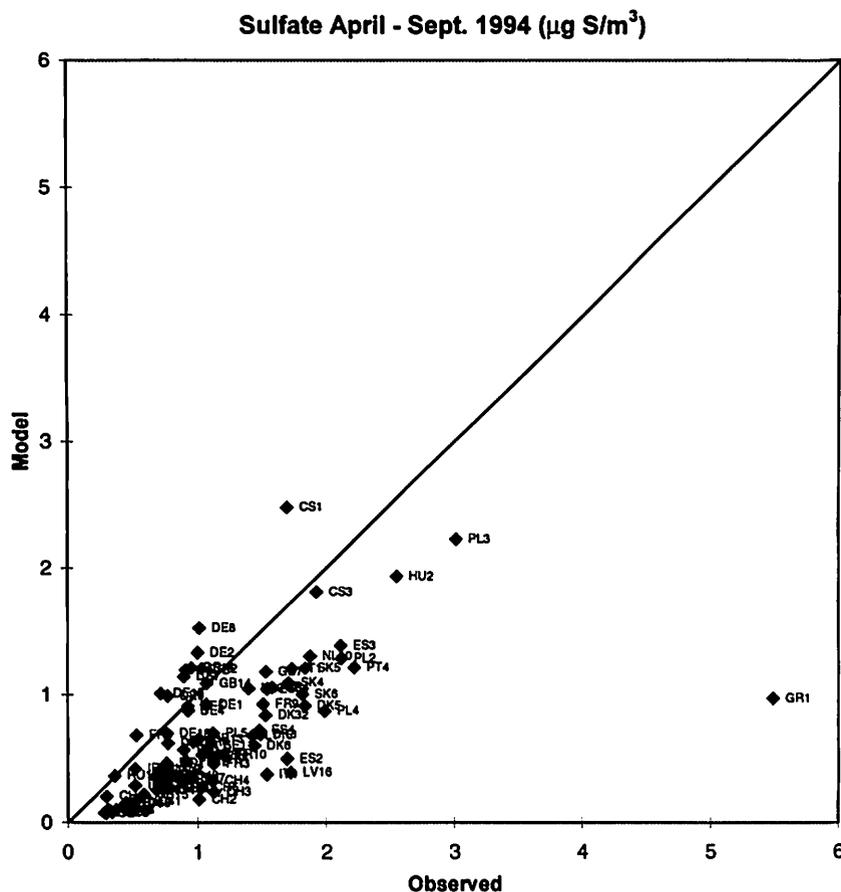| Station	Observed mean conc. ($\mu g\ S/m^3$)	Model mean conc. ($\mu g\ S/m^3$)	Correlation coefficient
DK32	1.53	0.83	0.80
ES01	0.89	0.56	0.38
ES02	1.70	0.49	0.38
ES03	2.11	1.38	0.50
ES04	1.48	0.72	0.69
ES05	1.54	1.04	0.68
FI04	0.48	0.15	0.77
FI09	0.87	0.33	0.62
FI17	0.92	0.34	0.73
FI22	0.37	0.10	0.49
FR03	1.12	0.46	0.55
FR05	0.53	0.67	0.30
FR08	0.97	0.62	0.66
FR09	1.51	0.92	0.67
FR10	1.20	0.52	0.11
FR11	0.74	0.29	0.56
FR12	0.91	0.47	0.63
GB02	0.76	0.42	0.67
GB04	1.58	1.05	0.57
GB06	0.79	0.27	0.71
GB07	1.53	1.18	0.64
GB13	1.01	0.65	0.50
GB14	1.07	1.09	0.61
GB15	0.58	0.22	0.53
GB16	0.70	0.36	0.78
GR01	5.49	0.97	0.13
HU02	2.55	1.93	0.34
IE01	0.52	0.29	0.67
IE02	0.52	0.42	0.74
IT01	1.74	1.20	0.42
IT04	1.54	0.37	0.37
LV10	1.05	0.54	0.36
LV16	1.73	0.39	0.30
LT15	1.43	0.67	0.48
NL09	1.40	1.04	0.75
NL10	1.88	1.30	0.57
NO01	0.76	0.46	0.68
NO08	0.73	0.41	0.82
NO15	0.32	0.10	0.81
NO30	0.28	0.077	0.30
NO39	0.44	0.15	0.77
NO41	0.53	0.17	0.72
NO43	0.82	0.36	0.68
NO44	0.69	0.25	0.64
PL02	2.12	1.28	0.39
PL03	3.01	2.23	0.42
PL04	1.99	0.87	0.51
PL05	1.12	0.69	0.57
PT04	2.22	1.21	0.08
RU01	0.36	0.36	0.19
RU13	0.31	0.10	0.19
RU14	0.75	0.27	0.42
SE02	1.12	0.51	0.78
SE05	0.34	0.081	0.66
SE08	1.04	0.52	0.83
SE11	1.10	0.60	0.69
SE12	0.75	0.32	0.76
SE13	0.29	0.073	0.68
SK02	1.04	1.20	0.40
SK04	1.71	1.09	0.37
SK05	1.84	1.20	0.42
SK06	1.82	1.00	0.34
TR01	0.67	0.35	0.35

Figure 3.12   Scatterplot of observed and model calculated six-month (April-September 1994) average surface concentrations of SO_4^{2-}. Units: μg S/m^3.

3.3.2   Carbonyl compounds

For nine sites measurements of some carbonyl compounds were available. The observed components that are included in the model are formaldehyde (HCHO), acetaldehyde (CH_3CHO), 2-butanone ($CH_3COCH_2CH_3$) and the two α-dicarbonyls: 1,2-ethanedione (glyoxal, $(CHO)_2$) and 1,2-propanedione (methylglyoxal, CH_3COCHO).

Table 3.6 gives correlation coefficients and observed and calculated averages for the available carbonyls. The observed values are mean values of a number of eight-hour measurements 0800 - 1600 UTC, while the model values are based on three-hour averages, 0900-1200 UTC, for the corresponding days (due to storage limitations). The difference in "sampling period" could lead to deviations between the model and observed values since the concentration of aldehydes and ketones varies during the day. The effect of different sampling periods is, however, expected to be small compared to other uncertainties. Just as for the hydrocarbons the values given in the table can not be considered as long-time averages for the given station and components, since the number of measurements is small. Also, in many cases the concentrations of some carbonyls, especially the α-dicarbonyls, were below the detection limit. In the comparison these measurements have been treated as giving zero concentration.

Since the hydrocarbons in the chemical mechanism are used as representatives for several different organic molecules, the carbonyls in the mechanism will, in a sense, also model several different compounds. This should lead to higher model concentrations than observed concentrations. The difference is expected to be especially large for 2-butanone since n-butane

31

Table 3.6. Carbonyl concentrations in air and correlation coefficients between observed and calculated concentrations (values within parenthesis are cases with more than half of the measurements giving concentrations below the detection limit; these measurements have been treated as if they had given zero concentration of the carbonyl)

	Station	Correlation coefficient	Observed mean concentration (ppb)	Model mean concentration (ppb)
Formaldehyde	CS03	0.51	1.48	1.11
	DE02	0.65	1.23	1.09
	FR08	0.42	1.34	2.40
	GB36	0.70	1.57	1.05
	IE31	0.62	0.48	0.44
	IT01	0.62	2.20	1.26
	IT04	0.39	2.86	1.47
	LV10	0.00	1.02	0.65
	NO01	0.45	0.69	0.75
Acetaldehyde	CS03	0.29	0.70	0.27
	DE02	0.75	0.44	0.26
	FR08	0.42	0.62	0.66
	GB36	0.83	0.67	0.34
	IE31	0.45	0.20	0.07
	IT01	0.45	0.96	0.35
	IT04	0.20	1.16	0.31
	LV10	-0.02	0.43	0.11
	NO01	0.47	0.29	0.15
Butanone	CS03	0.44	0.14	0.62
	DE02	0.76	0.10	0.52
	FR08	0.37	0.13	1.16
	GB36	0.76	0.16	0.59
	IE31	0.68	0.04	0.09
	IT01	0.20	0.20	0.61
	IT04	0.21	0.24	0.80
	LV10	0.38	0.06	0.30
	NO01	0.54	0.05	0.32
Glyoxal	CS03	(-0.27)	(0.016)	0.115
	DE02	0.30	0.031	0.094
	FR08	(0.15)	(0.005)	0.208
	GB36	(-0.07)	(0.004)	0.061
	IE31		(0.000)	0.018
	IT01	0.29	0.057	0.105
	IT04	0.24	0.045	0.156
	LV10	(-0.26)	(0.015)	0.048
	NO01	(0.13)	(0.002)	0.063
Methylglyoxal	CS03	(-0.35)	(0.025)	0.195
	DE02	(0.00)	(0.039)	0.209
	FR08	(0.40)	(0.011)	0.496
	GB36	(0.56)	(0.010)	0.206
	IE31		(0.000)	0.036
	IT01	0.22	0.097	0.239
	IT04	0.12	0.089	0.392
	LV10	(-0.28)	(0.017)	0.071
	NO01	(0.02)	(0.002)	0.109

is used to model butane and all heavier saturated hydrocarbons, as well as propane. In the model 2-butanone is also used as a surrogate for hydroxyacetone ($HOCH_2COCH_3$) in the propene chemistry. This means that 2-butanone is used to model a large number of different carbonyls.

Glyoxal and methylglyoxal concentrations are also likely to be substantially overestimated in the model since the o-xylene chemistry, which simulates all of the aromatic chemistry, is modeled in a very simplified way, where every o-xylene molecule eventually gives rise to the

formation of two methylglyoxal molecules and one glyoxal molecule. This is, of course, an extremely simplified mechanism and it will overestimate the formation of the α-dicarbonyls drastically. (Experimental methylglyoxal yield from the OH-radical initiated reactions of monocyclic aromatic hydrocarbons has been reported to be about 8-64 % and the glyoxal yield about 3-23% (see Atkinson, 1990).)

For formaldehyde, HCHO, the calculated average concentrations are within a factor of two from the observed for all stations. At most locations the model actually underestimates the formaldehyde concentration. The reasons for this could be many, e.g., unrealistic model hydrocarbon emission mix (the actual mix is different at different locations, while we have used the same mix all over Europe) or uncertainties in the wet scavenging. The simplified isoprene chemistry is also likely to underestimate HCHO concentrations (see Appendix A).

The acetaldehyde concentration is underestimated at all stations except one. The difference between the calculated and observed concentration is up to a factor of four. Possible explanations are again the accuracy of the emissions, the formulation of the chemical mechanism and uncertainties in precipitation scavenging.

At all sampling locations except Rucava (LV10) the correlation coefficient between calculated and observed concentrations are positive for the two simple aldehydes. The highest correlation coefficients are those for the Harwell station (GB36). For this location r is 0.83 for acetaldehyde.

The correlation coefficients for 2-butanone are also positive but the model overestimates the butanone concentration everywhere, from a factor of 2 at Mace Head (IE31) to a factor of 9 at Donon (FR8).

For the α-dicarbonyls the deviations between observed and model concentrations are even greater. For glyoxal the model overestimates the concentration from a factor of 2 (IT1) to a factor of 42 (FR8) and for methylglyoxal by a factor of 2 (IT1) to a factor of 54 (NO1). The correlation is low for the α-dicarbonyls, with several of the stations actually showing negative correlation coefficients. It should be noted that for most of the stations the glyoxal and methylglyoxal concentrations were below the detection limit at more than half of the measurements. For Mace Head (IE31) the α-dicarbonyls were measured at 22 different days and every time the concentrations were below the detection limit.

The reasonable agreement between calculated and observed concentrations for formaldehyde indicates that the model may be of some use for studying the distribution of this compound. The model chemistry is, however, not intended for calculating realistic concentrations of the α-dicarbonyls and butanone.

3.3.3   PAN

The comparison of observed and calculated PAN concentrations is complicated by the fact that the model component PAN represents a number of different molecules. Detailed simulations with explicit representation of different PAN-like components indicate that up to 30% of the PAN in the model calculations is due to other components and not to PAN itself (Altenstedt, 1998). Figure 3.13 shows a timeseries of observed and calculated PAN concentrations at the station Kollumerwaard in the Netherlands. This is the only location where we have had access to observations of PAN. There is a good correspondence on both daily and longer time scales. The correlation coefficient between the observed and calculated three-hour average concentrations is 0.58 and the calculated average PAN concentration for the whole six-month period is 0.60 ppb(v) which can be compared to an observed value of 0.49 ppb(v).
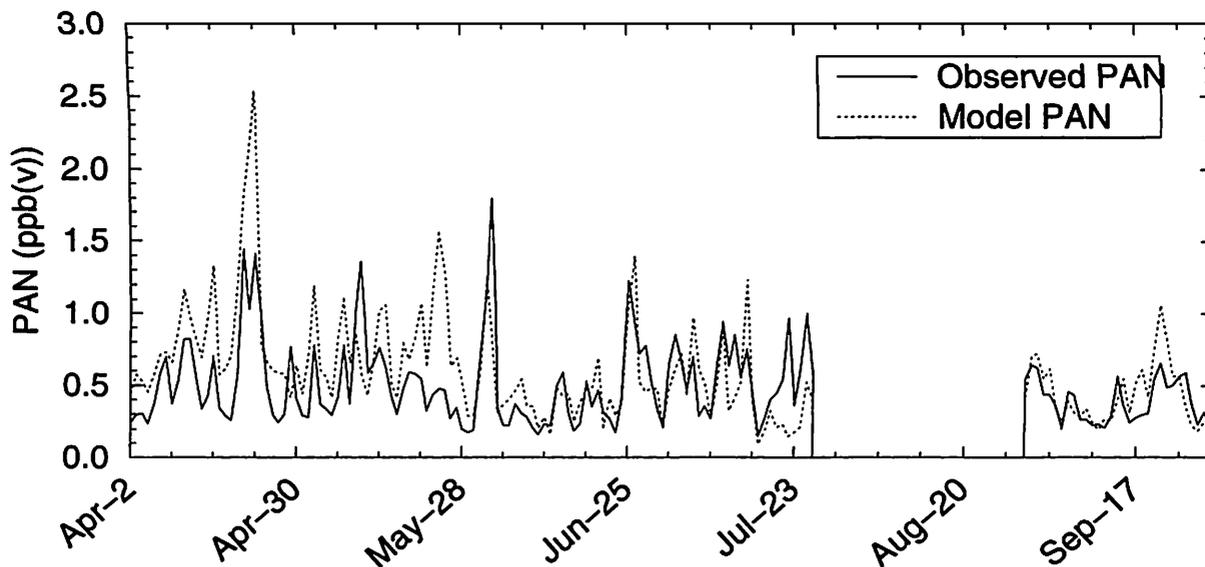
Figure 3.13 Observed and model calculated timeseries of diurnal average surface concentration of PAN at Kollumerwaard in 1994. Units: ppb(v).

3.4 Ozone

One of the primary aims of the present work has been to develop a model capable of simulating the concentration of surface ozone for time periods up to several months. A more exhaustive evaluation of the performance with regard to ozone is therefore presented below.

Figure 3.14 shows monthly average surface ozone concentrations for the six simulated months in 1994. The model predicts a distinct seasonal variation over large parts of the land area of western and central Europe, with monthly average concentrations exceeding 40 ppb(v) in July and lower concentrations in spring and fall. The highest concentrations are however found over the surrounding ocean areas. This is due to the low dry deposition velocity applied to ozone over water surfaces.

Figure 3.15 shows a comparison between timeseries of observed hourly average and model calculated three-hourly average concentrations of ozone at 14 selected stations.

Figure 3.16 shows a scatterplot comparing average concentrations for the whole six-month period. All of the calculated averages except one are within a plus/minus 40% of the observations. The exception is the Swiss station Sion (CH31), for which the model overestimates the mean ozone concentration by more than 60%. The model does not reproduce the extremely low ozone concentrations at night at this station. This is true also for some other stations but at these the model underestimates the high ozone concentrations at daytime, which leads to the effect that the model mean concentration is fairly close to the observed one.

Correlation coefficients and observed and calculated averages for all the stations are listed in Table 3.7. For more than half of the stations the correlation coefficient, r, is above 0.5 and only for 14 of the 81 stations r is below 0.4. The average correlation is 0.54.
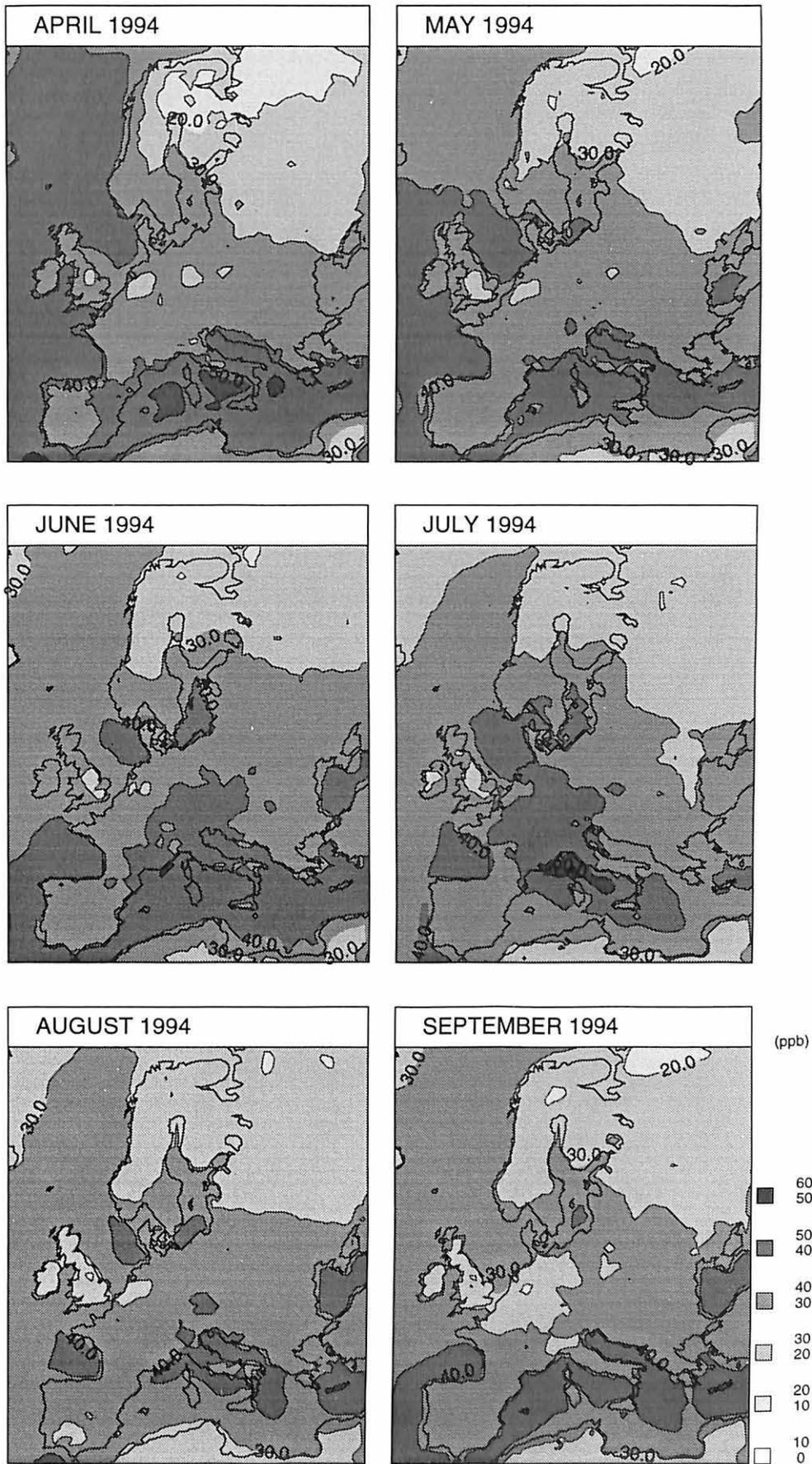
Figure 3.14 Surface ozone for April-September 1994, model calculated monthly average concentration. Unit: ppb(v).
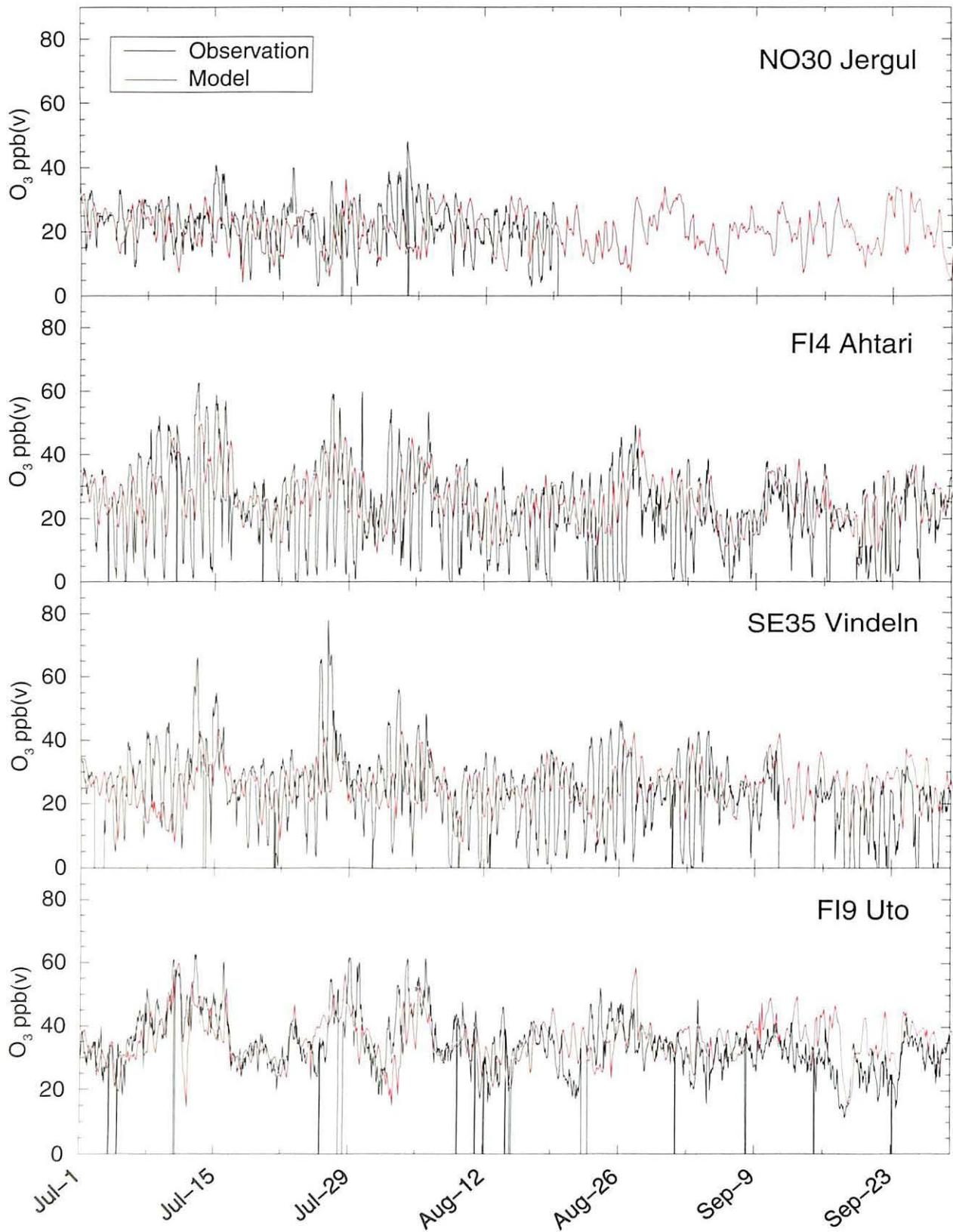
Figure 3.15a Timeseries of observed (1-h) and model calculated (3-h) average surface concentration of ozone at Jergul, Ähtäri, Vindeln and Utö in 1994. Units: ppb(v).
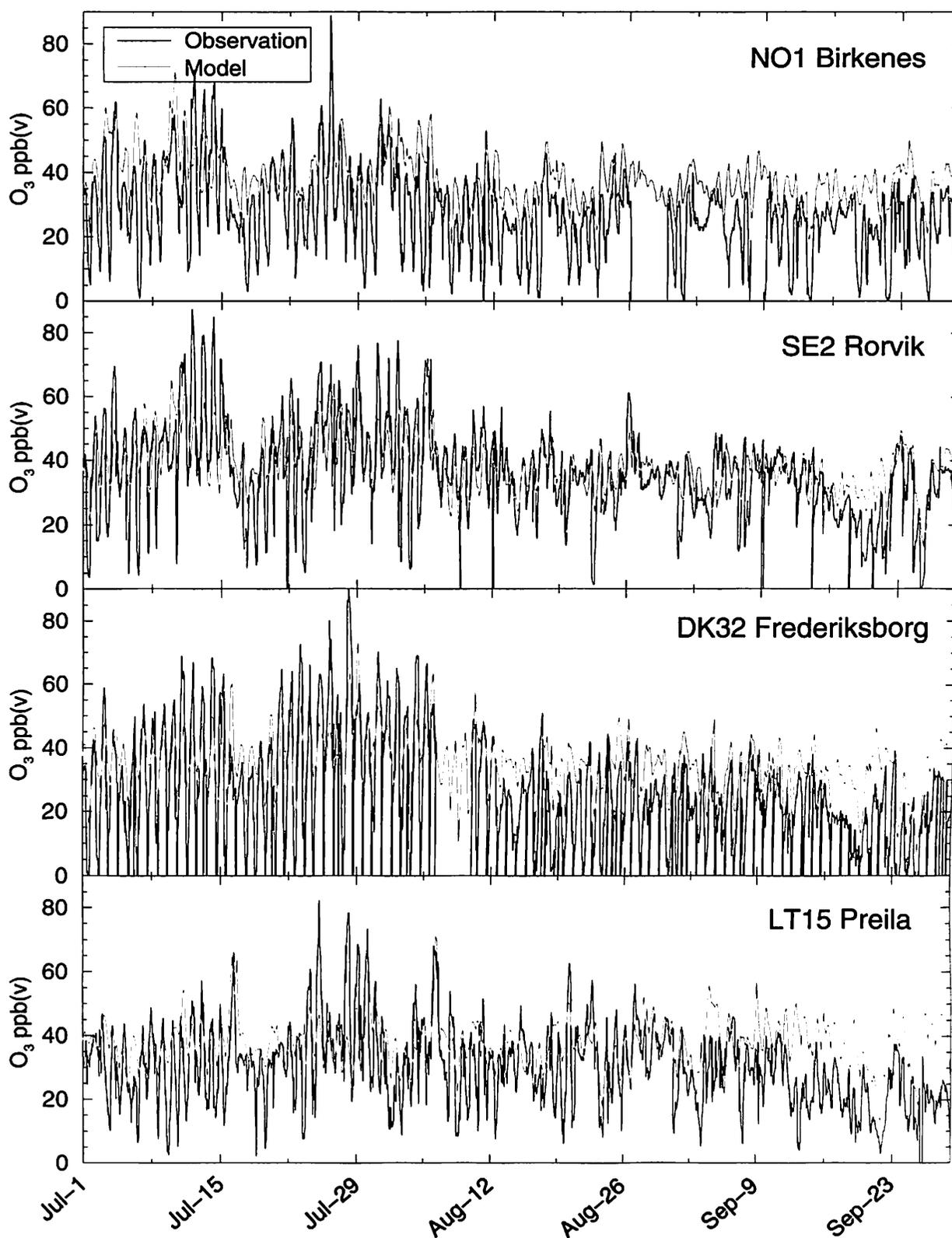
Figure 3.15b Timeseries of observed (1-h) and model calculated (3-h) average surface
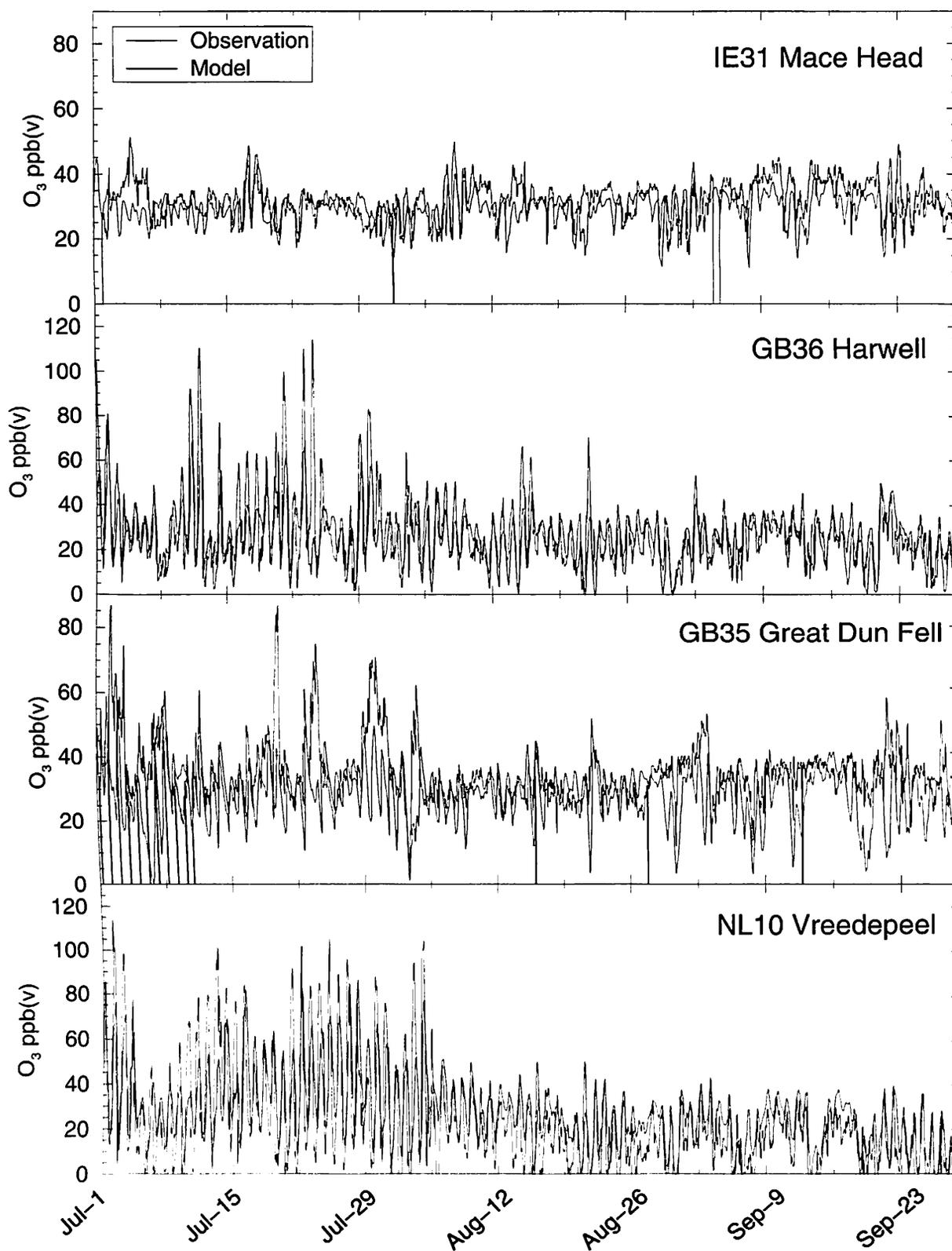concentration of ozone at Birkenes, Rörvik, Frederiksborg and Preila in 1994.
Units: ppb(v).

37

Figure 3.15c Timeseries of observed (1-h) and model calculated (3-h) average surface
concentration of ozone at Mace Head, Harwell, Great Dun Fell and
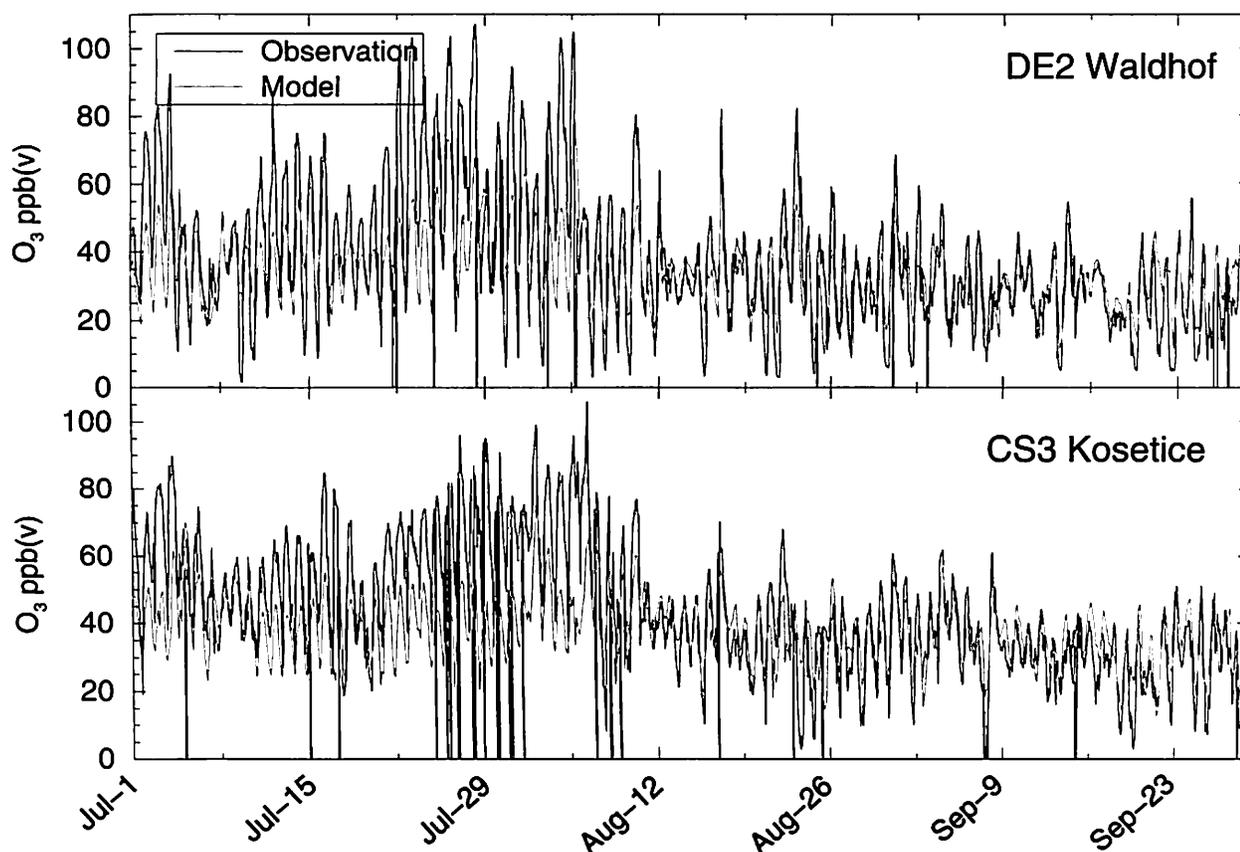Kollumerwaard in 1994. Units: ppb(v).

Figure 3.15d Timeseries of observed (1-h) and model calculated (3-h) average surface concentration of ozone at Waldhof and Kosetice in 1994. Units: ppb(v).

Table 3.7. Ozone concentration (ppb(v)) and correlation coefficients between observed and calculated diurnal mean concentrations

Station	Observed mean conc.	Model mean conc.	Correlation coefficient
AT02	40.2	37.1	0.69
AT03	33.1	36.3	0.63
AT04	47.9	39.2	0.48
CH02	32.2	36.7	0.65
CH03	33.7	37.3	0.71
CH04	47	39	0.62
CH05	46.4	35	0.60
CH31	23.2	37.4	0.42
CS01	50.5	35.9	0.53
CS03	43.8	38.1	0.72
DE01	37.1	37	0.58
DE02	37.9	34.1	0.79
DE03	50.1	37.5	0.56
DE04	39.8	36.5	0.72
DE05	53.2	38.7	0.41
DE07	33.6	37.9	0.70
DE08	41.1	35.6	0.53
DE09	35	36.9	0.60
DE11	31.1	34.6	0.63
DE12	36.2	33.8	0.80
DE17	29.3	36	0.78
DE26	30	40.3	0.71

Station	Observed mean conc.	Model mean conc.	Correlation coefficient
DE35	33.2	33.4	0.53
DK31	36.3	35.8	0.48
DK32	30.3	36.2	0.46
ES01	43.5	34.3	0.25
ES02	35.6	36.4	0.56
ES03	30.1	36.5	0.11
ES04	36.6	35.1	0.50
ES05	36.3	36.7	0.02
FI04	28	26.2	0.43
FI09	33.5	36.2	0.45
FI17	27.1	32.1	0.45
FI22	31.3	21.5	0.32
GB02	30.1	31.3	0.67
GB06	25.9	32.8	0.68
GB13	31.2	33.1	0.61
GB14	33.9	30	0.66
GB15	36.6	34	0.68
GB31	35.6	29.6	0.58
GB32	23.6	24.1	0.71
GB33	30.1	29.1	0.63
GB34	22.2	24.6	0.66
GB35	35.9	31.5	0.35
GB36	30.6	27.5	0.72
GB37	30.8	24.8	0.56
GB38	34.8	28.9	0.70
GB39	32.9	33	0.70
GB41	32.7	31.6	0.54
IE31	35.6	33	0.66
IT04	34	35.6	0.56
LT15	30.2	38.3	0.45
LV10	31.6	36.9	0.44
NL02	25.6	33.5	0.73
NL09	29.7	38.5	0.72
NL10	25.8	28.8	0.76
NO01	30.3	38.8	0.57
NO15	32.3	28.8	0.46
NO30	29.6	21.3	0.08
NO39	28.3	31.2	0.50
NO41	33.1	30.2	0.46
NO43	31.3	35.5	0.72
NO44	27.4	32.1	0.53
NO45	37.2	35.5	0.71
NO47	23.8	21.3	0.23
NO48	32.7	31.5	0.54
NO51	34.7	38.7	0.58
PT04	30.2	37.8	0.35
SE02	38	38.8	0.64
SE11	35.9	37.3	0.60
SE12	35.7	38.3	0.53
SE13	35.7	22.5	0.08
SE32	39.4	35.5	0.54
SE35	29.7	26.1	0.30
SI31	41.3	38.4	0.39
SI32	48.3	37.3	0.30
SI33	38.6	37.3	0.39
SK04	39.5	36.3	0.55
SK06	28.4	35.2	0.26
TR01	47.1	34.8	0.47

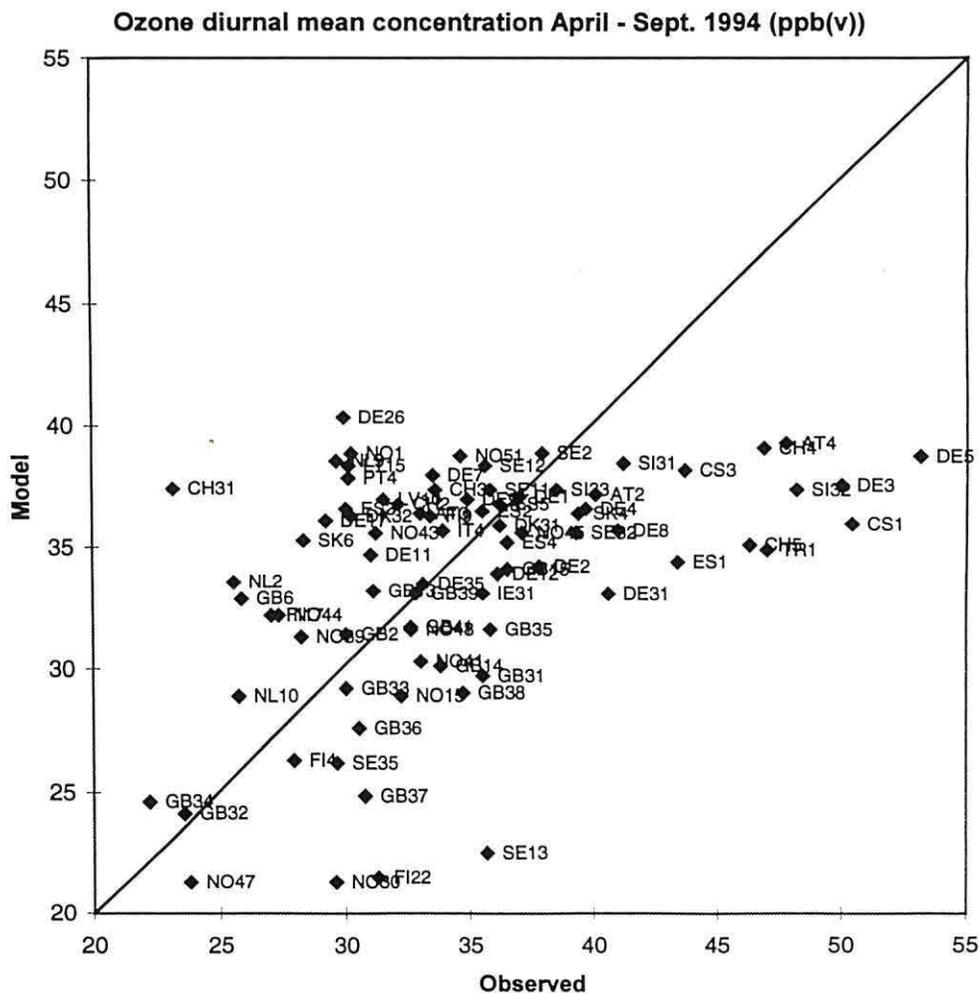**Ozone diurnal mean concentration April - Sept. 1994 (ppb(v))**

Figure 3.16 Scatterplot of observed and model calculated six-month (April-September 1994) average surface concentrations of ozone. Units: ppb(v).

3.4.1 *AOT40 and AOT60*

The comparison with observed concentrations presented above provides a good description of the general performance of the model with regard to predicting surface concentrations. However, effects on vegetation and on human health have been found to correlate better with accumulated ozone exposure over certain threshold concentrations, AOT. Taking AOT40 as an example the definition is given by:

$$AOT40 = \int_{t=0}^{t=T} \max(O_3 - 40, 0)dt$$

where $\max(x, 0) = x$ if $x > 0$; $\max(x, 0) = 0$ if $x < 0$.

The currently recommended threshold concentrations and integration periods for crops and forests derive from a UN-ECE workshop in Kuopio, Finland (Kärenlampi and Skärby, 1996). For crops the threshold is set to 40 ppb(v) and the AOT value should be evaluated for daylight
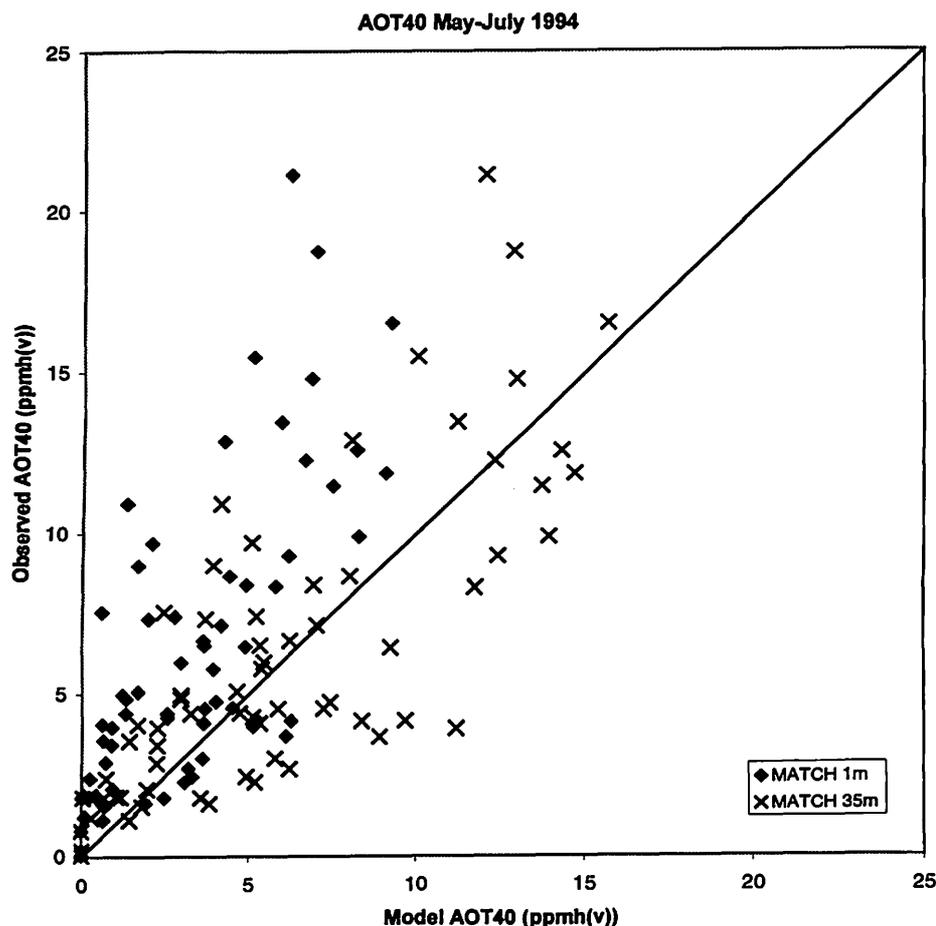
41

AOT40 May-July 1994

Figure 3.17a Scatterplot of observed and model calculated AOT40 May-July 1994. Units: ppmh(v).

hours (defined as those hours with mean global radiation exceeding 50 W m^{-2}), over a three month growing season (May-July). The critical level is set to 3000 ppb hours. For forests 40 ppb(v) is also used as the threshold concentration but the evaluation should be over a six month growing season (April-September). The critical level in this case is set to 10000 ppb hours. For health effects a threshold concentration of 60 ppb(v) can be used, based on the revised WHO standard of 120 μg m^{-3} as an 8-hour moving average. Here we use AOT60 as a preliminary measure of ozone levels above the WHO guideline.

In this model study we have used a somewhat simplified method to calculate AOT40 values. Instead of using the true daylight hours for computing the AOT40 we have simply used the 12-hour period 0600 - 1800 UTC and evaluated the AOT40 only for these hours. This means that the AOT40 values calculated do not correspond exactly with the UN-ECE recommendation but the deviation is expected to be reasonably small. The same hours were used for calculating both the "observed" and model AOT40 but an important difference between the two values is that the ozone observations used are hourly measurements while the model concentrations are three-hour mean values. This is expected to lead to some underestimation of the AOT40 value by the model. In order to investigate the size of this deviation we have checked how much the AOT40 value changes when the observed concentrations are first converted to three-hour mean concentrations before the calculation of
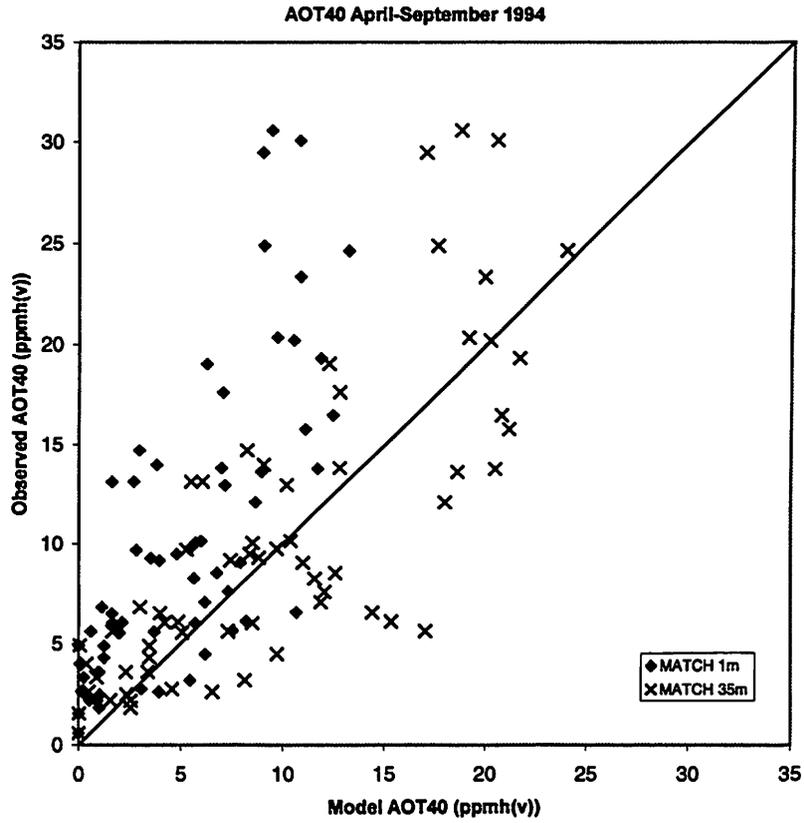
42

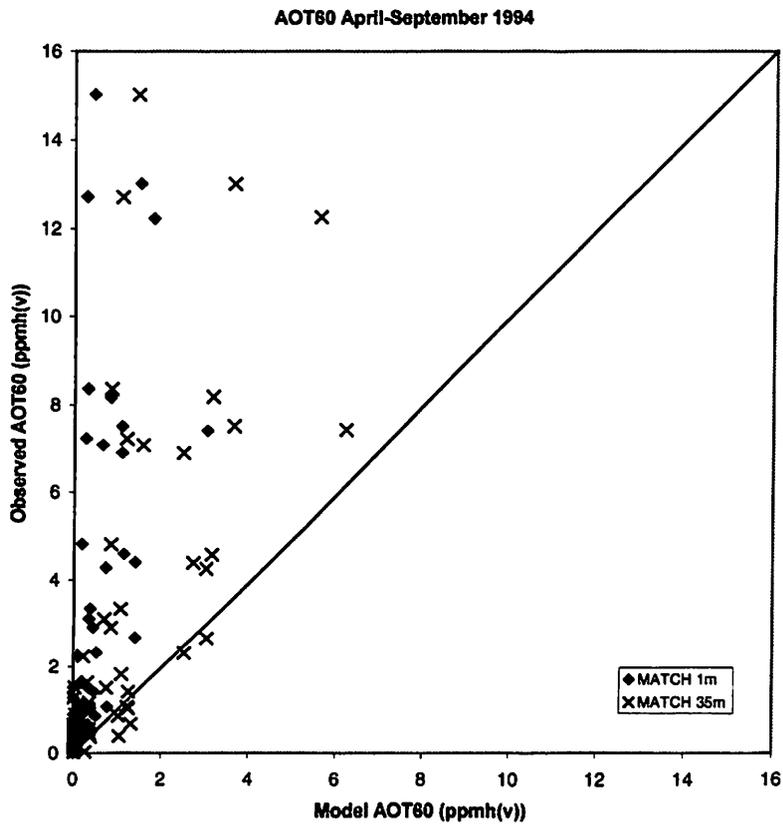Figure 3.17b Scatterplot of observed and model calculated AOT40 April-September 1994. Units: ppmh(v).

Figure 3.17c Scatterplot of observed and model calculated AOT60 April-September 1994. Units: ppmh(v).
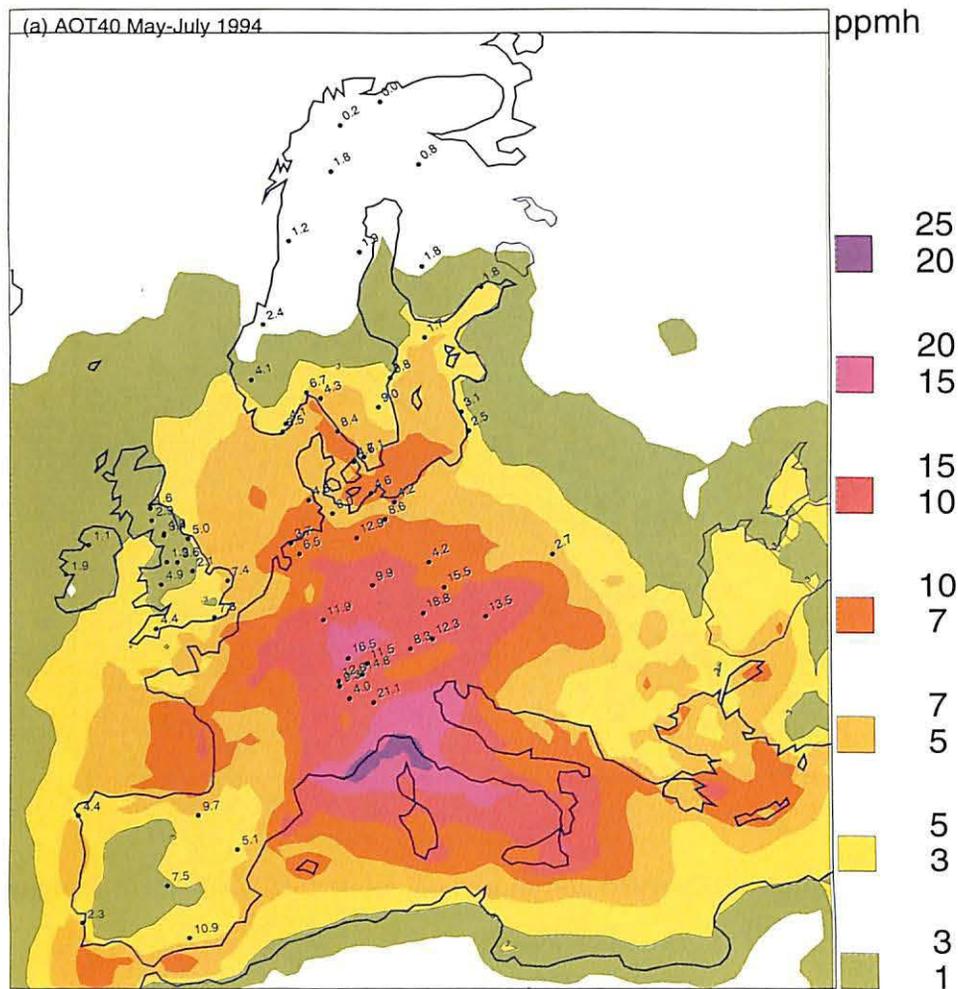
Figure 3.18a Observed and model calculated AOT40 May-July. Units: ppmh(v).

the AOT. For most of the stations the difference turns out to be small for the AOT40-values. For AOT60 the difference is much larger.

Figure 3.17 shows scatterplots comparing observed and model calculated AOT40 for crops and forest and AOT60. The same information is also given in Tables 3.8 and 3.9. Results are given for both the lowest model level and adjusted to the one meter level (c.f. section 3). Looking at the results for one meter the model shows a clear tendency towards underestimation for all three statistics. For 35 m the bias is much smaller for AOT40 while AOT60 is still underestimated. This highlights that the model has difficulties in catching the high ozone concentrations since these are important in determining the AOT statistics, but it is also clear that knowledge of the actual observation height and surface characteristics around the measurement stations are important factors to consider when evaluating model calculations. The correlation coefficients are 0.72, 0.73 and 0.59 for AOT40 crops, AOT40 forest and AOT60, respectively, for the one meter level. The corresponding values for the 35 m level are 0.78, 0.78 and 0.68.

Figure 3.18 shows the model calculated distribution of the three AOT statistics evaluated at 35 m, also indicated are the observed values. These figures show that the overall pattern is in good agreement with the observations although the model underestimates AOT60. The calculations indicate exceedance of the critical levels for AOT40 for large parts of western and central Europe.
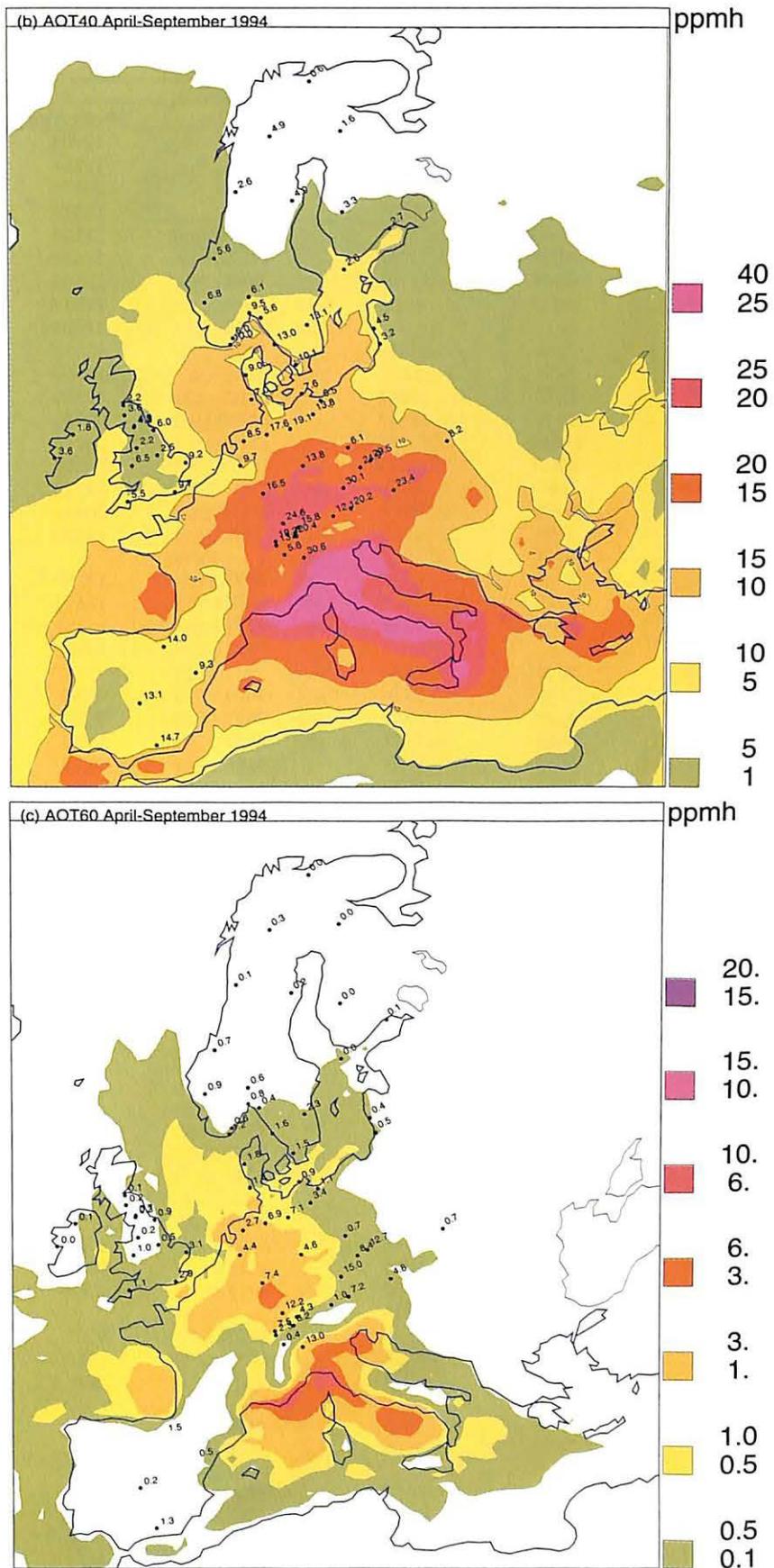
Figure 3.18b Observed and model calculated AOT40 April-September and AOT60 April-September for. Units: ppmh(v).

Table 3.8. AOT40 (ppb h)

Station	May-July Model 1m	Model 35m	Observed	April-Sept Model 1m	Model 35m	Observed
AT02	5894	11146	13467	10827	19904	23352
AT03	5788	11750	8322	8634	17961	12094
AT04	6626	12284	12265	10490	20175	20208
CH02	6164	12386	9277	8917	18574	13629
CH03	7460	13680	11471	11070	21105	15781
CH04	8157	14268	12568	11822	21621	19318
CH05	6791	12908	14795	9688	19105	20351
CH31	5136	11235	4016	7544	17038	5627
CS01	-	-	-	8953	17004	29478
CS03	5080	9968	15479	9038	17571	24899
DE01	4015	7458	4780	6198	11869	7049
DE02	4200	8004	12882	6232	12221	19053
DE03	9190	15653	16517	13200	23981	24639
DE04	9021	14644	11856	12408	20739	16470
DE05	6964	12853	18767	10777	20523	30089
DE07	4395	7989	8643	6962	12772	13812
DE08	8248	13890	9877	11680	20448	13775
DE09	4522	7268	4582	7339	12050	7578
DE11	2964	5447	5981	-	-	-
DE12	-	-	-	6997	12750	17626
DE26	6296	8412	4203	10680	14419	6546
DE35	5232	9708	4246	8221	15353	6102
DK31	-	-	-	7924	10981	9037
DK32	3684	5890	4563	-	-	-
ES01	570	2430	7546	1604	5492	13137
ES02	1307	4128	10936	2931	8207	14722
ES03	1672	4638	5077	3525	8820	9280
ES04	2072	5060	9705	3788	9019	13980
ES05	2552	4734	4429	-	-	-
FI04	190	666	1828	262	884	3334
FI09	1907	3838	1665	3948	6563	2603
FI17	2468	3581	1843	3076	4586	2742
FI22	0	0	811	3	21	1563
GB02	720	2260	2905	1014	3400	3591
GB06	656	1436	1138	1006	2564	1838
GB13	1309	3266	4410	1994	5084	5550
GB14	1200	2965	4985	1645	4209	6047
GB31	1308	2962	4867	1620	3988	6516
GB32	928	1951	2099	1040	2362	2478
GB33	698	1816	1569	918	2558	2178
GB34	438	1042	1867	535	1562	2213
GB35	890	2268	3984	1240	3473	4901
GB37	640	1422	3579	-	-	-
GB38	1977	3685	7327	2800	5269	9706
GB39	2762	5214	7407	3944	7445	9159
GB41	890	2268	3444	1240	3473	4302
IE31	482	1170	1854	950	2325	3586
IT04	6176	11998	21130	9404	18730	30597
LT15	3336	4949	2488	5468	8161	3169
LV10	3641	5823	3056	6221	9735	4468
NL02	4900	9261	6459	6782	12596	8527
NL09	6138	8950	3733	-	-	-
NL10	-	-	-	5432	9701	9746
NO01	3664	5339	4119	5726	8513	5998
NO15	98	300	1223	162	503	2638
NO30	0	1	201	-	-	-
NO39	245	738	2408	598	1635	5634
NO43	2562	5139	4306	3695	7326	5593
NO44	-	-	-	2118	4867	6063
NO45	3635	6235	6655	4800	8376	9474
NO47	0	0	40	0	5	585
NO48	600	1677	4069	1130	2991	6827
NO51	3664	5339	6512	5726	8513	10044
PT04	3108	5216	2324	-	-	-
SE02	4899	6916	8374	7136	10165	12951
SE11	4166	7039	7133	5992	10377	10135
SE12	3926	5379	5781	-	-	-
SE13	2	34	1825	12	71	4919

SE32	1666	3910	8998	2666	6038	13148
SE35	54	242	1893	84	384	3997
SK06	3212	6260	2738	5659	11572	8248

Table 3.9. AOT60 (ppb h)

Station	Model 1m	Model 35m	Observed
AT02	174	830	4831
AT03	332	1242	1040
AT04	256	1174	7240
CH02	512	2507	2343
CH03	712	2989	4294
CH04	1068	3615	7526
CH05	809	3134	8180
CH31	93	1043	391
CS01	261	1061	12717
CS03	296	829	8375
DE01	459	1247	1432
DE02	634	1548	7100
DE03	1772	5570	12242
DE04	3004	6184	7421
DE05	440	1426	15022
DE07	369	1050	3360
DE08	1119	3115	4617
DE09	499	1023	869
DE12	1074	2461	6924
DE26	764	1221	1085
DE35	333	1306	680
DK31	758	1082	1841
ES01	0	0	237
ES02	0	0	1275
ES03	27	147	521
ES04	0	32	1518
FI04	0	0	15
FI09	102	264	31
FI17	30	91	133
FI22	0	0	2
GB02	0	18	201
GB06	27	44	72
GB13	157	333	1050
GB14	39	146	874
GB31	80	350	1015
GB32	23	101	550
GB33	0	0	121
GB34	2	10	168
GB35	3	89	727
GB38	434	840	2923
GB39	346	689	3127
GB41	3	89	328
IE31	0	0	7
IT04	1473	3596	13018
LT15	234	367	457
LV10	148	386	380
NL02	1386	3018	2693
NL10	1379	2694	4426
NO01	242	358	556
NO15	0	0	141
NO39	0	0	662
NO43	47	160	448
NO44	6	43	610
NO45	41	166	772
NO47	0	0	4
NO48	10	50	891
NO51	242	358	1179
SE02	172	315	1650
SE11	342	746	1523
SE13	0	0	323
SE32	108	216	2254
SE35	0	0	232
SK06	0	70	712

3.5   Deposition

Observations of wet deposition are available from the EMEP network for a range of inorganic components on a daily basis. Here we focus on deposition of oxidized nitrogen and sulfur.

Before looking at the results some comments on the quality of the precipitation fields used in the calculations are appropriate. In the present study we have used the forecasted precipitation fields from the HIRLAM model. It is generally difficult to forecast precipitation accurately and relatively large errors in both location and amounts of precipitation are common for current NWP models compared to forecasts for parameters like wind speed or temperature. In addition it takes time to spin up the hydrological cycle in the NWP models, which means that the precipitation forecast is usually better for longer forecast lengths, e.g. between 6 and 12 hours. In the present study we have only had access the precipitation from the 3- and 6- hour forecast which means that we have not used the optimum forecasted precipitation.

For more detailed assessment work it would be possible use observed precipitation or a combination of observations and forecasted precipitation. Such information can, however, not be used in forecast mode.

The description of wet scavenging (c.f. section 2.4) is also quite simple. A more advanced scheme, which accounts for the differences between convective and stratiform precipitation, could be implemented

3.5.1   Oxidized nitrogen

Figure 3.19 shows the calculated accumulated dry and wet deposition for the simulated six-month period. The geographical distribution reflects roughly the distribution of the emissions, especially for dry deposition. The efficiency of the dry deposition of some of the nitrogen components is lower over water surfaces, which is clearly reflected in the dry deposition field. The wet deposition is strongly influenced by the distribution of precipitation. This can be seen for example along the west coast of Norway.

Figure 3.20 shows a comparison between observed and model calculated wet deposition for the six-month period. The model has a tendency to overestimate wet deposition, but for almost all of the stations the model predictions are within a factor of two from observed, which is encouraging considering the uncertainties in the precipitation fields used. Correlation coefficients are given in Table 3.10.

3.5.2   Sulfur

The calculated dry and wet deposition of sulfur are shown in Figure 3.21. As for oxidized nitrogen the geographical distribution reflects roughly the distribution of emissions. The difference in dry deposition between water and land surfaces is not as pronounced as for the nitrogen components.

Figure 3.22 shows a comparison between observed and model calculated wet deposition for the six-month period. As for oxidized nitrogen the model has a tendency to overestimate wet deposition. In this case the overestimation is more pronounced, but for the majority of the stations the model predictions are within a factor of two from observed. Correlation coefficients are given in Table 3.10.
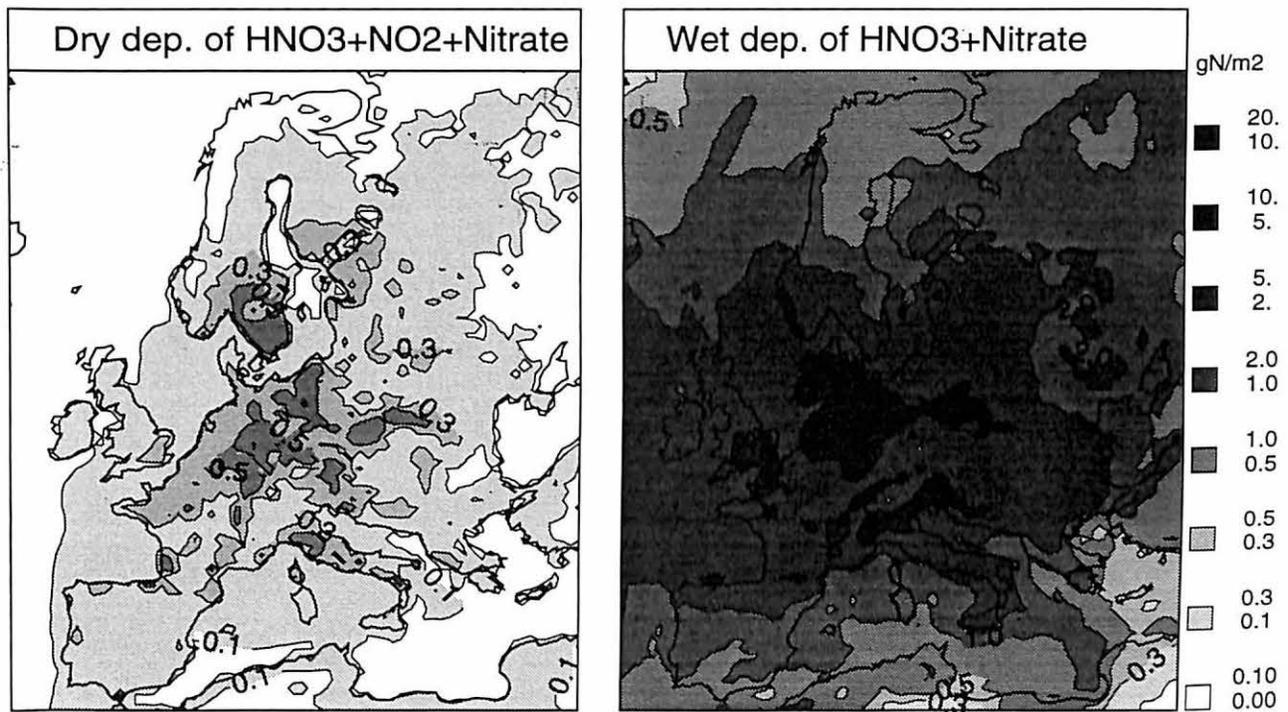
Figure 3.19 Six-month accumulated (April-September 1994) model calculated dry and wet deposition of NO_3^-. Units: mg N/m^2
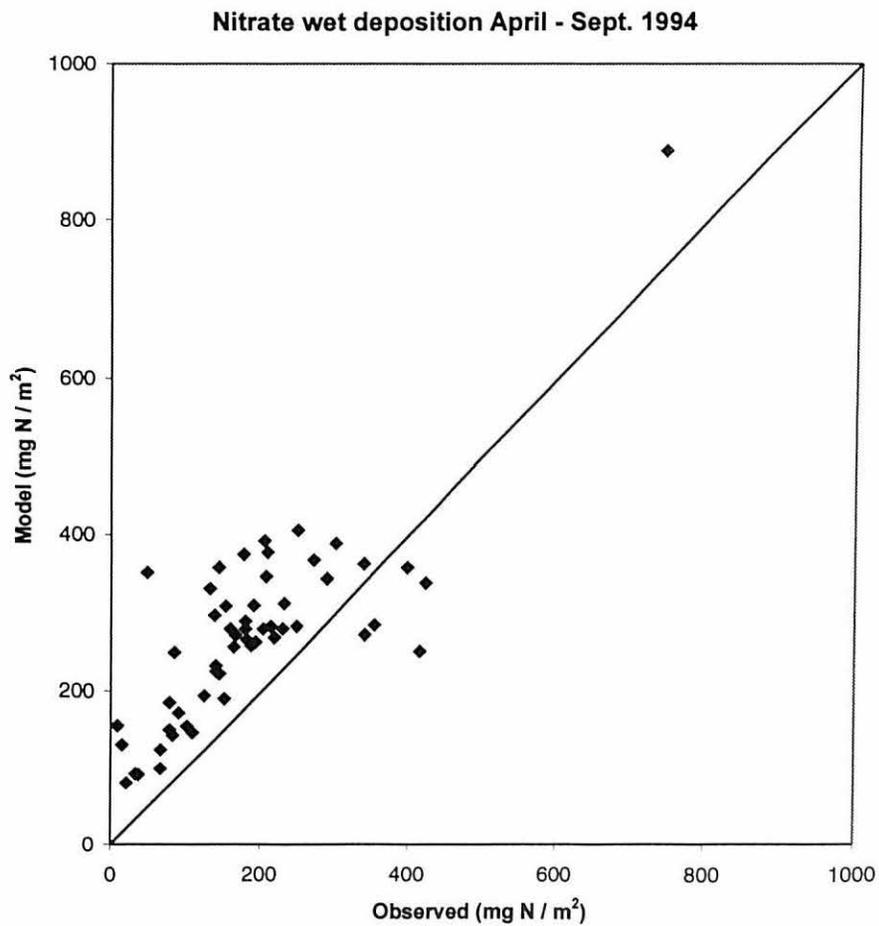

Figure 3.20 Scatterplot of observed and model calculated wet deposition of NO_3^- for April-September 1994. Units: mg N/m^2.
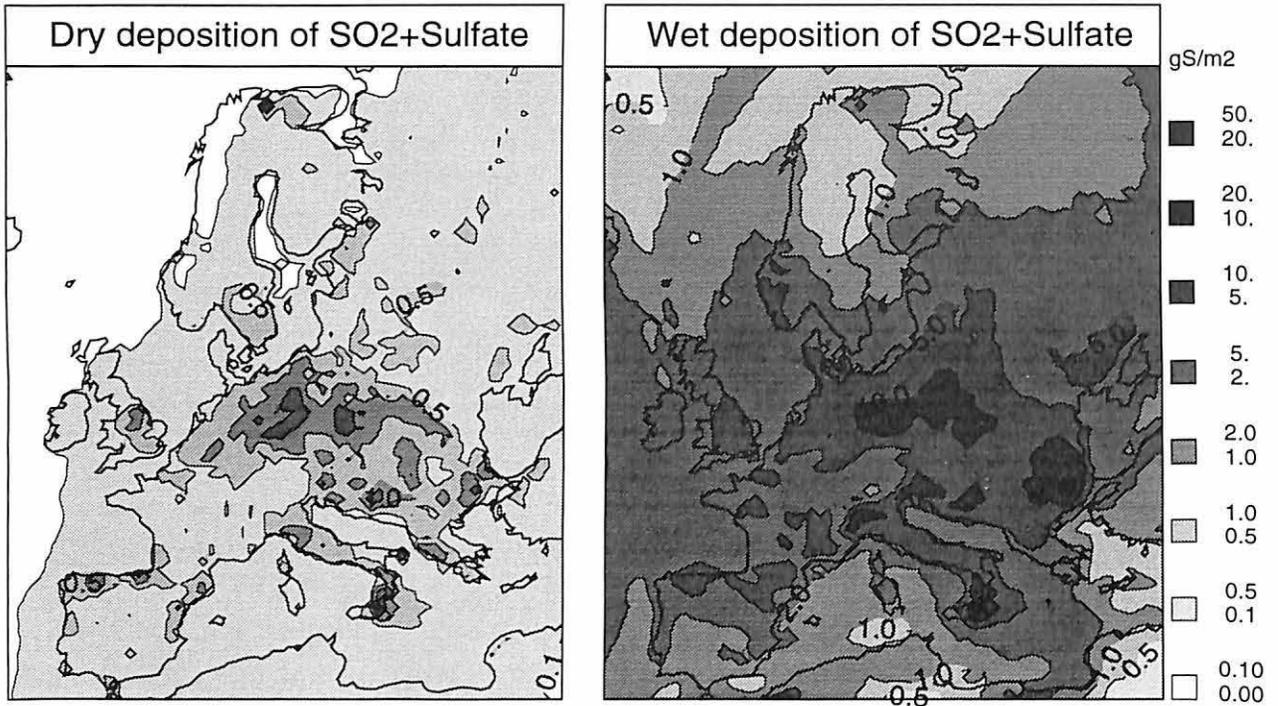
49

Figure 3.21 Six-month accumulated (April-September 1994) model calculated dry and wet deposition of SO_4^{2-}. Units: mg S/m²
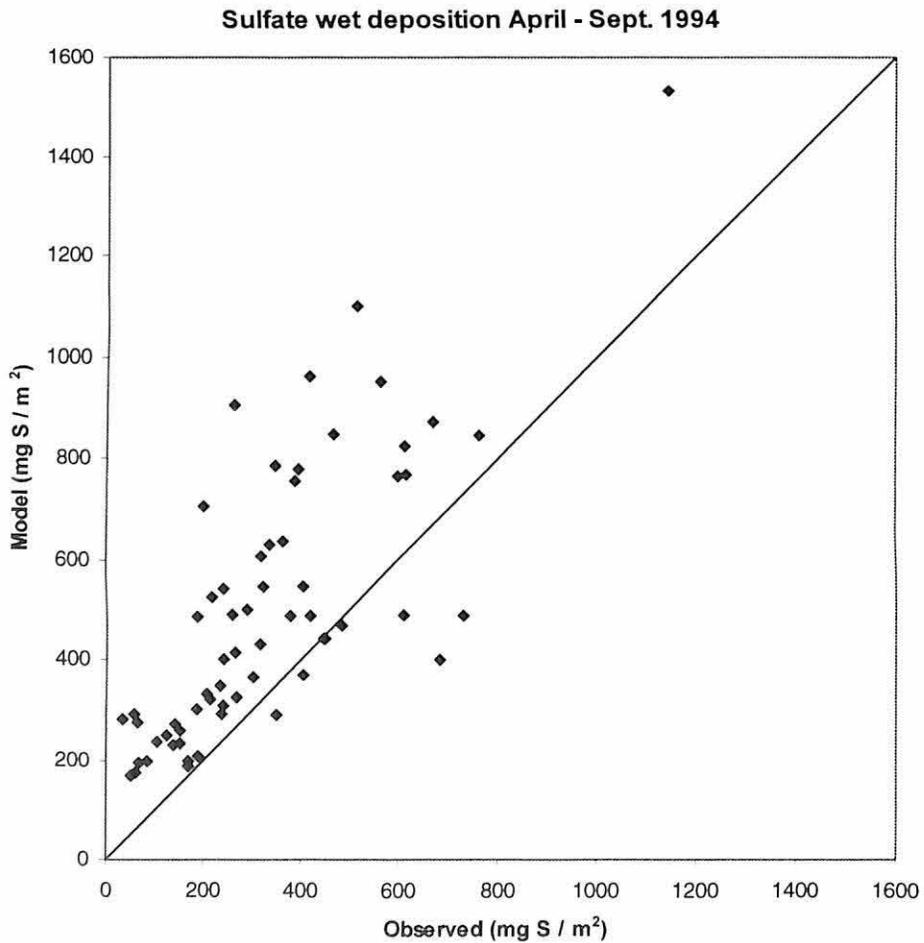

Figure 3.22 Scatterplot of observed and model calculated wet deposition of SO_4^{2-} for April-September 1994. Units: mg S/m².

Table 3.10. Wet deposition of oxidized nitrogen and sulfur for the six-month period April – September, 1994 (mg N/m^2, mg S/m^2) and correlation coefficients between observed and calculated daily deposition

Station	N measured dep.	model dep.	correl. coeff.	S measured dep.	model dep.	correl. coeff.
AT02	158	281	0.01	334	629	0.01
AT03	204	392	0.11	257	488	0.08
AT04	288	344	0.09	416	483	0.04
CH02	202	281	0.10	302	365	0.08
CS01	230	313	0.36	507	1096	0.26
CS03	186	260	0.14	344	784	0.08
DE01	270	367	0.16	403	543	0.09
DE02	249	405	0.08	385	753	0.07
DE03	421	338	0.13	679	396	0.13
DE04	208	377	0.12	289	498	0.08
DE05	217	270	0.12	374	485	0.09
DE07	176	375	0.06	392	778	0.06
DE08	300	388	0.08	594	765	0.15
DE09	152	310	0.12	241	541	0.11
DK03	206	347	0.23	322	542	0.13
DK05	189	311	0.25	319	606	0.18
ES01	-	-	-	188	209	0.00
ES02	66	100	0.00	170	189	0.00
ES03	151	191	-0.01	198	705	0.05
ES04	84	250	0.04	218	525	0.04
ES05	-	-	-	350	290	0.01
FI04	66	125	0.20	138	232	0.17
FI09	82	144	0.24	153	261	0.17
FI17	101	156	0.43	268	324	0.34
FI22	37	92	-0.02	83	199	-0.02
FR03	165	273	0.01	240	399	0.00
FR08	396	357	0.10	604	483	0.07
FR09	143	359	0.02	186	486	0.00
FR10	247	284	0.02	404	367	0.04
GB02	139	233	0.42	263	412	0.05
GB06	-	-	-	213	322	-0.03
GB13	180	267	0.38	241	401	0.21
GB14	137	298	0.08	262	905	0.02
GB15	-	-	-	57	294	0.05
HR02	338	362	0.05	611	767	0.14
HR04	413	252	0.40	728	486	0.41
HU02	178	281	0.06	462	846	0.05
IE01	-	-	-	185	302	0.03
IT04	741	888	0.41	1140	1531	0.32
NL09	48	352	0.10	-	-	-
NO01	352	285	0.53	443	438	0.40
NO08	339	273	0.26	482	464	0.18
NO15	-	-	-	68	195	0.48
NO30	21	81	0.00	52	170	0.00
NO39	-	-	-	126	249	0.00
NO41	78	151	0.32	104	239	0.17
NO43	124	195	0.16	236	292	0.09
NO44	108	148	0.15	153	234	0.06
PL05	192	264	0.34	363	633	0.30
PT01	9	156	-0.01	35	282	-0.02
PT03	78	186	0.03	241	309	0.01
PT04	15	131	0.03	64	276	0.04
RU01	-	-	-	141	273	-0.01
RU13	-	-	-	169	197	-0.02
RU14	-	-	-	447	439	0.07
SE02	144	223	0.19	232	347	0.12
SE05	33	93	0.44	61	177	0.37
SE11	163	258	0.22	315	429	0.20
SE12	90	173	0.19	206	332	0.10
SK02	228	281	0.06	760	847	0.12
SK04	178	291	0.13	558	950	0.07
SK05	212	284	0.04	610	823	0.05
SK06	131	332	0.04	412	960	0.07
YU05	140	226	0.01	666	870	0.04

4. Summary and conclusions

An atmospheric chemistry module with 56 chemical components has been implemented in the MATCH model. The aim has been to develop a model platform that can be used as a basis for a range of regional scale studies in atmospheric chemistry, including assessment of the importance of different sources of pollutants to the levels of photochemical oxidants and air pollutant forecasting. Meteorological input data to MATCH was taken from archived output from the operational version of HIRLAM at SMHI. The evaluation of model calculations over Europe for a six-month period in 1994 shows good results considering known sources of error and uncertainties in input data and model formulation.

The results for primary components show the largest deviations between model calculations and observations. Apart from difficulties with the representativity of the observations this can to a large extent be attributed to uncertainties in emission data and to the limited horizontal and vertical resolution of the model. The correlation coefficient between daily observed and calculated values is above 0.5 at more than a third of the stations for SO_2. For NO_2 the correlation between the observed and calculated concentration is generally lower than for SO_2.

A limited amount of observational data is available for primary hydrocarbons. A surprisingly good correspondence between model calculations and observations was found for several of the hydrocarbons of anthropogenic origin. The results are best for the hydrocarbons with long residence times like ethane and n-butane. For these components the average calculated concentrations are within a factor of two from the corresponding observed hydrocarbon concentrations for most stations and the correlation coefficient is above 0.8 at four stations for ethane. The agreement for hydrocarbons with shorter residence times is worse but still rather good considering the uncertainties related to emission data and formulation of the chemical scheme.

For isoprene, the only biogenic hydrocarbon included, the results are not so good, with low and sometimes negative correlation and large deviations between observed and calculated average concentrations, exceeding a factor of 10 at several locations. This indicates that the isoprene emissions used are probably quite far from being realistic.

The results for secondary components are generally better than for primary components. Average concentrations of HNO_3 + NO_3^- are with few exceptions within a factor of two from the observations. The correlation coefficients are above 0.5 for more than half of the stations. For sulfate the model has a tendency for underprediction but the correlation is generally higher than for HNO_3 + NO_3^-, with r-values above 0.8 for several stations.

The agreement between calculated and observed concentrations for formaldehyde is reasonably good, indicating that the model may be of some use for studying the distribution of this compound.

Comparison of model calculations with over 80 stations with hourly measurements of ozone shows that the model is capable of predicting average surface concentrations of ozone within plus/minus 40%, with a correlation coefficient above 0.5 for more than half of the stations. The general geographical variation of surface ozone is well described by the model. When looking at AOT40 and AOT60 statistics it is evident, however, that the model underestimates high ozone concentrations. This is probably due to a combination of several factors, including model resolution and formulation and incomplete knowledge about emissions and surface characteristics.

The calculated wet deposition of nitrate and sulfate show a tendency for overprediction compared to the observed deposition. Accumulated deposition for the six-month period is

within a factor of 2 for most of the stations. Given that model derived, and not observed, precipitation fields were used, this result is encouraging, considering also that the precipitation fields were not taken from the optimal forecast lengths and that a fairly simple description of wet scavenging was used.

In summary we think that the combination of meteorological data from HIRLAM, the MATCH model and the modified chemical scheme from the EMEP model gives good results considering known sources of error. With limited further work the system is sufficiently good to be applied for scenario studies and for regional scale air pollutant forecasts. Future work to improve and extend the capabilities of the model system include:

- Improved treatment of radiation and calculation of photolysis rates
- Improved description of dry deposition using more detailed information about landcover
- Improved description of cloud and precipitation processes including aqueous phase chemistry
- Use of observed precipitation and improved wet scavenging scheme
- Higher resolution and nesting

Acknowledgment

References

Altenstedt, J. (1998) IVL, Personal communication.

Andersson-Sköld Y. and Simpson D. (1997) Comparison of the chemical schemes of the EMEP MSC-W and the IVL photochemical trajectory models. EMEP/MSC-W Note 1/97, Blindern, Oslo 3, Norway.

Atkinson, R. (1990) Gas-phase tropospheric chemistry of organic compounds: a review. *Atmos. Environ.* 24A, 1.

Barrett, K., Seland, Ø, Foss, A., Mylona, S., Sandnes, H., Styve, H. and Tarrasón, L. (1995) European transboundary acidifying air pollution. Ten years of calculated fields and budgets to the end of the first sulphur protocol. EMEP/MSC-W Report 1/95, The Norwegian Meteorological Institute.

Berge, E., Styve, H. and Simpson, D. (1995) Status of the emission data at MSC-W. EMEP MSC-W Note 2/95.

Blackburn, W. J. and Proctor, J. T. A. (1983) Estimating photosyntethically active radiation from measured solar irradiance. *Solar Energy* 31, 233-234.

Bott, A. (1989a) A positive definite advection scheme obtained by non-linear renormalization of advective fluxes. *Monthly Weather Rev.* **117**, 1006-1015.

Bott, A. (1992) Monotone flux limitation in the area preserving flux-form advection algorithm. *Monthly Weather Rev.* **120**, 2592-2602.

Berkowicz, R., Olesen, H. R. and Torp, U. (1986) The Danish Gaussian air pollution model (OML): Description, test and sensitivity analysis in view of regulatory applications. In *Proceedings of the 15th NATO/CCMS International Technical Meeting on Air Pollution Modelling and Its Application,* Plenum Press, New York.

Bringfelt, B. (1996) Tests of a new land surface treatment in HIRLAM, HIRLAM Technical Report No 23, Swedish Meteorological and Hydrological Institute, Norrköping, Sweden.

Builtjes, P.J., Stern, R.M. and Pankrath, J., PHOXA: The use of a photochemical dispersion model for several episodes in North-Western Europe, in *Air Pollution Modelling and its Application, Vol VI,* H. van Dop, ed., Plenum Press, New York (1988).

Burridge, D. M. and Gadd A. J. (1977) The meteorological office operational 10-level numerical weather prediction model. United Kingdom Meteorological Office. *Sc. Paper No 34*, 1-39.

Businger, J. A., Wyngaard, J. C., Izumi, Y. and Bradley, E. F. (1971) Flux-profile relationships in the atmospheric surface layer. *J. Atm. Sci.* **28**, 181-189.

Carmichel, G. and Peters, L. K. (1984) An Eulerian transport/transformation/removal model for SO_2 and sulfate - I. Model development. *Atmos. Environ.* **18**, 937-951.

Carter W. P. L. (1996) Condensed atmospheric photooxidation mechanisms for isoprene. *Atmos. Environ. 30,* 4275-4290.

Chamberlain, A. C. and Chadwick, R. C. (1965) Transport of iodine from atmosphere to ground. *Tellus* **18**, 226-237.

Chang, J. S., Brost, R. A., Isaksen, I. S. A., Madronich, S., Middleton, P, Stockwell, W. R. and Walcek, C. J. (1987) A three-dimensional Eulerian acid deposition model. Physical concepts and model formulation. *J. Geophys. Res.* **92**, 14681-14700.

Derwent, R. G. and Jenkin, M. E. (1990) Hydrocarbon involvement in photochemical ozone formation in Europe. *AERE Report* **R13736** (HMSO), London.

Derwent, R. G. and Jenkin, M. E. (1991) Hydrocarbons and the long-range transport of ozone and PAN across Europe. *Atmos. Environ.* **8**, 1661-1678.

European Space Agency (ESA) (1992) Remote Sensing Forest Map of Europe.

Hass, H., Memmesheimer, M., Geiß, H., Jakobs, H. J., Laube, M. and Ebel, A. (1990) Simulation of the Chernobyl radioactive cloud using the Eurad model. *Atmos. Environ.* **23A**, 673-692.

Hass, H., Builtjes, P.J.H., Simpson, D. and Stern, R. (1997) Comparison of model results obtained with several European regional air quality models. *Atmos. Environ.* **31**, 3259.

Henderson-Sellers, A., Wilson, M. F., Thomas, G., Dickinson, R. E. (1986) Current global land-surface data sets for use in climate related studies, NCAR/TN/272+STR, Atmospheric Analysis and Prediction Division, National Center for Atmospheric Research, Boulder, CO.

HIRLAM documentation manual, System 2.5, E. Källén (ed.), Swedish Meteorological and Hydrological Institute (1996).

Holtslag, A. A. M., Meijgard, E. and De Rooy, W. C. (1995) A comparison of boundary layer diffusion schemes in unstable conditions over land. *Boundary-Layer Met.* **76**, 69-95.

Josefsson, W. (1989) Computed global radiation using interpolated, gridded cloudiness from the meso-beta analysis compared to measured global radiation. Swedish Meteorological and Hydrological Institute, Report Meteorology No: 101.

Langner, J., Persson, C. and Robertson, L. (1995) Concentration and deposition of acidifying air pollutants over Sweden: Estimates for 1991 based on the MATCH model and observations, *Water, Air, and Soil Pollut.* **85**, 2021.

Langner, J., Robertson, L., Persson, C. and Ullerstig, A. (1998) Validation of the operational emergency response model at the Swedish Meteorological and Hydrological Institute using data from ETEX and the Chernobyl accident. *Atmos. Environ.* In press.

Moxim, W. J., Levy II, H., Kasibhatla, P. S. (1996) Simulated global tropospheric PAN: Its transport and impact on NO_x. *J. Geophys. Res.* **101**, 12621-12638.

Nielsen, L. B., Berkowicz, R., Conradsen, K. and Prahm, L. P. (1981) Net incoming radiation estimated from hourly global radiation and/or cloud observations. *J. Clim.* **1**, 255-272.

Pleijel K., Altenstedt J. and Andersson-Sköld Y. (1996) Comparison of chemical schemes used in photochemical modelling - Swedish conditions, IVL-report B 1151, IVL, Box 470 86, 402 58 Göteborg, Sweden.

Pudykiewiz, J. (1989) Simulation of the Chernobyl dispersion with a 3-D hemispheric tracer model, *Tellus* **41B**, 391.

Robertson, L., Langner J. and Engardt M. (1996) MATCH-Meso-scale atmospheric transport and chemistry modelling system. Basic transport model description and control experiments with Rn^{222}. Swedish Meteorological and Hydrological Institute RMK-70.

Robertson, L., Rodhe, H. and Granat, L. (1995) Modelling of sulfur deposition in the southern Asian region, *Water, Air, and Soil Pollut.* **85**, 2337.

Simpson, D. (1992) Long-period modelling of photochemical oxidants in Europe. Model calculations for July 1985. *Atmos. Environ.* **26A**, 1609.

Simpson, D., Guenther, A., Hewitt, C.N. and Steinbrecher, R. (1995) Biogenic emissions in Europe. 1. Estimates and uncertainties. *J. Geophys. Res.* **100**, 22,875.

Simpson, D. (1995) Biogenic emissions in Europe. 2. Implications for ozone control strategies. *J. Geophys. Res.* **100**:22,891.

Simpson, D., Andersson-Sköld Y. and Jenkin M. E. (1993) Updating the chemical scheme for the EMEP MSC-W oxidant model: current status. EMEP MSC-W Note 2/93.

Zlatev, Z, Christensen, J. and Eliassen, A. (1993) Studying high ozone concentrations by using the Danish eulerian model, *Atmos. Environ,* **27A**, 845.

Van Ulden, A. P. and Holtslag A. A. M. (1985) Estimation of atmospheric boundary layer parameters for diffusion applications. *J. Climate Appl. Met.* **24**, 1196-1207.

Verver, J.G., Blom, J.G., van Loon, M. and Spee, E.J. (1996) A comparison of stiff ODE solvers for atmospheric chemistry problems, *Atmos. Environ.* **30**, 49.

Zilitinkevich, S. and Moronov D. V. (1996) A multi-limit formulation for the equilibrium depth of a stably stratified boundary layer. *Boundary-Layer Met.* **81**, 321-351.

APPENDIX A: COMPARISON OF THREE WAYS TO DESCRIBE THE CHEMISTRY OF ISOPRENE

A1. Introduction

In Eulerian modelling, the number of species treated is critical in order to minimize computing time and costs. In the work presented here, three chemical schemes representing the degradation of isoprene in the atmosphere, i.e. the EMEP MSC-W mechanisms (Simpson *et al.*, 1993), and two mechanisms described by Carter (Carter, 1996), have been compared.

The comparison has been performed in a number of hypothetical chemical environments, including European conditions.

In the EMEP isoprene scheme, species are represented by characteristic species representing groups. All characteristic species are treated in an explicit way. In the Carter isoprene schemes, species are represented by using both representative species and chemical operators as in the SAPRC mechanism (Carter, 1990).

A2. The EMEP isoprene chemical scheme

The EMEP MSC-W model (Simpson *et al.*, 1993) is a trajectory model simulating long range transport of pollutants over Europe. The chemical scheme is compressed and uses characteristic species as representatives for groups of VOC. The chemical behaviour of each characteristic species is treated explicitly. The alkanes are, besides methane, represented as ethane and n-butane, alkenes are represented as ethene, propene and isoprene. The aromatics, alcohols, aldehydes and ketones are represented by o-xylene, ethanol and methanol, formaldehyde and acetaldehyde, and methyl-ethyl-ketone respectively. The isoprene chemistry is represented by 18 species in 28 reactions as shown in Table A1.

A2.1 The Carter isoprene chemical schemes

The chemical degradation of isoprene has been described in detail in Carter and Atkinson (1996), where observations from chamber studies have been compared to model results. In most cases the results were within the uncertainty of the data, although the PAN yield from isoprene degradation was underestimated by a factor of around 2. Two condensed mechanisms were developed based on this detailed mechanism (Carter, 1996). The schemes used in this comparison study are described in Table A2 and A3. The condensed mechanisms gave very close predictions to those of the detailed mechanism for both ozone, OH, and PAN (Carter, 1996), while HCHO was underpredicted by the 1-product mechanism.

A3. Model set-up and simulations

A3.1 The IVL chemical scheme

The principle of the photochemical trajectory model used for the comparison, is the same as in the Harwell model which initially was developed to simulate the formation of ozone and other oxidants in the London plume (Derwent and Hov, 1979; Derwent and Hough, 1988). The model has been further developed and adapted to fit Swedish conditions (Andersson-Sköld *et al.*, 1992; Pleijel et al. 1992; Andersson-Sköld, 1995).

Table A1. Isoprene chemical description used in the EMEP MSC-W model (Simpson *et al.*, 1993) including recommendations from Simpson (1997).

Species representing the isoprene chemistry:
isop   *isoprene*
macr   *methacrolein*
mvk   *methyl vinyl ketone*
isro2   *RO2 from isoprene degradation*
isni   *org. nitrate from isoprene degradation*
mvko2 RO2 from mvk degradation
isro2h, macro2, mpan, ch2cch3, isnir, isni1, isono3, isono3h, macro2h, mvko2h, ch2co2hch3, isnirh

Isoprene chemistry
kro2no=4.2d-12*exp(180./temp) ;
kho2ro2=1.0d-11 ;

% 12.3d-15*exp(-2013/temp)	*:isop+o3 = *0.67:macr,*0.26:mvk,*0.3:o,*
	*0.55:oh,*0.07:c3h6,*0.8:hcho,*0.06:ho2,*0.05:co;
% 2.54e-11*exp(410./temp)	*: isop+oh = isro2;*
% kro2no	*: isro2+no = *0.32:macr,*0.42:mvk,*
	*0.74:hcho,*0.14:isni,*0.12:isro2,*0.78:ho2,*0.86:no2;
% 4.13d-12*exp(452./temp)	*: mvk+oh = mvko2 ;*
% kro2no	*: mvko2+no = *0.684:ch3cho,*
	*0.684:ch3coo2,*0.266:mglyox,
	*0.266:hcho,*0.05:isni,*0.95:no2,*0.95:ho2 ;
% kho2ro2	*: isro2+ho2 = isro2h;*
% 2.0d-11	*: isro2h+oh = oh+isro2;*
% 8.0d-18	*: isro2h+o3 = *0.7:hcho;*
% 1.86d-11*exp(175./temp)	*: macr+oh = *0.5:macro2;*
% 1.0d-11	*: macro2+no2 = mpan;*
% 1.34d+16*exp(-13330./temp)	*: mpan = macro2+no2;*
% 2.0d-11	*: macro2+no = ch2cch3+no2;*
% kro2no	*: ch2cch3+no = no2+ch3coc2h5+ho2;*
% 4.32d-15*exp(-2016./temp)	*: mvk+o3=*0.82:mglyox,*0.8:hcho,*0.2:o,*
	*0.05:co,*0.06:ho2,*0.04:ch3cho,*0.08:oh;
% 3.35d-11	*: isni+oh = isnir;*
% kro2no	*: isnir+no = *0.05:isni1,*0.05:ho2,*
	*1.9:no2,*0.95:ch3cho,*0.95:ch3coc2h5;
% 7.8d-13	*: isop+no3 = isono3;*
% kro2no	*: isono3+no = *1.10:no2,*0.8:ho2,*
	*0.85:isni,*0.1:macr,*0.15:hcho,*0.05:mvk;
% kho2ro2	*: mvko2+ho2 = mvko2h;*
% kho2ro2	*: macro2+ho2 = macro2h;*
% kho2ro2	*: ch2cch3+ho2 = ch2co2hch3;*
% kho2ro2	*: isono3+ho2 = isono3h;*
% 3.2d-11	*: ch2co2hch3+oh = ch2cch3;*
% 2.0d-11	*: isono3h+oh = isono3;*
% 2.2d-11	*: mvko2h+oh = mvko2;*
% 3.7d-11	*: macro2h+oh = macro2;*
% kho2ro2	*: isnir+ho2 = isnirh;*
% 3.7d-11	*: isnirh+oh = isnir;*

The model describes the chemical development in a trajectory passing over emission sources. The chemical development is described by the rate expressions, dC_i/dt, for each species treated in the investigated model. For a species i in the boundary layer, the differential equation which represents the concentration development in time, C_i, will be expressed as in the equation below.

$$\frac{dC_i}{dt} = P_i - L_i C_i - \frac{V_{i,g} C_i}{h} + \frac{E_i}{h} \qquad \text{(A1)}$$

where:

C_i is the concentration of species i in $\left[molecules \cdot cm^{-3}\right]$ in the boundary layer,

P_i is the chemical production rate in $\left[molecules \cdot cm^{-3} \cdot s^{-1}\right]$ for species i,

L_i is the chemical loss rate coefficient in $\left[s^{-1}\right]$ for species i,

$V_{i,g}$ is the dry deposition rate in $\left[cm \cdot s^{-1}\right]$ for species i,

h is the height of the mixing layer in $\left[cm\right]$,

E_i is the emission rate in $\left[molecules \cdot cm^{-2} \cdot s^{-1}\right]$ for species i,

The differential equations were solved using the calculation program FACSIMILE/CHEKMAT (Curtis and Sweetenham, 1987), employing Gear's method (Gear, 1969) on a Sun Workstation.

A3.2 Chemical modifications

In order to make the various models as strictly comparable as possible, all identical chemical reactions in the different schemes were set using the same rate coefficients, i.e. the ones used in the IVL scheme (Andersson-Sköld, 1995). Since the Carter chemical descriptions are based on the SAPRC chemical mechanism (Carter, 1990), using chemical operators and not explicit species as in the EMEP and the IVL model, it was necessary to make some modifications of the schemes. In this study the 4-product mechanism is used as the most detailed mechanism.

The adapted Carter 4-product mechanism is described by 16 species in 48 reactions, as shown in Table A2. The following modifications are made compared to the original (Carter, 1996) scheme. No carbon counters are used, methacrolein is used as in the EMEP-version, which only treats the OH reaction and not the O_3 or NO_3 reactions, nor photolysis. Methyl vinyl ketone is used as in the EMEP-version including no photolysis. No ISOPROD photolysis is included, as photolysis of methacrolein is excluded in EMEP. Peroxy radical formation from methacrolein degradation is used in the EMEP-version as macro2, not as MA-RCO3, and macro2 has no reaction with RO2 or RCO3. RO2 and RCO3-species are counted all through the EMEP chemical scheme in order to be used correctly in the X + RO2/RCO3-reactions described in the SAPRC-way.

The adapted Carter 1-product mechanism is described by 7 species in 27 reactions, as shown in Table A3. The following modifications are made compared to the original (Carter, 1996) scheme as described in Carter (1997), where an adaptation to the RADM-II mechanism was made. Photolysis of ISOPROD is not included, as photolysis of methacrolein is excluded in EMEP.

Table A2. Condensed chemical scheme used in this study to represent the Carter 4-product isoprene mechanism (Carter, 1996).

Species representing the isoprene chemistry:

ISOP, ISOPROD, HCHO, CCCCO2, CCCCHO2, HCOCHO2, HOCCHO2, C2O2CHO, C2O2COH, RO2N, CH3OOH, RNO3, RO2R, R2O2, RO2, RCO3

Rkcal = 1.99E-3 kcal/mole/K;
kro2no=4.2d-12*exp(180./temp) ;
kho2ro2=1.0d-11 ;
falloff = k0/(1+k0kinf)*0.27@((1+(log10(k0kinf))@2)@-1);
k0=m*1.95E-28*((TEMP/300)@-4);
kinf=8.4E-12;
k0kinf=k0/kinf;

Isoprene chemistry

% 2.54E-11*exp(0.81/Rkcal/TEMP):	ISOP + OH = *0.088: RO2N, *0.912: RO2R,*0.629: HCHO,*0.23: macr, *0.32: MVK,*0.362:ISOPROD, *0.079: R2O2,*1.079: RO2;
% 7.86E-15*exp(-3.80/Rkcal/TEMP):	ISOP + O3 = *0.4: HCHO, *0.39: macr,*0.16: MVK,*0.55: HCHO2,*0.2:CCCCO2, *0.2: CCCCHO2,*0.05: ISOPROD;
% 1.0:	HCHO2 = *0.7:HCOOH,*0.12:OH,*0.12:HO2,*0.12:CO, *0.18:H2;
% 3.60E-11:	ISOP + O = *0.75: ISOPROD,*0.25: macro2, *0.25:RCO3,*0.5:HCHO, *0.25:RO2R,*0.25:RO2;
% 3.03E-12*exp(-0.89/Rkcal/TEMP):	ISOP + NO3 = RO2,*1.05:CH3CHO, *0.8:RNO3,*0.8:RO2R,*0.2:ISOPROD, *0.2:R2O2,*0.2:NO2;
% 1.50E-19:	ISOP + NO2 = RO2,* 1.05:CH3CHO,*0.8:RNO3, *0.8:RO2R,*0.2:ISOPROD,*0.2:R2O2,*0.2:NO;

% 1.86d-11*exp(175./temp)	:	macr+oh = *0.5:macro2;
% 1.0d-11	:	macro2+no2 = mpan;
% 1.34d+16*exp(-13330./temp)	:	mpan = macro2+no2;
% 2.0d-11	:	macro2+no = ch2cch3+no2;
% kro2no	:	ch2cch3+no = no2+ch3coc2h5+ho2;
% kho2ro2	:	macro2+ho2 = macro2h;
% 3.7d-11	:	macro2h+oh = macro2;

% 4.13d-12*exp(452./temp)	:	mvk+oh = mvko2 ;
% kro2no	:	mvko2+no = *0.684:ch3cho, *0.684:ch3coo2,*0.266:mglyox, *0.266:hcho,*0.05:isni,*0.95:no2, *0.95:ho2 ;
% 4.32d-15*exp(-2016./temp)	:	mvk+o3=*0.82:mglyox,*0.8:hcho,*0.2:o, *0.05:co,*0.06:ho2,*0.04:ch3cho,*0.08:oh;
% 3.35d-11	:	isni+oh = isnir;
% kro2no	:	isnir+no = *0.05:isni1,*0.05:ho2, *1.9:no2,*0.95:ch3cho,*0.95:ch3coc2h5;
% 6.19E-11:		ISOPROD + OH = *0.418:CO, *0.125:CH3CHO,*0.02:HCHO, *0.124:glyox,*0.082:CH3CHO,*0.145:mglyox,

	*0.48:ch3coc2h5,*0.688:RO2R, *0.313:macro2,*0.688:RO2, *0.313:RCO3;
% 4.18E-18:	ISOPROD + O3 = *0.062:CH3CHO,*0.007:HCHO,*0.031:glyox, *0.622:mglyox,*0.278:ch3coc2h5, *0.063:HCHO2, *0.278:HCOCHO2,*0.559:HOCCHO2, *0.069:C2O2CHO, *0.031:C2O2COH;
% 1.00E-13:	ISOPROD + NO3 = RNO3 + HO2 + R2O2 + RO2,*0.668:CO,*0.332:HCHO, *0.438:CH3CHO;
% 1.0:	CCCCO2 = OH + R2O2 + HCHO + macro2 + RO2 + RCO3;
% 1.0:	CCCCHO2 = *0.989:CH3CHO,*0.25:ISOPROD;
% 1.0:	C2O2CHO = OH + R2O2 + HCHO + HO2 + RO2 + RCO3;
% 1.0:	HOCCHO2 = *0.6:OH,*0.3:CH3COO2,*0.3:RCO3, *0.3:RO2R,*0.3:HCHO,*0.3:CO,*0.3:RO2;
% 1.0:	HCOCHO2 = *0.12:HO2,*0.24:CO,*0.12:OH, *0.51:HCHO;
% 1.0:	C2O2COH = OH + mglyox + HO2 + R2O2 + RO2;
% 4.200E-12*exp(0.36/Rkcal/TEMP):	RO2N + NO = RNO3;
% 3.40E-13*exp(1.59/Rkcal/TEMP):	RO2N + HO2 = CH3OOH + CH3COC2H5;
% 1.0E-15:	RO2N + RO2 = RO2 + CH3COC2H5, *0.5:HO2;
% 1.86E-12*exp(1.053/Rkcal/TEMP):	
	RO2N + RCO3 = RCO3 + CH3COC2H5, *0.5:HO2;
% 2.191E-11*exp(-1.408/Rkcal/TEMP):	
	RNO3+OH = NO2, *0.155:CH3COC2H5, *1.384:CH3CHO,*0.16:HCHO, *1.39:R2O2,*1.39:RO2;
% 4.200E-12*exp(0.36/Rkcal/TEMP):	RO2R + NO = NO2 + HO2;
% 3.40E-13*exp(1.59/Rkcal/TEMP):	RO2R + HO2 = CH3OOH;
% 1.0E-15:	RO2R + RO2 = RO2, *0.5:HO2;
% 1.86E-12*exp(1.053/Rkcal/TEMP):	RO2R + RCO3 = RCO3, *0.5:HO2;
% 4.200E-12*exp(0.36/Rkcal/TEMP):	R2O2 +NO = NO2;
% 3.40E-13*exp(1.59/Rkcal/TEMP):	R2O2 + HO2 =;
% 1.0E-15:	R2O2 + RO2 = RO2;
% 1.86E-12*exp(1.053/Rkcal/TEMP):	R2O2 + RCO3 = RCO3;
% 4.200E-12*exp(0.36/Rkcal/TEMP):	RO2 + NO = NO;
% 3.40E-13*exp(1.59/Rkcal/TEMP):	RO2+HO2 = HO2;
% 1.0E-15:	RO2 + RO2 =;
% 1.86E-12*exp(1.053/Rkcal/TEMP):	RO2 + RCO3 = ;
% 5.10E-12*exp(0.397/Rkcal/TEMP):	RCO3+ NO = NO;
% falloff :	RCO3 + NO2 = NO2;
% 3.40E-13*exp(1.59/Rkcal/TEMP):	RCO3 + HO2 = HO2;
% 2.80E-12*exp(1.053/Rkcal/TEMP):	RCO3 + RCO3 = ;

60

Table A3. Condensed chemical scheme used in this study to represent the Carter 1-product isoprene mechanism (Carter, 1996; Carter, 1997).

Species representing the isoprene chemistry:
ISOP, ISORO2, XO2, ONIT, ISOPROD, ISONRO2, IPRO2

Rkcal = 1.99E-3 kcal/mole/K;
j<7> = the fotolysis rate for hno3 -> no2+oh;

% 2.54E-11*exp(0.81/Rkcal/TEMP):	ISOP + OH = ISORO2,*0.079:XO2;
% 4.20E-12*exp(0.358/Rkcal/TEMP):	ISORO2 + NO = *0.088:ONIT,
	*0.912:NO2,*0.912:HO2,*0.912:isoprod,
	*0.629:HCHO;
% 7.70E-14 *exp(2.583/Rkcal/TEMP):	ISORO2 + HO2 = C2H5OOH;
% 8.40E-14 *exp(0.437/Rkcal/TEMP):	ISORO2 + ch3coo2 = isoprod,
	*0.5:HO2,*0.5:ch3o2,*0.5:ch3cooh;
% 3.40E-14 *exp(0.437/Rkcal/TEMP):	ISORO2 + CH3O2 = isoprod,
	*0.5:HCHO,*0.5:HO2;
% 7.86E-15*exp(-3.80/Rkcal/TEMP):	ISOP + O3 = ,*0.4 :HCHO,
	*0.6:ISOPROD,*0.39:HCOOH,*0.07:OH,
	*0.07:HO2,*0.07:CO,
	*0.2:OH,*0.2:XO2,*0.2:HCHO,*0.2:CH3COO2,
	*0.15: CH3CHO,*0.05:ISOPROD;
% 3.60E-11:	ISOP + O =,*0.75:ISOPROD,*0.25:CH3COO2,
	*0.25:HCHO,*0.25:CH3O2;
% 3.03E-12*exp(-0.89/Rkcal/TEMP):	ISOP + NO3 = ISONRO2;
% 4.20E-12*exp(0.358/Rkcal/TEMP):	ISONRO2 + NO = NO2,
	*0.8:CH3CHO,*0.8:ONIT,*0.8:HO2,
	*0.2:ISOPROD,*0.2:NO2;
% 7.70E-14*exp(2.583/Rkcal/TEMP):	ISONRO2 + HO2 = ONIT;
% 8.40E-14*exp(0.437/Rkcal/TEMP):	ISONRO2 + CH3COO2 = CH3CHO +
	ONIT,*0.5: HO2,*0.5:CH3O2,*0.5: CH3COOH;
% 3.40E-14*exp(0.437/Rkcal/TEMP):	ISONRO2 + CH3O2 = CH3CHO + ONIT,*0.5:HCHO,*0.5:HO2;
% 3.36E-11:	ISOPROD + OH = 0.5:CH3COO2,*0.5:IPRO2,*0.2:XO2;
% 4.20E-12*exp(0.358/Rkcal/TEMP):	IPRO2 + NO = NO2 + HO2,*0.59:CO,
	*0.55:CH3CHO,*0.25:HCHO,*0.08:glyox,
	*0.34:mglyox,*0.63: CH3COC2H5;
% 7.70E-14*exp(2.583/Rkcal/TEMP):	IPRO2 + HO2 = C2H5OOH;
% 8.40E-14*exp(0.437/Rkcal/TEMP):	IPRO2 + CH3COO2 = ,*0.5:HO2,*0.5:CH3O2,*0.5:CH3COOH,
	*0.5:CH3CHO,*0.5:CH3COC2H5;
% 3.40E-14*exp(0.437/Rkcal/TEMP):	IPRO2 + CH3O2 = ,*0.5:HCHO,
	*0.5:HO2,*0.5:CH3CHO,*0.5:CH3COC2H5;
% 7.11E-18 :	ISOPROD + O3 = ,*0.268:OH,*0.10:HO2,
	*0.114:CH3COO2,*0.054:CH3O2,*0.07:XO2,
	*0.155:CO,*0.146:HCHO,
	*0.02:CH3CHO,*0.01:glyox,
	*0.85:mglyox,*0.09:CH3COC2H5,*0.462:HCOOH;
% 1.0E-15:	ISOPROD + NO3 = ,*0.075:CH3COO2,*0.075:HNO3,
	*0.643:CO,*0.282:HCHO,*0.925:ONIT,
	*0.282:CH3CHO,*0.925:HO2,*0.925:XO2;
% 7.7E-14*exp(1300/TEMP):	XO2 + HO2 = C2H5OOH;
% 1.7E-14*exp(220/TEMP):	XO2 + CH3O2 = HCHO + HO2;
% 4.2E-14*exp(220/TEMP):	XO2 + CH3COO2 = CH3O2;
% 3.6E-16*exp(220/TEMP):	XO2 + XO2 = ;
% 4.2E-12*exp(180/TEMP):	XO2 + NO = NO2;
% 2.891*j<7>:	ONIT = HO2 + NO2, *0.2:CH3CHO,*0.8:CH3COC2H5;
% 1.55E-11*exp(-540/TEMP):	ONIT + OH = NO2, *0.843:secc4h9o2;

61

A3.3 Dry deposition

The dry deposition rates are chosen to correspond to the dry deposition over an average Swedish terrain with a 50 % forest coverage. The dry deposition velocities used in the simulations are given as diurnal mean values in Table A4 below.

Table A4. Dry deposition velocities used in the model simulations.

	O_3	HNO_3	NO_2	H_2O_2	SO_2	PAN
V_d [cm s^{-1}]	0.5	2.0	0.15	0.5	0.5	0.2

A3.4 Initial concentrations

The simulations were conducted for a hypothetical air mass passing over European emission sources. The concentrations of ozone, nitrogen oxides and volatile organic compounds, used at the start of the simulation, were set as in Table A5. The data are representing a clean air-mass arriving at the Swedish TOR station situated at Rörvik (Lindskog), apart from o-xylene.

Table A5. Initial concentrations used in the model set-up. Concentrations are based on data from a typical clean airmass reaching the Swedish west-coast (Lindskog), apart from o-xylene.

Species	Initial concentration (ppbv)
ozone	see Table A6.
NO_2	1.3
NO	0.3
ethane	1.3
n-butane	0.7
ethene	0.15
propene	0.05
o-xylene	0.5
SO_2	1

A3.4 Emission scenarios

The emission scenarios of NOx, VOC, CO and isoprene per km^2 and year along the simulated trajectory are given in Table A6. In the normal case emissions representative for average Swedish emissions are chosen. The distribution of the VOC emitted along the simulated trajectory were taken from data for southern Sweden (Janhäll and Andersson-Sköld, 1996).

A3.5 Meteorology

The highest ozone concentrations are expected when the solar radiation is high. For the simulation of an ozone episode the meteorological parameters were chosen to correspond to a cloudfree high pressure situation in the middle of the summer. The meteorological conditions chosen are shown in Table A3.4. The diurnal variation of the solar radiation at the 21st of June was used at 55°N. Clouds in the model are assumed to only reduce the solar radiation below them. The values chosen for this comparison study are shown in Table A7.

Table A6. Emission scenarios used in the comparison of three isoprene mechanisms.

	Name of run	Anthropogenic emissions (tonnes km^{-2} year^{-1})			Biogenic emissions	Initial concentration (ppbv)
No.		NO$_x$	VOC	CO	Isoprene	ozone
6	**Normal**	3	3	9	3	50
7	N - low NO$_x$	0.3	3	9	3	50
8	N - high NO$_x$	30	3	9	3	50
9	N - low VOC	3	0.3	0.9	3	50
10	N - high VOC	3	30	90	3	50
11	N - low isoprene	3	3	9	0.3	50
12	N - high isoprene	3	3	9	30	50
13	N - low ozone	3	3	9	3	20
14	N - high ozone	3	3	9	3	100
15	**Low**	0.3	0.3	0.9	0.3	50
16	L - norm isoprene	0.3	0.3	0.9	3	50
17	L - high isoprene	0.3	0.3	0.9	30	50
18	**High**	30	30	90	30	50
19	H - norm isoprene	30	30	90	3	50
20	H - low isoprene	30	30	90	0.3	50
21	H - low NO$_x$	0.3	30	90	30	50
22	H - low VOC	30	0.3	0.9	30	50

Table A7. Meteorological data used in the model simulations.

	Summer episode
Date	21st of June
Latitude	55°N
Height of boundary layer	1000 [m]
Temperature	25 °C
Relative humidity	70 %
Cloudiness	0/8

A4. Results from the comparison study

The cases studied vary from extreme hypothetical cases to normal realistic cases. The ozone and PAN result from the normal case simulation is shown in Figure A1 and Figure A2.

Figure A1. Ozone concentration in the Normal case using three different methods to represent the isoprene chemistry. In **Carter 4** the four-product mechanism is used, in **Carter 1** the one-product mechanism is used and in **EMEP** the EMEP mechanism is used, as described in the text.
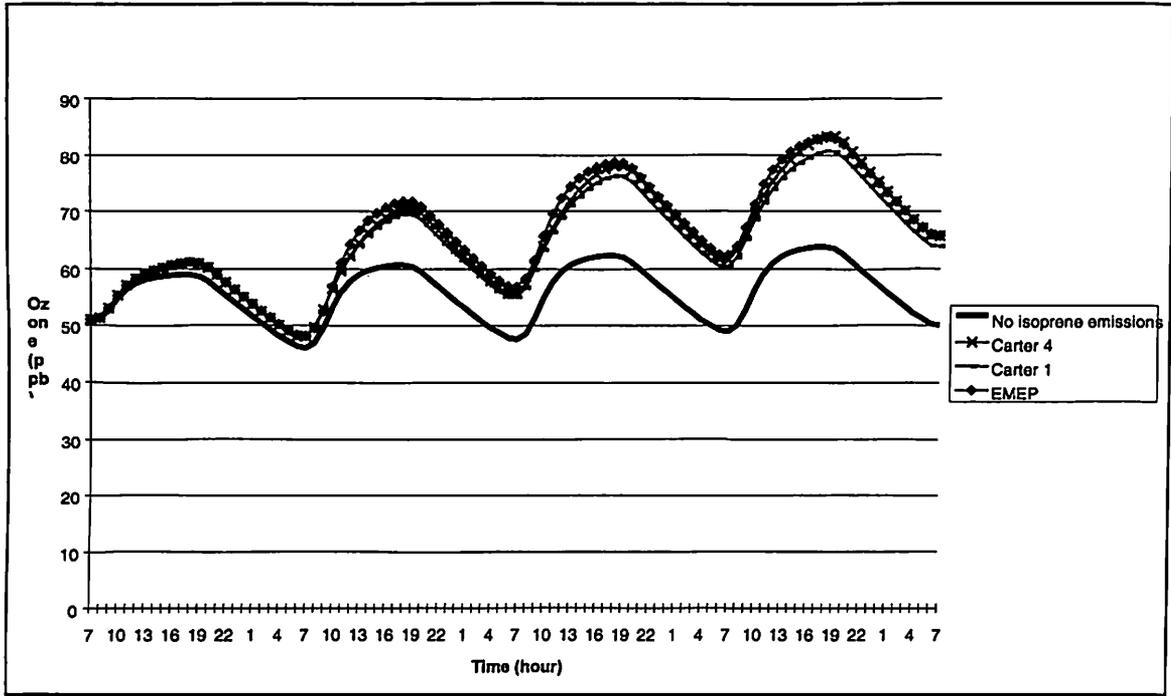

Figure A2. PAN concentration in the Normal case using three different methods to represent the isoprene chemistry. In **Carter 4** the four-product mechanism is used, in **Carter 1** the one-product mechanism is used and in **EMEP** the EMEP mechanism is used, as described in the text.
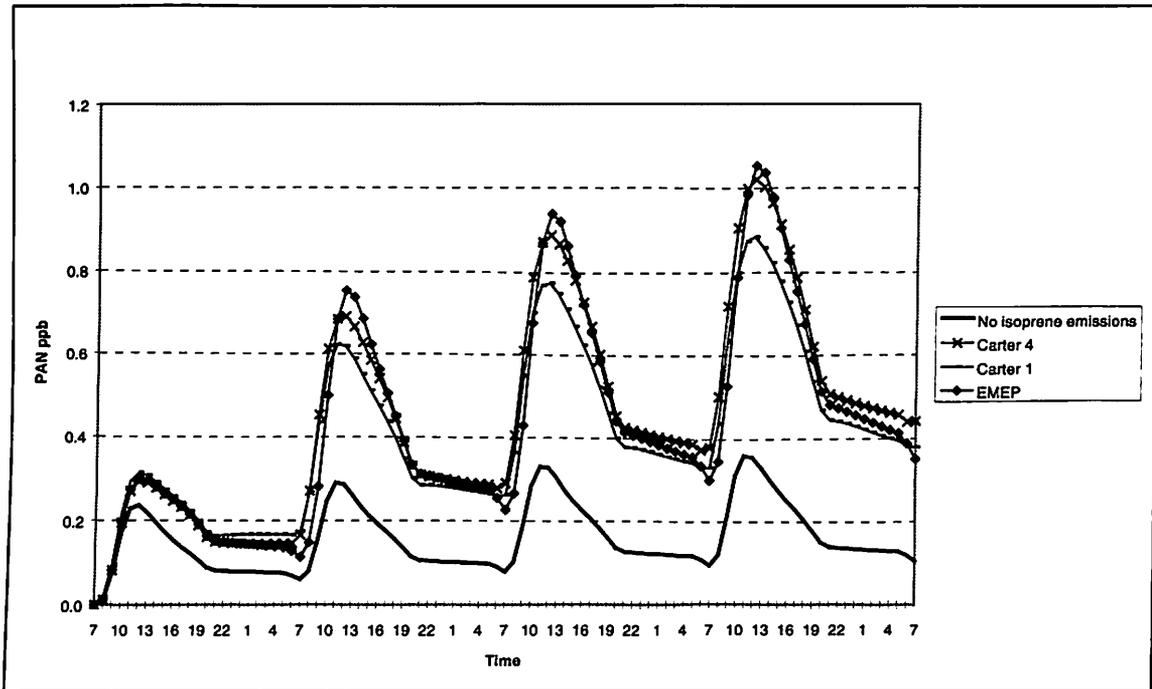
64

The results from all simulations are shown in Table A8. The ozone and PAN production from isoprene emissions in the simulations are shown as average over the time of simulation (i.e. 4 days) and as the maximum production from isoprene emissions. Since the Carter 4 mechanism is the most detailed mechanism, it is used as a reference. The percentage difference between Carter 1 and Carter 4, as well as between EMEP and Carter 4 are shown in the last columns of the table.

Numbers in the tables indicated in bold, italic show the cases which are most relevant for simulations in Northern Europe. The northern parts of Europe are normal to low in NO_x emissions. In these four simulations (number 6, 7, 10 and 21), the Carter 1 mechanism gives results for ozone in closest agreement with the most detailed mechanism.

A5. Summary

Three published chemical schemes for treating isoprene have been compared in a large number of chemical conditions. There are no large differences between the results, when the focus is on the simulation of ozone concentration. The chemical descriptions of isoprene that are used in the more detailed mechanisms (Simpson *et al.*, 1993; Carter, 1996), using 16-18 species, could thus be replaced by the mechanism using only 7 species (Carter, 1996).

References

Andersson-Sköld Y., Grennfelt P. and Pleijel K. (1992) Photochemical ozone creation potentials: a study of different concepts, *J. Air & Waste Management Ass.*, **42**, pp 1152-1158.

Andersson-Sköld Y. (1995) Updating the chemical scheme for the IVL photochemical trajectory model, IVL-report B 1151, IVL, Box 470 86, 402 58 Göteborg, Sweden.

Carter W. P. L. (1990) A detailed mechanism for the gas-phase atmospheric reactions of organic compounds. *Atmos. Environ.* **24A**, pp. 481-518.

Carter W. P. L. (1996) Condensed atmospheric photooxidation mechanisms for isoprene. *Atmos. Environ.* **30**, pp. 4275-4290.

Carter W. P. L. (1997) Communication via e-mail, feb. 1997.

Carter W. P. L. and Atkinson R. (1996) Development and evaluation of a detailed mechanism for the atmospheric reactions of isoprene and NOx. *Int. J. Chem. Kinet.* **28**, 497-530.

Curtis A.R. and Sweetenham W.P. (1987) FACSIMILE/CHEKMAT User's manual. AERE R 12805, Harwell Laboratory, Oxfordshire, England.

Derwent R.G. and Hough A.M. (1988) The impact of possible future emission control regulations on photochemical ozone formation in Europe, AERE R 12919, Harwell Laboratory, Oxfordshire, England.

Derwent R.G. and Hov Ø. (1979) Computer modelling studies of photochemical air pollution formation in north west Europe, AERE R-9434, Harwell Laboratory, Oxfordshire, England.

Gear C.W. (1969) The automatic integration of stiff ordinary differential equations. *Information Processing 68*, Ed. A. J. H. Morell, North Holland, Amsterdam, pp 187-193.

Janhäll S. and Andersson-Sköld Y. (1997) Emission inventory of NMVOC (non methane volatile organic compounds) and simulations of ozone formation due to emissions of NOxand NMVOC in Sweden, IVL-report B 1193, IVL, Box 470 86, 402 58 Göteborg, Sweden.

Lindskog L. IVL, Personal communication

Pleijel K., Andersson-Sköld Y. and Omstedt G. (1992) The importance of chemical and meteorological processes on mesoscale atmospheric ozone formation (in Swedish), IVL-report B 1056, IVL, Box 470 86, 402 58 Göteborg, Sweden.

Simpson D., Andersson-Sköld Y. and Jenkin M.E. (1993) Updating the chemical scheme for the EMEP MSC-W oxidant model: current status, EMEP MSC-W Note 2/93.

Simpson D. (1997) DNMI, Personal communication.

Table A8. Ozone and PAN production from isoprene emission in different scenarios, using three descriptions of the isoprene chemistry. The scenarios are described in Table A6. The percentage difference between the simulation conducted with the Carter 4 (C4) mechanism and the two more simplified mechanisms are shown in the last columns.

		Ozone production (ppb)			PAN production (ppb)			% ozone diff. from C4		% PAN diff. from C4	
		Carter 4	Carter 1	EMEP	Carter 4	Carter 1	EMEP	Carter 1	EMEP	Carter 1	EMEP
6	*Average*	*9.7*	*8.7*	*10.4*	*0.29*	*0.25*	*0.27*	*-10.3*	*7.0*	*-14.9*	*-6.9*
6	*Maximum*	*19.7*	*17.0*	*19.3*	*0.67*	*0.53*	*0.70*	*-13.7*	*-2.0*	*-21.4*	*5.0*
7	*Average*	*0.8*	*0.9*	*1.6*	*0.05*	*0.07*	*0.05*	*6.4*	*103.4*	*30.4*	*5.1*
7	*Maximum*	*2.2*	*2.5*	*5.2*	*0.12*	*0.13*	*0.15*	*17.0*	*138.0*	*6.9*	*27.7*
8	Average	7.0	6.7	6.7	0.06	0.06	0.05	-3.7	-4.2	8.0	-7.2
8	Maximum	18.0	17.1	16.4	0.18	0.18	0.20	-5.0	-8.7	4.2	10.6
9	Average	11.8	10.4	11.9	0.26	0.22	0.24	-11.9	0.6	-14.5	-7.2
9	Maximum	23.1	19.7	21.9	0.66	0.53	0.68	-14.6	-5.2	-20.3	3.5
10	*Average*	*0.2*	*0.9*	*3.6*	*0.19*	*0.18*	*0.23*	*358.8*	*1784.7*	*-5.1*	*21.4*
10	*Maximum*	*3.8*	*4.6*	*8.4*	*0.49*	*0.48*	*0.60*	*22.0*	*121.9*	*-3.3*	*21.8*
11	Average	1.2	1.0	1.2	0.03	0.02	0.02	-16.2	0.9	-18.0	-8.6
11	Maximum	2.3	1.9	2.2	0.07	0.05	0.07	-19.0	-6.3	-27.1	2.5
12	Average	22.3	23.9	28.4	1.33	1.92	1.45	7.1	27.4	43.6	8.8
12	Maximum	46.3	50.1	63.7	2.88	3.65	3.55	8.2	37.4	27.0	23.3
13	Average	10.1	9.1	10.6	0.28	0.24	0.26	-9.5	5.8	-14.2	-6.4
13	Maximum	19.6	17.1	19.3	0.66	0.53	0.70	-13.0	-1.6	-20.6	5.4
14	Average	9.3	8.2	10.1	0.31	0.26	0.28	-11.6	8.7	-16.3	-8.3
14	Maximum	19.7	16.8	19.3	0.68	0.53	0.71	-14.9	-2.3	-21.9	4.4
15	Average	0.5	0.5	0.8	0.01	0.01	0.01	-4.5	61.9	-8.1	-4.2
15	Maximum	1.5	1.4	1.8	0.02	0.02	0.02	-7.1	20.3	-16.8	7.0
16	Average	2.9	2.8	3.8	0.07	0.08	0.07	-4.5	31.3	14.2	4.5
16	Maximum	7.1	6.9	10.0	0.17	0.16	0.20	-2.5	41.0	-1.9	18.3
17	Average	-2.5	-4.0	-8.1	0.09	0.17	0.03	57.6	221.0	94.7	-66.9
17	Maximum	5.9	7.2	5.9	0.21	0.33	0.17	23.5	0.1	55.7	-18.7
18	Average	71.7	69.5	78.4	9.66	8.31	9.10	-3.1	9.3	-13.9	-5.8
18	Maximum	111.9	100.5	116.1	18.26	14.92	17.96	-10.2	3.7	-18.3	-1.7
19	Average	11.4	10.2	11.1	0.97	0.80	0.92	-10.6	-2.9	-17.2	-5.7
19	Maximum	21.2	20.5	19.4	2.05	1.64	1.82	-3.3	-8.8	-19.8	-11.0
20	Average	1.2	1.1	1.2	0.10	0.08	0.09	-11.3	-4.3	-17.1	-5.4
20	Maximum	2.3	2.2	2.1	0.20	0.17	0.18	-4.0	-8.6	-18.9	-10.7
21	*Average*	*-14.8*	*-16.0*	*-19.9*	*-0.11*	*-0.01*	*-0.17*	*8.1*	*34.0*	*-89.6*	*56.5*
21	*Maximum*	*2.6*	*2.7*	*2.1*	*0.03*	*0.21*	*0.02*	*2.9*	*-21.8*	*569.5*	*-45.1*
22	Average	158.7	149.6	158.9	8.70	7.09	8.23	-5.8	0.1	-18.5	-5.4
22	Maximum	284.9	260.0	281.0	17.98	14.02	17.92	-8.7	-1.4	-22.0	-0.3

APPENDIX B: CHEMICAL REACTION SCHEME

The chemical scheme used in the model is mainly based on the EMEP MSC-W mechanism (Simpson *et al.*, 1993). The isoprene chemistry has, however, been modified. An adapted version of the Carter 1-product mechanism (Carter, 1996) is used instead of the EMEP isoprene mechanism. The reaction scheme is presented in Table B1 below.

Table B1.   The chemical scheme

#EQUATIONS {EMEP-93 Simpson et al., 1993, modified}	
REACTION	**RATE CONSTANT**
{**Inorganic chemistry**}	
{ 1.} O + O2 + M = O3	: KOO2;
{ 5.} O + NO + M = NO2	: KONO;
{ 7.} O1D + M = O	: ARR(2.0E-11, 100.0);
{ 8.} O1D + H2O = 2 OH	: 2.2e-10;
{ 11.} O3 + NO = NO2	: ARR(1.8E-12, -1370.);
{ 12.} O3 + NO2 = NO3	: ARR(1.2E-13, -2450.);
{ 13.} O3 + OH = HO2	: ARR(1.9E-12, -1000.);
{ 14.} O3 + HO2 = OH	: ARR(1.4E-14, -600.);
{ 15.} NO + NO3 = 2 NO2	: ARR(1.8E-11, 110.);
{ 17.} NO + HO2 = NO2 + OH	: ARR(3.7E-12, 240.);
{ 19.} NO2 + NO3 = NO + NO2	: ARR(7.2E-14, -1414.);
{ 20.} NO2 + NO3 = N2O5	: 1.4E-12;
{ 21.} NO2 + OH = HNO3	: 1.4E-11;
{ 26.} NO3 + H2O2 = HO2 + HNO3	: 4.1E-16;
{ 29.} N2O5 = NO2 + NO3	: ARR(7.1E+14, -11080.);
{ 30.} OH + HO2 = H2O	: ARR(4.8E-11, 250.);
{ 31.} OH + H2O2 = HO2	: ARR(2.9E-12, -160.);
{ 33.} OH + H2 = HO2	: ARR(7.7E-12, -2100.);
{ 35.} OH + HNO3 = NO3	: ARR(1.0E-14, 785.);
{ 36.} 2 HO2 = H2O2	: FH2O*ARR(2.3E-13, 600.);
{ 37.} 2 HO2 + M = H2O2	: FH2O*ARR(1.7E-33, 1000.);
{**Sulfur chemistry**}	
{ 39.} OH + SO2 = HO2 + SULFATE	: 1.35E-12;
{ 40.} CH3O2 + SO2 = HCHO + HO2 + SULFATE	: 4.0E-17;
{**Aerosol reactions**}	
{ 43.} H2O2 = AEROSOL	: R_AEROSOL;
{ 43.} CH3O2H = AEROSOL	: R_AEROSOL;
{ 44.} N2O5 = 2 NITRATE	: R_AEROSOL;
{ 45.} HNO3 = NITRATE	: R_AEROSOL;
{**Methane chemistry**}	
{ 59.} OH + CH4 = CH3O2	: ARR(3.9E-12, -1885.);
{ 60.} CH3O2 + NO = HCHO + HO2 + NO2	: KRO2NO;
{ 61.} 2 CH3O2 = 2 HCHO + 2 HO2	: ARR(5.5E-14, 365.);
{ 62.} 2 CH3O2 = CH3OH + HCHO	: ARR(5.5E-14, 365.);
{ 63.} OH + CH3OH = HO2 + HCHO	: ARR(3.3E-12, -380.);
{ 65.} HO2 + CH3O2 = CH3O2H	: ARR(3.8E-13, 780.);
{ 66.} OH + HCHO = CO + HO2	: 9.6E-12;
{ 67.} CH3O2H + OH = HCHO + OH	: ARR(1.0E-12, 190.);
{ 68.} CH3O2H + OH = CH3O2	: ARR(1.9E-12, 190.);
{ 69.} NO3 + HCHO = HNO3 + CO + HO2	: 5.8E-16;
{ 70.} OH + CO = HO2	: 2.4E-13;

{**Ethane chemistry**}
{ 71.} OH + C2H6 = C2H5O2   : ARR(7.8E-12, -1020.);
{ 72.} C2H5O2 + NO = HO2 + CH3CHO + NO2   : 8.9E-12;
{ 74.} C2H5O2 + HO2 = C2H5OOH   : ARR(6.5E-13, 650.);
{76A.} C2H5OOH + OH = CH3CHO + OH   : 5.8*ARR(1.0E-12, 190.);
{76B.} C2H5OOH + OH = C2H5O2   : KRC92;
{ 75.} OH + CH3CHO = CH3COO2   : ARR(5.6E-12, 310.);
{ 77.} CH3COO2 + NO2 = PAN   : 1.0E-11;
{ 78.} PAN = CH3COO2 + NO2   : ARR(1.34E+16, -13330.);
{ 79.} CH3COO2 + NO = NO2 + CH3O2   : 2.0E-11;
{ 80.} CH3O2 + CH3COO2 = HCHO + HO2 + CH3O2   : 5.5E-12;
{ 80.} CH3O2 + CH3COO2 = CH3COOH + HCHO   : 5.5E-12;
{ 94.} 2 CH3COO2 = 2 CH3O2   : ARR(2.8E-12, 530.);
{ 88.} CH3COO2 + HO2 = CH3COO2H   : ARR(1.3E-13, 1040.);
{ 90.} CH3COO2H + OH = CH3COO2   : KRC92;
{ 89.} CH3COO2 + HO2 = CH3COOH + O3   : ARR(3.0E-13, 1040.);

{**Ethanol chemistry**}
{ 64.} OH + C2H5OH = CH3CHO + HO2   : 3.2E-12;

{**n-butane chemistry**}
{ 81.} OH + NC4H10 = SECC4H9O2   : ARR(1.64E-11, -559.);
{ 83.} NO + SECC4H9O2 =   : KRO2NO;
NO2 + 0.65 HO2 + 0.65 CH3COC2H5 + 0.35 CH3CHO + 0.35 C2H5O2
{ 86.} OH + CH3COC2H5 = CH3COCHO2CH3   : 1.15E-12;
{105.} CH3COCHO2CH3 + NO = NO2 + CH3COO2 + CH3CHO   : KRO2NO;
{104.} CH3COCHO2CH3 + HO2 = CH3COCHO2HCH3   : 1.0E-11;
{107.} CH3COCHO2HCH3 + OH = CH3COCHO2CH3   : 4.8E-12;
{108.} SECC4H9O2 + HO2 = SECC4H9O2H   : KHO2RO2;
{   } SECC4H9O2H + OH = SECC4H9O2   : KRC92;
{   } SECC4H9O2H + OH = OH + CH3COC2H5   : KRC91;

{**Ethene chemistry**}
{109.} C2H4 + OH = CH2O2CH2OH   : ARR(1.66E-12, 474.);
{110.} CH2O2CH2OH + NO = NO2 + 2 HCHO + HO2   : KRO2NO;
{113.} CH2O2CH2OH + HO2 = CH2OOHCH2OH   : KHO2RO2;
{   } CH2OOHCH2OH + OH = CH3CHO + OH   : KRC91;
{   } CH2OOHCH2OH + OH = CH2O2CH2OH   : KRC92;
{112.} C2H4 + O3 = HCHO + 0.44 CO + 0.12 HO2 + 0.13 H2   : ARR(1.2E-14, -2630.);

{**Propene chemistry**}
{123.} O3 + C3H6 = 0.5 HCHO + 0.5 CH3CHO + 0.07 CH4 + 0.4 CO +   : ARR(6.5E-15, -1880.);
0.28 HO2 + 0.15 OH + 0.31 CH3O2 + 0.07 H2
{125.} OH + C3H6 = CH3CHO2CH2OH   : 2.86E-11;
{126.} NO + CH3CHO2CH2OH = NO2 + CH3CHO + HCHO + HO2   : KRO2NO;
{122.} CH3CHO2CH2OH + HO2 = CH3CHOOHCH2OH   : KHO2RO2;
{   } CH3CHOOHCH2OH + OH = CH3COC2H5 + OH   : KRC91;
{   } CH3CHOOHCH2OH + OH = CH3CHO2CH2OH   : KRC92;

{**o-xylene chemistry**}
{234.} OXYLENE + OH = OXYO2   : 1.37E-11;
{236.} OXYO2 + NO = MGLYOX + MAL + HO2 + NO2   : KRO2NO;
{237.} OXYO2 + HO2 = OXYO2H   : KHO2RO2;
{235.} OXYO2H + OH = OXYO2   : 1.7E-11;
{219.} MAL + OH = MALO2   : 2.0E-11;
{220.} MALO2 + NO = NO2 + HO2 + MGLYOX + GLYOX   : KRO2NO;
{ 85.} MALO2 + HO2 = MALO2H   : KHO2RO2;
{223.} MALO2H + OH = MALO2   : 2.4E-11;
{221.} OH + GLYOX = HO2 + 2 CO   : 1.1E-11;
{222.} OH + MGLYOX = CH3COO2 + CO   : 1.70E-11;

69

{**Isoprene chemistry**, version recommended by IVL, Sep 1997}
```
{    } C5H8 + OH = ISRO2 + 0.079 XO2                           : ARR(2.54E-11, 408.);
{    } ISRO2 + NO = 0.088 ONIT + 0.912 NO2 + 0.912 HO2 +       : ARR(4.20E-12, 180.);
0.912 ISOPROD + 0.629 HCHO
{    } ISRO2 + HO2 = C2H5OOH                                   : ARR(7.70E-14, 1301.);
{    } ISRO2 + CH3COO2 =                                       : ARR(8.40E-14, 220.);
ISOPROD + 0.5 HO2 + 0.5 CH3O2 + 0.5 CH3COOH
{    } ISRO2 + CH3O2 = ISOPROD + 0.5 HCHO + 0.5 HO2            : ARR(3.40E-14, 220.);
{    } C5H8 + O3 = 0.6 HCHO + 0.65 ISOPROD + 0.27 OH + 0.07 HO2 : ARR(7.86E-15, -1914.);
+ 0.07 CO + 0.2 XO2 + 0.2 CH3COO2 + 0.15 CH3CHO + 0.39 HCOOH
{    } C5H8 + O =                                              : 3.6E-11;
0.75 ISOPROD + 0.25 CH3COO2 + 0.25 HCHO + 0.25 CH3O2
{    } C5H8 + NO3 = ISONRO2                                    : ARR(3.03E-12, -448.);
{    } ISONRO2 + NO =                                          : ARR(4.20E-12, 180.);
1.2 NO2 + 0.8 CH3CHO + 0.8 ONIT + 0.8 HO2 + 0.2 ISOPROD
{    } ISONRO2 + HO2 = ONIT                                    : ARR(7.70E-14, 1301.);
{    } ISONRO2 + CH3COO2 =                                     : ARR(8.40E-14, 220.);
CH3CHO + ONIT + 0.5 HO2 + 0.5 CH3O2 + 0.5 CH3COOH
{    } ISONRO2 + CH3O2 = CH3CHO + ONIT + 0.5 HCHO + 0.5 HO2    : ARR(3.40E-14, 220.);
{    } ISOPROD + OH = 0.5 CH3COO2 + 0.5 IPRO2 + 0.2 XO2        : 3.36E-11;
{    } IPRO2 + NO = NO2 + HO2 + 0.59 CO + 0.55 CH3CHO +        : ARR(4.20E-12, 180.);
0.25 HCHO + 0.08 GLYOX + 0.34 MGLYOX +0.63 CH3COC2H5
{    } IPRO2 + HO2 = C2H5OOH                                   : ARR(7.70E-14, 1301.);
{    } IPRO2 + CH3COO2 = 0.5 HO2 + 0.5 CH3O2 + 0.5 CH3COOH +   : ARR(8.40E-14, 220.);
0.5 CH3CHO +0.5 CH3COC2H5
{    } IPRO2 + CH3O2 =                                         : ARR(3.40E-14, 220.);
0.5 HCHO + 0.5 HO2 + 0.5 CH3CHO + 0.5 CH3COC2H5
{    } ISOPROD + O3 = 0.268 OH + 0.1 HO2 + 0.114 CH3COO2 +     : 7.11E-18;
0.054 CH3O2 + 0.07 XO2 + 0.155 CO +0.146 HCHO + 0.02 CH3CHO +
0.01 GLYOX + 0.85 MGLYOX + 0.09 CH3COC2H5 +0.462 HCOOH
{    } ISOPROD + NO3 = 0.075 CH3COO2 + 0.075 HNO3 + 0.643 CO + : 1.0E-15;
0.282 HCHO + 0.925 ONIT + 0.282 CH3CHO + 0.925 HO2 + 0.925 XO2
{    } XO2 + HO2 = C2H5OOH                                     : ARR(7.7E-14, 1300.);
{    } XO2 + CH3O2 = HCHO + HO2                                : ARR(1.7E-14, 220.);
{    } XO2 + CH3COO2 = CH3O2                                   : ARR(4.2E-14, 220.);
{    } XO2 + XO2 = M                                           : ARR(3.6E-16, 220.);
{    } XO2 + NO = NO2                                          : ARR(4.2E-12, 180.);
{    } ONIT + OH = NO2 + 0.843 SECC4H9O2                       : ARR(1.55E-11, -540.);
```

{**Photolysis reactions**}
```
{ 1.} O3 + hv = O1D                                    : 2.00E-4*EXP(-1.4*SECT)*BETA ;
{ 2.} O3 + hv = O                                      : 1.23E-3*EXP(-0.6*SECT)*BETA ;
{ 3.} NO2 + hv = NO + O                                : 1.45E-2*EXP(-0.4*SECT)*BETA ;
{ 4.} NO3 + hv = NO2 + O                               : 8.94E-2*EXP(-0.059*SECT)*BETA ;
{ 5.} NO3 + hv = NO                                    : 3.53E-2*EXP(-0.081*SECT)*BETA ;
{ 6.} N2O5 + hv = NO2 + NO3                            : 3.32E-5*EXP(-0.567*SECT)*BETA ;
{ 7.} H2O2 + hv = 2 OH                                 : 2.20E-5*EXP(-0.75*SECT)*BETA ;
{ 8.} HNO3 + hv = NO2 + OH                             : 3.00E-6*EXP(-1.25*SECT)*BETA ;
{ 9.} HCHO + hv = 2 HO2 + CO                           : 5.40E-5*EXP(-0.79*SECT)*BETA ;
{10.} HCHO + hv = H2 + CO                              : 6.65E-5*EXP(-0.6*SECT)*BETA ;
{11.} CH3CHO + hv = CH3O2 + HO2 + CO                   : 1.35E-5*EXP(-0.94*SECT)*BETA ;
{12.} CH3COC2H5 + hv = CH3COO2 + C2H5O2                : 2.43E-5*EXP(-0.877*SECT)*BETA ;
{14.} GLYOX + hv = CO + HCHO                           : 2.*6.65E-5*EXP(-0.6*SECT)*BETA ;
{15.} CH3O2H + hv = OH + HCHO + HO2                    : 2.27E-5*EXP(-0.62*SECT)*BETA;
{16.} MGLYOX + hv = CO + CH3COO2 + HO2                 : 4.*5.40E-5*EXP(-0.79*SECT)*BETA;
{17.} C2H5OOH + hv = OH + CH3CHO + HO2                 : 2.27E-5*EXP(-0.62*SECT)*BETA;
{18.} CH3COO2H + hv = OH + CH3O2                       : 2.27E-5*EXP(-0.62*SECT)*BETA;
{20.} CH3COCHO2HCH3 + hv = OH + CH3CHO + CH3COO2       : 2.27E-5*EXP(-0.62*SECT)*BETA;
{21.} SECC4H9O2H + hv =                                : 2.27E-5*EXP(-0.62*SECT)*BETA;
OH + 0.65 HO2 + 0.65 CH3COC2H5 + 0.35 CH3CHO + 0.35 C2H5O2
```

{22.} CH2OOHCH2OH + hv = OH + HO2 + 1.56 HCHO + 0.22 CH3CHO	: 2.27E-5*EXP(-0.62*SECT)*BETA;
{23.} CH3CHOOHCH2OH + hv = CH3CHO + HCHO + HO2 + OH	: 2.27E-5*EXP(-0.62*SECT)*BETA;
{24.} OXYO2H + hv = OH + MGLYOX + MAL + HO2	: 2.27E-5*EXP(-0.62*SECT)*BETA;
{25.} MALO2H + hv = OH + MGLYOX + GLYOX + HO2	: 2.27E-5*EXP(-0.62*SECT)*BETA;
{ivl} ONIT + hv = HO2 + NO2 + 0.2 CH3CHO + 0.8 CH3COC2H5	: 8.67E-6*EXP(-1.25*SECT)*BETA ;

Rate expressions:

Read ARR(2.0E-11, 100.0) as $2.0*10^{-11}*exp(100.0/T)$, where T is the temperature in K.

Read 2.00E-4*EXP(-1.4*SECT)*BETA as $2.00*10^{-4}*exp(-1.4*sec\,(\theta)\,)*\beta$, where θ is the solar zenith angle and β is a scaling factor depending on the total cloud cover.

$KOO2 = 5.7*10^{-34}*(T/300.0)^{-2.8}$

$KONO = 9.6*10^{-32}*(T/300.0)^{-1.6}$

$FH2O = (1+1.4*10^{-21}*[H2O]*exp(2200/T))$, where [H2O] is the concentration of H_2O-molecules

$R\_AEROSOL = 10^{-4}$ if relative humidity > 0.9

$\qquad\qquad\quad = 10^{-5}$ if relative humidity <= 0.9

$KRO2NO = ARR(4.2E-12, 180.0)$

$KRC92 = ARR(1.9E-12, 190.0)$

$KHO2RO2 = 10^{-11}$

$KRC91 = ARR(5.8E-12, 190.0)$

The units for the rate constants are s^{-1} for first order reactions, cm^3 molecule^{-1} s^{-1} for second order reactions and cm^6 molecule^{-2} s^{-1} for third order reactions.

Abbreviations:

GLYOX	Glyoxal (1,2-ethanedione)
IPRO2	Peroxy radical formed from ISOPROD + OH
ISOPROD	Lumped organic product species from reactions of isoprene, ISRO2 and ISONRO2
ISONRO2	Isoprene-NO3 adduct
ISRO2	Peroxy radical from isoprene + OH
M	Any air molecule
MAL	CH3COCH=CHCHO
MALO2	Peroxy radical from MAL + OH
MALO2H	Hydroperoxide from MALO2
MGLYOX	Methylglyoxal (1,2-propanedione)
ONIT	Organic nitrate
OXYO2	Peroxy radical formed from o-xylene + OH
OXYO2H	Hydroperoxide from OXYO2
PAN	Peroxyacetyl nitrate
XO2	Chemical operator accounting for additional NO to NO2 conversions affected by lumped organic species

References

Carter W. P. L. (1996) Condensed atmospheric photooxidation mechanisms for isoprene. *Atmos. Environ. 30*, pp. 4275-4290.

Simpson, D., Andersson-Sköld Y. and Jenkin M. E. (1993) Updating the chemical scheme for the EMEP MSC-W oxidant model: current status. EMEP MSC-W Note 2/93.

SMHIs publications

SMHI publishes six report series. Three of these, the R-series, are intended for international readers and are in most cases written in English. For the others the Swedish language is used.

Names of the Series	Published since
RMK (Report Meteorology and Climatology)	1974
RH (Report Hydrology)	1990
RO (Report Oceanography)	1986
METEOROLOGI	1985
HYDROLOGI	1985
OCEANOGRAFI	1985

Earlier issues published in serie RMK

1 Thompson, T., Udin, I., and Omstedt, A. (1974)
Sea surface temperatures in waters surrounding Sweden.

2 Bodin, S. (1974)
Development on an unsteady atmospheric boundary layer model.

3 Moen, L. (1975)
A multi-level quasi-geostrophic model for short range weather predictions.

4 Holmström, I. (1976)
Optimization of atmospheric models.

5 Collins, W.G. (1976)
A parameterization model for calculation of vertical fluxes of momentum due to terrain induced gravity waves.

6 Nyberg, A. (1976)
On transport of sulphur over the North Atlantic.

7 Lundqvist, J.-E., and Udin, I. (1977)
Ice accretion on ships with special emphasis on Baltic conditions.

8 Eriksson, B. (1977)
Den dagliga och årliga variationen av temperatur, fuktighet och vindhastighet vid några orter i Sverige.

9 Holmström, I., and Stokes, J. (1978)
Statistical forecasting of sea level changes in the Baltic.

10 Omstedt, A., and Sahlberg, J. (1978)
Some results from a joint Swedish-Finnish sea ice experiment, March, 1977.

11 Haag, T. (1978)
Byggnadsindustrins väderberoende, seminarieuppsats i företagsekonomi, B-nivå.

12 Eriksson, B. (1978)
Vegetationsperioden i Sverige beräknad från temperaturobservationer.

13 Bodin, S. (1979)
En numerisk prognosmodell för det atmosfäriska gränsskiktet, grundad på den turbulenta energiekvationen.

14 Eriksson, B. (1979)
Temperaturfluktuationer under senaste 100 åren.

15 Udin, I., och Mattisson, I. (1979)
Havsis- och snöinformation ur datorbearbetade satellitdata - en modellstudie.

16 Eriksson, B. (1979)
Statistisk analys av nederbördsdata. Del I. Arealnederbörd.

17 Eriksson, B. (1980)
Statistisk analys av nederbördsdata. Del II. Frekvensanalys av månadsnederbörd.

18   Eriksson, B. (1980)
     Årsmedelvärden (1931-60) av nederbörd,
     avdunstning och avrinning.

19   Omstedt, A. (1980)
     A sensitivity analysis of steady, free floa-
     ting ice.

20   Persson, C., och Omstedt, G. (1980)
     En modell för beräkning av luftförore-
     ningars spridning och deposition på me-
     soskala.

21   Jansson, D. (1980)
     Studier av temperaturinversioner och verti-
     kal vindskjuvning vid Sundsvall-Härnö-
     sands flygplats.

22   Sahlberg, J., and Törnevik, H. (1980)
     A study of large scale cooling in the Bay of
     Bothnia.

23   Ericson, K., and Hårsmar, P.-O. (1980)
     Boundary layer measurements at Klock-
     rike. Oct. 1977.

24   Bringfelt, B. (1980)
     A comparison of forest evapotranspiration
     determined by some independent methods.

25   Bodin, S., and Fredriksson, U. (1980)
     Uncertainty in wind forecasting for wind
     power networks.

26   Eriksson, B. (1980)
     Graddagsstatistik för Sverige.

27   Eriksson, B.(1981)
     Statistisk analys av nederbördsdata. Del
     III. 200-åriga nederbördsserier.

28   Eriksson, B. (1981)
     Den "potentiella" evapotranspirationen i
     Sverige.

29   Pershagen, H. (1981)
     Maximisnödjup i Sverige (perioden
     1905-70).

30   Lönnqvist, O. (1981)
     Nederbördsstatistik med praktiska tillämp-
     ningar.
     (Precipitation statistics with practical ap-
     plications.)

31   Melgarejo, J.W. (1981)
     Similarity theory and resistance laws for
     the atmospheric boundary layer.

32   Liljas, E. (1981)
     Analys av moln och nederbörd genom
     automatisk klassning av AVHRR-data.

33   Ericson, K. (1982)
     Atmospheric boundary layer field experi-
     ment in Sweden 1980, GOTEX II, part I.

34   Schoeffler, P. (1982)
     Dissipation, dispersion and stability of
     numerical schemes for advection and dif-
     fusion.

35   Undén, P. (1982)
     The Swedish Limited Area Model. Part A.
     Formulation.

36   Bringfelt, B. (1982)
     A forest evapotranspiration model using
     synoptic data.

37   Omstedt, G. (1982)
     Spridning av luftförorening från skorsten i
     konvektiva gränsskikt.

38   Törnevik, H. (1982)
     An aerobiological model for operational
     forecasts of pollen concentration in the air.

39   Eriksson, B. (1982)
     Data rörande Sveriges temperaturklimat.

40   Omstedt, G. (1984)
     An operational air pollution model using
     routine meteorological data.

41   Persson, C., and Funkquist, L. (1984)
     Local scale plume model for nitrogen
     oxides. Model description.

42   Gollvik, S. (1984)
     Estimation of orographic precipitation by
     dynamical interpretation of synoptic model
     data.

43   Lönnqvist, O. (1984)
     Congression - A fast regression technique
     with a great number of functions of all pre-
     dictors.

44   Laurin, S. (1984)
     Population exposure to So and NO_x from
     different sources in Stockholm.

45   Svensson, J. (1985)
     Remote sensing of atmospheric tempera-
     ture profiles by TIROS Operational
     Vertical Sounder.

46 Eriksson, B. (1986)
Nederbörds- och humiditetsklimat i
Sverige under vegetationsperioden.

47 Taesler, R. (1986)
Köldperioden av olika längd och före-
komst.

48 Wu Zengmao (1986)
Numerical study of lake-land breeze over
Lake Vättern, Sweden.

49 Wu Zengmao (1986)
Numerical analysis of initialization
procedure in a two-dimensional lake
breeze model.

50 Persson, C. (1986)
Local scale plume model for nitrogen
oxides. Verification.

51 Melgarejo, J.W. (1986)
An analytical model of the boundary layer
above sloping terrain with an application to
observations in Antarctica.

52 Bringfelt, B. (1986)
Test of a forest evapotranspiration model.

53 Josefsson, W. (1986)
Solar ultraviolet radiation in Sweden.

54 Dahlström, B. (1986)
Determination of areal precipitation for the
Baltic Sea.

55 Persson, C. (SMHI), Rodhe, H. (MISU),
De Geer, L.-E. (FOA) (1986)
The Chernobyl accident - A meteorological
analysis of how radionucleides reached
Sweden.

56 Persson, C., Robertson, L. (SMHI), Grenn-
felt, P., Kindbom, K., Lövblad, G., och
Svanberg, P.-A. (IVL) (1987)
Luftföroreningsepisoden över södra
Sverige 2 - 4 februari 1987.

57 Omstedt, G. (1988)
An operational air pollution model.

58 Alexandersson, H., Eriksson, B. (1989)
Climate fluctuations in Sweden
1860 - 1987.

59 Eriksson, B. (1989)
Snödjupsförhållanden i Sverige -
Säsongerna 1950/51 - 1979/80.

60 Omstedt, G., Szegö, J. (1990)
Människors exponering för luftförore-
ningar.

61 Mueller, L., Robertson, L., Andersson, E.,
Gustafsson, N. (1990)
Meso-γ scale objective analysis of near
surface temperature, humidity and wind,
and its application in air pollution model-
ling.

62 Andersson, T., Mattisson, I. (1991)
A field test of thermometer screens.

63 Alexandersson, H., Gollvik, S.,
Meuller, L. (1991)
An energy balance model for prediction of
surface temperatures.

64 Alexandersson, H., Dahlström, B. (1992)
Future climate in the Nordic region -
survey and synthesis for the next century.

65 Persson, C., Langner, J., Robertson, L.
(1994)
Regional spridningsmodell för Göteborgs
och Bohus, Hallands och Älvsborgs län. (A
mesoscale air pollution dispersion model
for the Swedish west-coast region. In
Swedish with captions also in English.)

66 Karlsson, K.-G. (1994)
Satellite-estimated cloudiness from NOAA
AVHRR data in the Nordic area during
1993.

67 Karlsson, K-G. (1996)
Cloud classifications with the SCANDIA
model.

68 Persson, C., Ullerstig, A. (1996)
Model calculations of dispersion of lindane
over Europe. Pilot study with comparisons
to measurements around the Baltic Sea and
the Kattegat.

69 Langner, J., Persson, C., Robertson, L.,
and Ullerstig, A. (1996)
Air pollution Assessment Study Using the
MATCH Modelling System. Application
to sulfur and nitrogen compounds over
Sweden 1994.

70 Robertson, L., Langner, J., Engardt, M.
(1996)
MATCH - Meso-scale Atmosperic
Transport and Chemistry modelling
system.

71   Josefsson W. (1996)
      Five years of solar UV-radiation
      monitoring in Sweden.

72   Persson, C., Ullerstig, A., Robertson, L.,
      Kindbom, K., Sjöberg, K. (1996)
      The Swedish Precipitation Chemistry
      Network. Studies in network design using
      the MATCH modelling system and
      statistical methods.

73   Robertson, L. (1996)
      Modelling of anthropogenic sulfur
      deposition to the African and South
      American continents.

74   Josefsson, W. (1996)
      Solar UV-radiation monitoring 1996.

75   Häggmark, L., Ivarsson, K.-I. (SMHI),
      Olofsson, P.-O. (Militära vädertjänsten).
      (1997)
      MESAN - Mesoskalig analys.

76   Bringfelt, B, Backström, H, Kindell, S,
      Omstedt, G, Persson, C, Ullerstig, A.
      (1997)
      Calculations of PM-10 concentrations in
      Swedish cities- Modelling of inhalable
      particles

77   Gollvik, S. (1997)
      The Teleflood project, estimation of
      precipitation over drainage basins.

78   Persson, C., Ullerstig, A. (1997)
      Regional luftmiljöanalys för Västmanlands
      län baserad på MATCH modell-
      beräkningar och mätdata - Analys av 1994
      års data

79   Josefsson, W., Karlsson, J.-E. (1997)
      Measurements of total ozone 1994-1996.

80   Rummikainen, M. (1997)
      Methods for statistical downscaling of
      GCM simulations.

81   Persson, T. (1997)
      Solar irradiance modelling using satellite
      retrieved cloudiness - A pilot study

SMHI